Thesis for the degree of: **Doctor of Philosophy**

Dublin City University

CALIXARENES:

Molecular Modelling of and

Potentiometric Studies on Cation

Complexes

Paddy Kane, GRSC.

School Of Chemical Sciences

Supervisor: Dr. Dermot Diamond

September 1998.

Declaration

I hereby certify that this material, which I now submit for assessment on the programme of study leading to the award of **Doctor of Philosophy** is entirely my own work and has not been taken from the work of others save to the extent that such work has been cited and acknowledged within the text of my work.

Signed: *Paddy Kane*   **ID No.**: 94970459

Paddy Kane

Date: 2/10/98

Dedication

To My Parents,

John and Winnie

Quotation

42

Douglas Adams

Hitch Hiker's Guide To The Galaxy

Acknowledgements

I wish to thank my supervisor, Dr. Dermot Diamond, for his innovation, enthusiasm and endless patience. Mention must be made of the synchronised fiddle playing of Dermot and cohorts in The Snug (both of them) and other hip hostelries. Just ask me for directions.

I am indebted to Darren *"Tap no. 2, please"* Fayne, Kevin Kincaid and Tom McKittrick, for their assistance in the experimental work. I must not forget Dr.Steven Bell and Prof. M. A. McKervey, both of Queens University Belfast, for their advice with regard to the writing of papers.

Dr. Colin Barnes, Dr. Robert Forster, Dr. Joshua Howarth, Dr. Paraic James, Dr. Siobhan O'Keefe and members of the Computational Chemistry mailing list, all deserve thanks for their advice and discussions.

The technicans, especially Ann, Damian, Maurice, Mick and Veronica, were of tremendous help to me over the past few years and I wish to thank them for that.

I wish to thank Forbairt, The Irish American Partnership, City Research, and Dublin Corporation for their financial support.

Thanks to Mam and Dad for their support over the last few years.

I must thank *"The Thesis Busters"* - Carol (thanks also for the shower cap idea and introducing me, albeit indirectly, to the mysteries of magpies), Frances *The Burglar* and Linda (two of the kindest and warmest people that you will ever meet), 3-D Helen and Mairead.

If you are not mentioned in the following paragraph, it just means that I dislike you. Thanks to all at 64 and 66 D**n S***t road for the apple tart, chocolate gateaux and tea. Thanks also to Stefano and Luke (who have been verra gud and brillinth to me). And thanks to a cast of thousands including Michaela (for the pillows and the cushion), Raquel (for the fudge), Big Ben, Little Joe, Celine (thank you very much for arranging the courier), the wan and only Dominic, Teresa ("Aaaaah, Peddy!"), P. J. with the sexy chin, Mark with the sexy voice, Mark who thinks he's sexy, Shane (why not try Freebird again), *Ten Pin King* Frank, Richard I, Richard *The Bap*

v

Publications and Presentations

Publications

- **P. Kane**, K. Kincaid, D. Fayne, D. Diamond, *"Conformational Analysis of Complexes of calix-[4]-arenes with Group 1 and Group 2 Cations"*, in preparation.

- **P. Kane**, D. Fayne, D. Diamond, S. E .J. Bell and M. A. McKervey, *"Modelling of the Sodium Complex of a Calixarene Tetraester in the 1,3-Alternate Conformation"*, J. Molecular Modeling, **1998**, in press (9 pages).

- **S. E. J. Bell**, M. A. McKervey, D. Fayne, P. Kane and D. Diamond, *"Molecular Modelling of Calixarenes with Group 1 Metal Ions"* J. Molecular Modeling, **1998**, 4, 44-52.

- **S. O'Neill**, P. Kane, M. A. McKervey and D. Diamond., *"Comparison of the Performance of Calix[4]arene Phosphine Oxide and Ester Derivatives in Ion-Selective Electrodes"* Analytical Communications, **1998**, 35, 127-131.

- **P. Kane** and D. Diamond, *"Determination of Ion-Selective Electrode Characteristics by Curve Fitting"*, Talanta, **1997**, 44, 1847-1858.

Seminars

- **Irish Universities Research Colloquium** (Institute Of Chemistry Of Ireland and AGB Scientific), *"Understanding Selectivity in Calixarene Ionophores"* University College Galway, 8th May, 1998.

- **Young Molecular Modellers' Conference** (Molecular Modeling and Graphics Society), *"Molecular Modelling Of Calixarene:Guest Interactions"*, London, December 15th, 1997.

Posters

- **Research & Development Topics** (Royal Society Of Chemistry), Nottingham University, *"A Novel Method For The Determination of Ion-Selective Electrode Characteristics"*, 22-23 July, 1996.

Table Of Contents

Preface

- Where compounds are referenced by number in this thesis, the numbering used is as follows:

<C> <Chapter Number> - <Number>

For example, **C 1-1**, is the tetrahydroxycalix[4]arene.

- Note that the figures and tables for Chapters 3 and 4 are given at the end of those chapters, while the figures for Chapter 2 are given at the end of that chapter. .

ABSTRACT

Chapter 1: The three-dimensional nature of calixarenes and their applications in sensors are reviewed.

Chapter 2: Molecular mechanics was used to model the geometry of a sodium calixarene complex formed with a 1,3-alternate conformation. Partial charges were assigned to the calixarene ligands by a variety of methods. These included various semi-empirical methods (AM1, PM3 and MNDO) arbitrarily assigning formal charges to the ions and carrying out semi-empirical calculations on the full ligand:complex. An investigation into the effect of placing the cation in different starting positions was undertaken in the case of this complex also. The effect of using ligand partial charges calculated with the PM3 and MNDO semi-empirical methods is commented upon.

Chapters 3 and 4: A series of calixarene phosphine oxides were used to construct ion-selective electrodes, (i.e., potentiometric sensors) and were found to be selective for calcium in the presence of a range of Group 1 and Group 2 interfering ions. Estimations of the characteristics of these electrodes (the cell constant, the Nernstian Slope Factor and potentiometric selectivity coefficients) were obtained by simple but rigorous procedure, developed for a potassium-selective valinomycin ion-selective electrode. The procedure involved fitting the experimental data to a mathematical model by non-linear analysis. In this method, the interfering ion concentration is kept constant and the primary ion concentration is varied by means of a series of small volume 'spikes', added to a single solution, with the electrodes continually in contact, and measuring the cell potential after each addition.

Monte Carlo conformational searches with molecular mechanics geometry optimisation gave very clear and positive explanations for the selectivity several calixarenes for several Group 1 and Group 2 ion, while NMR spectroscopic studies supported the conclusions drawn from the modelling studies about changes in conformation upon complexation with metal ions.

1. Calixarenes: *Three-dimensional Structure and Applications in Sensors*

1.1. Introduction

The name calixarenes was introduced by Gutsche for the cyclic oligomers formed from the condensation of formaldehyde and *p*-alkylphenols under alkaline conditions.[1,2] The word 'calix' (which means 'chalice' in Latin or Greek) refers to the chalice-like shape of the so-called 'cone' conformation of the calix[4]arenes. The most common calixarenes are described in Figure 1-1. These calixarenes possess an upper rim, defined by the **R** substituents in the *p*- position of the aryl rings and a lower rim defined by the phenolic oxygens and the pendant groups attached to them. Between these two regions lies a hydrophobic cavity of aromatic rings.
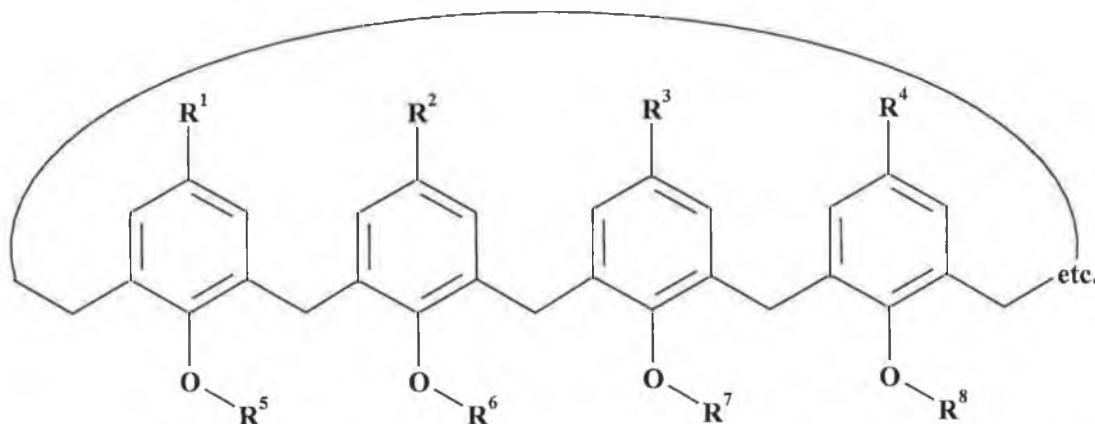
Figure 1-1. *Structure of common calix[n]arenes. Often, n = 4-8, $R^1 = R^2 = R^3 = R^4$, etc., = t-Bu or H and $R^5 = R^6 = R^7 = R^8$, etc, = H, alkyl or aryl.*

1

In Chapters 2 and 3, molecular modelling investigations of calixarenes is discussed while in Chapter Three, also reports on the work that Dr. Dermot Diamond and co-workers, including myself, have done on the use of calixarene phosphine oxides in ion-selective electrodes.   Thus, this chapter introduces the conformations of calixarenes and their use as recognition elements in sensor membranes.

1.2.   Conformations of Parent Calixarenes

The special appeal of calixarenes is the synergistic effect of the combination of the substituents present in the upper and lower rims and the three-dimensional nature of this combination.   Numerous conformations of calixarenes are possible through rotation of the phenolic moieties about the Ar-CH$_2$ bonds.   The four principal conformations of the calix[4]arenes which have been labelled by Gutsche,[3] are given Figure 1-1.

| cone | partial cone | 1,2-alternate | 1,3-alternate |
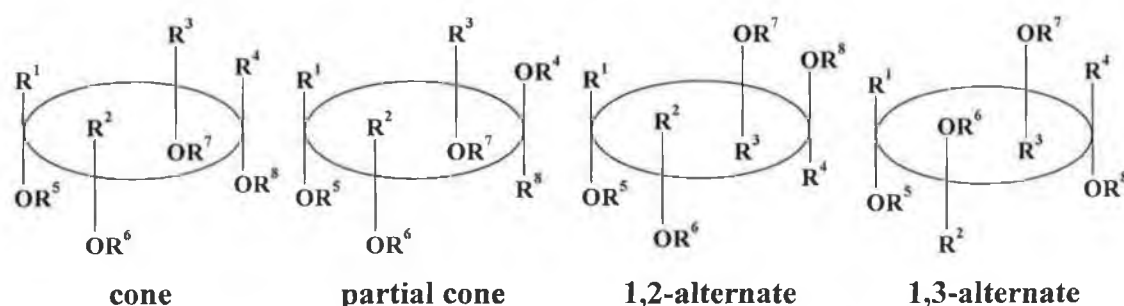
Figure 1-1. *The principal conformations of calix[4]arenes. R^1, R^2, R^3, R^4, R^5, R^6, R^7 and R^8 = H, alkyl or aryl.*

1.2.1.   *Conformations in The Solid State*

In the solid state, the cone conformation is exclusively observed for calix[4]arenes with four free hydroxyl groups, i.e., **C 1-1**,[4] because this arrangement is stabilised by intramolecular hydrogen bonding between the hydroxyl groups with each of these groups simultaneously acting as a hydrogen donor and acceptor.

The influence of hydrogen bonding is perhaps even more evident when calix[4]arenes with less than four hydroxyl groups are considered. For example, **C 1-2**[5,6] and **C 1-3**[5,6] adopt a 1,2-alternate conformation, while **C 1-7**[7,8] takes up a 1,3-alternate conformation. The SH groups are stronger electron donors but weaker

hydrogen acceptors. Furthermore, the 1,3-alternate conformation accommodates the larger size of the SH groups better than the cone conformation. **C 1-8** has a partial cone conformation.[9,10]

The cone conformation is again observed when the bulkiness of the pendant groups is great enough to prevent interconversion with other conformers. For example, **C 1-4**, **C 1-5** and **C 1-6** all adopt the cone conformation.[11]
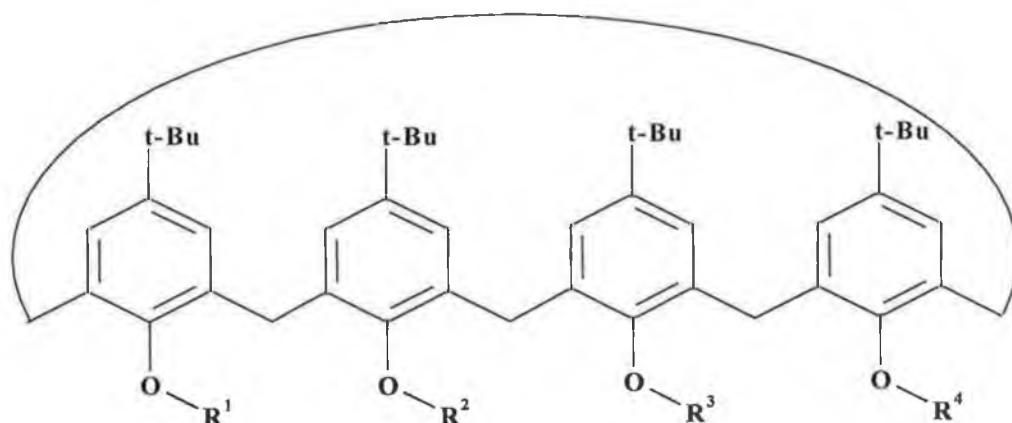
	R^1	R^2	R^3	R^4
C 1-1	OH	OH	OH	OH
C 1-2	OH	H	OH	H
C 1-3	H	H	H	H
C 1-4	CH_2CN	H	CH_2CN	H
C 1-5	CH_2COOEt	H	CH_2COOEt	H
C 1-6	CH_2COO-t-Bu	H	CH_2COO-t-Bu	H

C 1-7

C 1-8

3
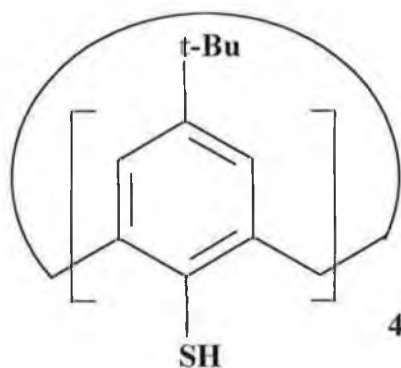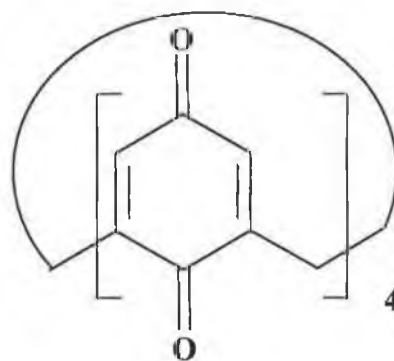
Calix[5]arenes show a cone-like conformation in the solid state with distances between neighbouring oxygen atoms (O….O distances) being larger than those in calix[4]arenes.[12] For example, in the X-ray structure of C 1-9,[12a] these distances range from 2.81 to 2.87 Å, while such distances in calix[4]arenes are ca. 2.65 to 2.67 Å,[4] indicating weaker intramolecular hydrogen bonds in the case of the calix[5]arene. These distances are similar but more variable in the X-ray structure of C 1-10, (2.75 to 2.88 Å) [12b] than that of C 1-9. The reason is probably due to the fact that the 1,1,3,3 tetramethyl R groups of C 1-10 are bulkier than the H's of C 1-9 and the molecule undergoes greater distortion to minimise repulsion between the R groups on neighbouring rings. Similar high variability in the distances between neighbouring oxygen atoms (2.74 to 2.88 Å) has been observed for C 1-11.[12d] In this case the bulkiness of the t-Bu groups is a factor. However, an additional factor is the inclusion of one of the t-Bu groups of a given molecule in the cavity of a neighbouring molecule to create a 'zipper' effect in the packing of the crystal.

In calix[6]arenes, two completely different conformation have so far been observed in the solid state:

a) all the hydroxyl groups are on the same side of the molecule, in a 'pinched' cone conformation, as exemplified by the X-ray structures of C 1-12,[13] C 1-13[13,14] and C 1-17.[15] The shape of the molecule in these cases is defined by the elliptical arrangements of the t-Bu groups on one side of the molecule and the oxygen atoms on the other side. For example, the O….O distances are ca. 2.57 to 2.65 Å in C 1-13,[14] i.e., this elliptical arrangement forces the neighbouring oxygen atoms to be similar to that found in calix[4]arenes.

b) groups of three neighbouring hydroxyl groups are on opposite sides of the molecule such as that found in the X-ray structure of C 1-18.[16] Such X-ray structures are described as a double partial cone as two sets of three aryl rings have a cone-like arrangement and are oriented in opposite directions. This conformation appears to be stabilised by intramolecular hydrogen bonding between the three phenolic oxygen atoms and the two hydrogen atoms. The O….O distances are in the range 2.50 to 2.64 Å. Of the X-ray structures observed of this type, this one is the most ideal.

4
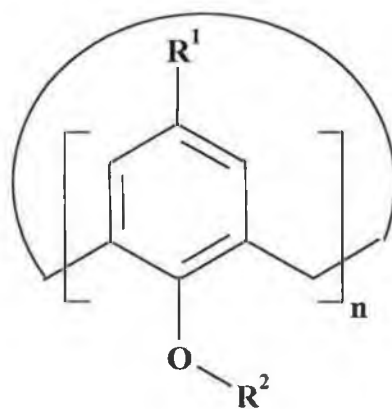
	n	R^1	R^2
C 1-9	5	H	H
C 1-10	5	$C(CH_3)_2CH_2C(CH_3)_3$	H
C 1-11	5	*t*-Bu	H
C 1-12	6	*i*_Pr	H
C 1-13	6	*t*-Bu	H
C 1-14	6	H	CH_2COOEt
C 1-15	7	*t*-Bu	H
C 1-16	8	*t*-Bu	H
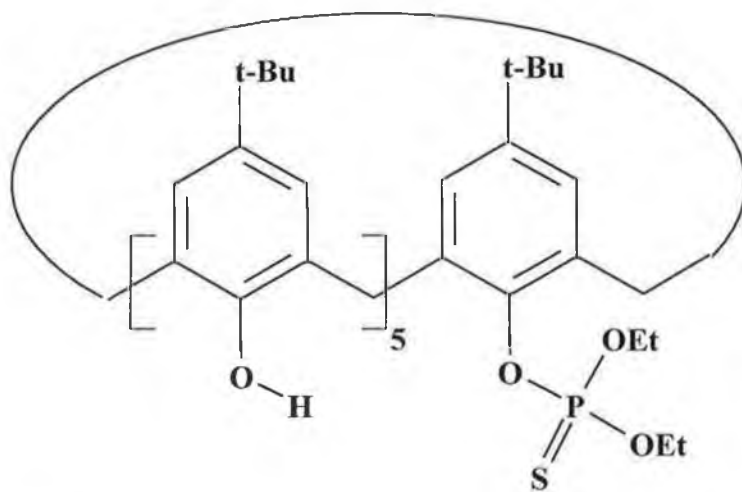
C 1-17
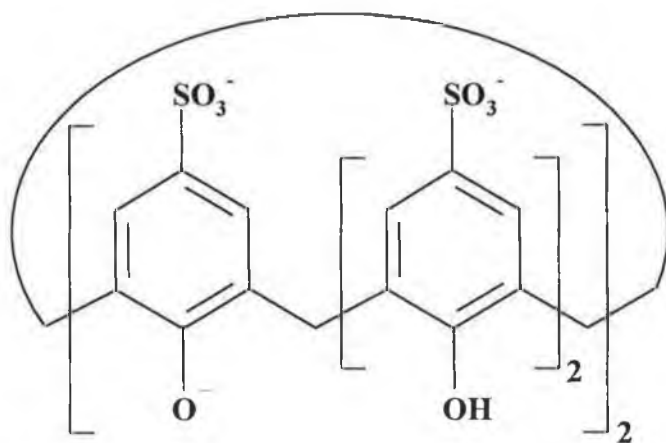
C 1-18

Wolfgong *et. al.*[17] report that **C 1-13** adopts a pinched cone conformation when it is recrystallised from benzene but when it is recrystallised from DMSO, acetone and dioxane/water, solvents which are capable of forming hydrogen bonds, the calixarene has a double partial cone conformation which is distorted. In the cases of the latter two solvents, the partial cones are severely distorted, with each unit containing an aryl ring approximately coplanar with the mean plane of the oxygen atoms in the macrocycle. The term double partial cone is inappropriate in these cases and the description 1,2,3-alternate is better. In the case of dioxane/water, the bulkiness of dioxane is obviously a factor in creating this distortion in addition to its ability to form hydrogen bonds.

The authors then go on to claim that the extent of the distortion which occurs in the case of hydrogen bonding solvents is dependent on the bulkiness of the solvent molecules and they support this argument by pointing out that in the X-ray structure of hexasubstituted esters such as **C 1-14**,[18] the cavity is 'filled' by one of the pendant groups and that the geometry of the macrocyclic ring is virtually identical to that of **C 1-13** when the latter compound is recrystallised from acetone and dioxane/water. However, their argument does not explain why less distortion is observed with DMSO than that observed with acetone since DMSO is bulkier than acetone because of its pyramidal geometry about the sulfur atom.

Calix[7]arenes[19] and calix[8]arenes[20,21] do not have a simple structure. For example, the X-ray structure of the calix[7]arene, **C 1-15** (as a calixarene:pyridine, 1:3 clathrate), consists of two substructures whose geometries are like that of a calix[4]arene and a calix[3]arene and that have mutually perpendicular axes.[19] Molecular mechanics, consisting of an exhaustive search of the conformational space combined with optimisation of the structures found, have confirmed this conformation as the global minimum.[22] The calix[4]arene-substructure is a distorted cone conformation with two hydrogen bonds of length 2.74 Å and two long contacts at 3.50 Å and 4.82 Å. Two very different conformations have been reported for the calix[8]arene, **C 1-16**. Gutsche *et. al.*[20] report what is referred to as a pleated loop conformation in which the eight hydroxyl groups are arranged in an almost planar, slightly undulating hydrogen bonded cyclic array. In contrast, the structure of this compound obtained by Czugler *et. al.*[21] consists of two sets of three aryl rings in the macrocycle at opposite ends of the molecule arranged in a partial cone manner and oriented in opposite directions. In between these two sets there are two aryl rings in approximately the same plane as each other and which are perpendicular to the axes of the aforementioned partial cones. The overall effect is that of a chair. The reason for these two different conformations must be related to the fact that the former structure contains no solvent molecules while the latter crystallised with eight pyridine molecules (one of which is bound to the host) even though the same solvent was used in both re-crystallisations.

1.2.2. *Conformations in Solution*

In solution, the vast majority of calix[4]arenes exist in the cone conformation. The ^{1}H NMR spectrum of **C 1-1** shows singlets for the hydroxyl, aromatic and *t*-butyl protons.[3] The two protons of each of the methylene bridges are non-equivalent and at low temperatures the resonance of these protons are observed as two doublets, meaning that these protons constitute an AB system with a coupling constant of 12-14 Hz, typical of geminal protons.[23] On the basis of Nuclear Overhausen Effect (NOE) experiments on **C 1-20**,[24,25] the high field doublet at ca. $\delta = 3.20$ ppm has been assigned to the equatorial protons (H_{eq}) and the other doublet at ca. $\delta = 4.89$ ppm to the axial protons (H_{ax}). See Figure 1-1a. That the axial peak is downfield from the

equatorial peak can be explained by their proximity of the axial protons to the phenoxy oxygen atoms which deshield the axial protons.

Computational studies predict that the symmetry of cone-calix[4]arenes is not C_{4v} but rather C_{2v}. For example, Figure 1-1b-d shows that the four aryl rings in **C 1-20** are non-equivalent, with the angle of inclination of the planes containing three of the atoms in rings **A** and **C** is 7.1° and that rings **B** and **D** are inclined at an angle of 77.2°. If such predictions are correct then interconversion must take place between two identical conformations with C_{2v} symmetry. Evidence for this interconversion is found in the variation in the ${}^1H$ NMR spectrum of **C 1-1** with temperature.[26] As the temperature is increased the methylene proton signals broaden, coalesce and become a sharp singlet. The interconversion rate at 47 °C has been calculated to be 150 s^{-1}.[27]

8

H_A the axial protons

H_B the equatorial protons
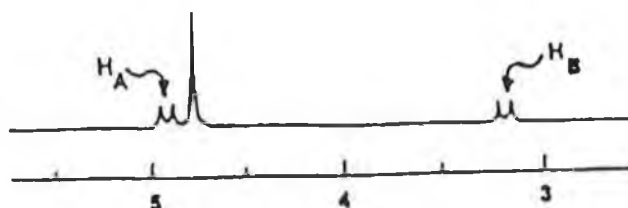
(a)
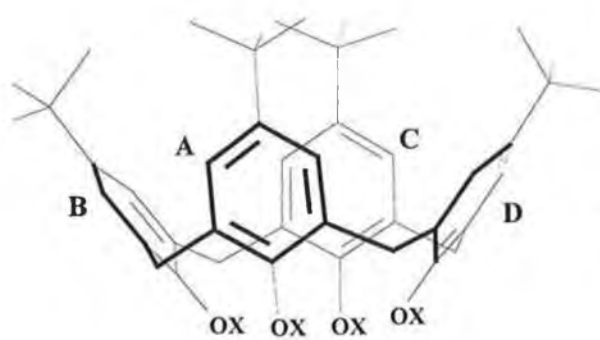
(b)
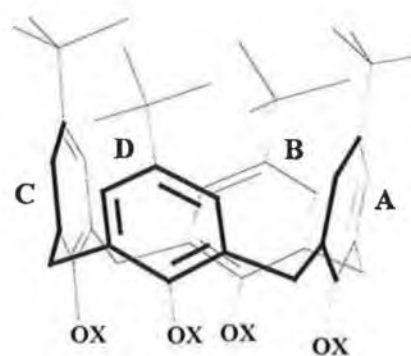
(c)
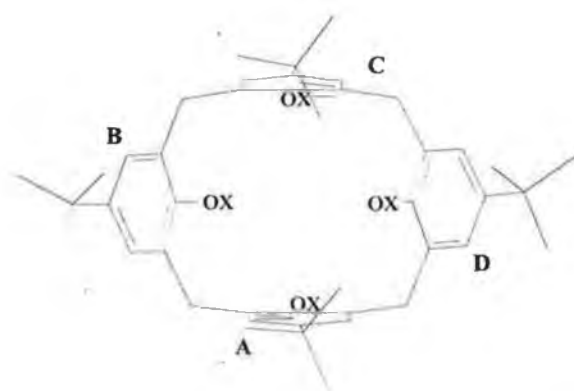
(c)
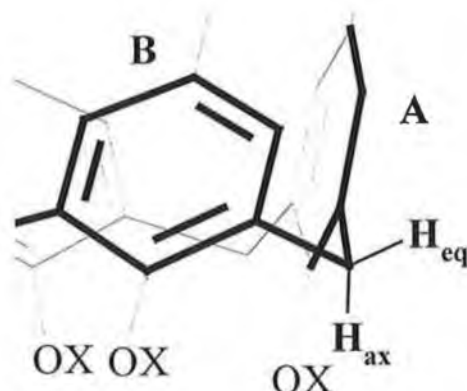
(d)

Figure 1-1. *C 1-20*, i.e., *X = CH₂COO-t-Bu.* *Partial ^1H NMR spectrum,*[25] *(a). Molecular Models: side on views, (b) and (c), view through cavity, (d) and expanded side-on view of one of the methylene bridging regions, showing the equatorial and axial protons, (e). The modelling procedure is detailed in Chapter Two.*

The details of the mechanism of interconversion are unknown but there is strong evidence that the hydroxyl groups pass through the interior of the calixarene. For **C 1-19**, it was found that the energy barriers for the coalescence of the signals due to the methyl protons on one side of the cavity and the methylene bridging protons in the macrocyclic ring on the other side, were the same within experimental error.[28] This unequivocally indicates that the interconversion takes place via the ring inversion route (route (b) in Figure 1-2) because this route, unlike route (a), involves the interconversion between the axial and equatorial protons in the aforementioned methylene bridges.
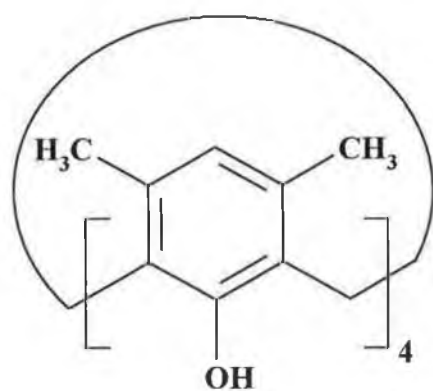
C 1-19
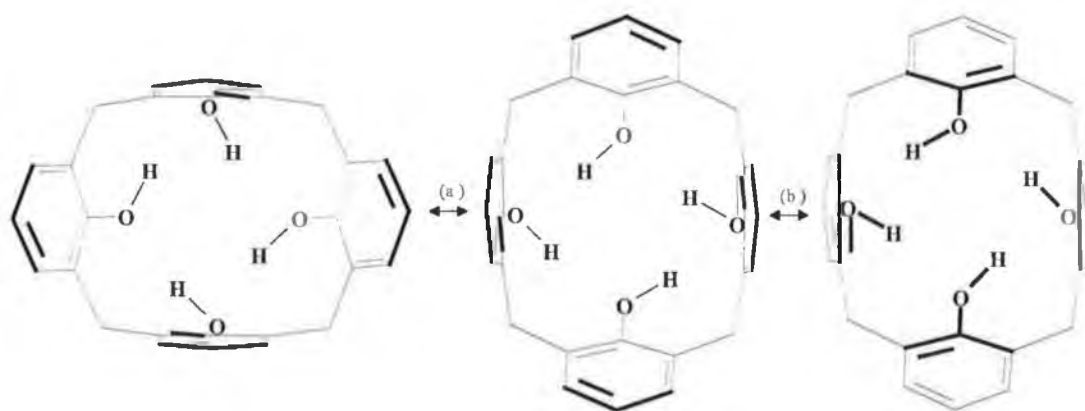
Figure 1-2. *Interconversion between the different possible cone conformers (with C_{2v} symmetry) of **C 1-19** by routes: pseudorotation, (a) and ring inversion, (b). The methyl groups have been omitted for clarity.*

10

Also, in the case of **C 1-1**, when CDCl$_3$ is used as a solvent, coalescence signal due to methylene protons occurs at 45 to 52 °C. However, when deuterated pyridine is used, the coalescence occurs at 15 °C,[26] indicating that pyridine, through hydrogen bonding, stabilises the intermediate with respect to the original conformer in this interconversion after the intramolecular hydrogen bonding has been broken or loosened. If the interconversion occurred via the pseudorotation route, the effect of using deuterated pyridine as a solvent would not be as dramatic.

The importance of intramolecular hydrogen bonding to the conformation is apparent when the hydroxyl groups are replaced. In **C 1-21**, for example, the lack of intramolecular hydrogen bonding and the relatively small size of the methyl groups mean that the compound is conformationally very mobile and the presence of several conformers was detected. The main conformation was determined to be partial cone because of the two pairs of doublets observed for the methylene bridging protons.[29] Similar results were obtained for **C 1-22**.

In contrast, the composition, as judged by ^{1}H NMR spectroscopy, of the product mixtures obtained from the synthesis of **C 1-23** and **C 1-24** (evidence of a mixture of the cone and partial cone conformers in an approximately 1:1 ratio were observed), did not change when the measurement temperature was increased to 60 °C or when refluxed for three days.[29] Thus the *n*-propyl and *n*-butyl groups are bulky enough to inhibit the interconversion between different conformers.
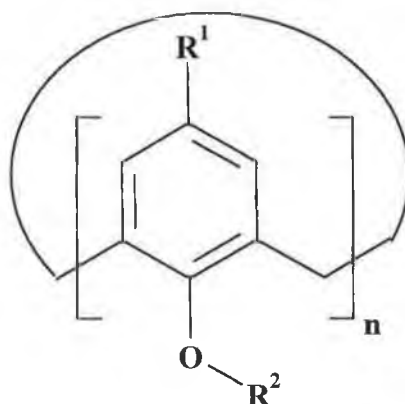
	n	R^1	R^2
C 1-20	4	t-Bu	CH_2COO-t-Bu
C 1-21	4	t-Bu	Me
C 1-22	4	t-Bu	Et
C 1-23	4	t-Bu	n-Pr
C 1-24	4	t-Bu	n-Bu
C 1-25	6	t-Bu	OCH_3
C 1-26	6	t-Bu	CH_2-Ph
C 1-27	6	t-Bu	CH_2-C_6H_4-CN

The ^{1}H NMR spectrum of **C 1-7** shows a singlet for the methylene protons across a large temperature range (-60 to 100 °C).[7,8] This could be interpreted as meaning that **C 1-7** exists as pair of very rapidly interconverting cone or 1,3-alternate conformers. However, it seems more likely that the geometry of the compound in solution is fixed in the 1,3-alternate conformation, considering the invariance of the spectrum at low temperatures and that the compound has this conformation in the crystalline state.[7,8] In contrast, Böhmer[23] reports that the conformations of calix[4]arenes with *exo* hydroxyl groups such as **C 1-28** (where intramolecular hydrogen bonding between all four hydroxyl groups is impossible) and **C 1-2** (where there are no hydroxyl groups) *do* undergo such interconversion.

R = CH$_3$ or t-Bu
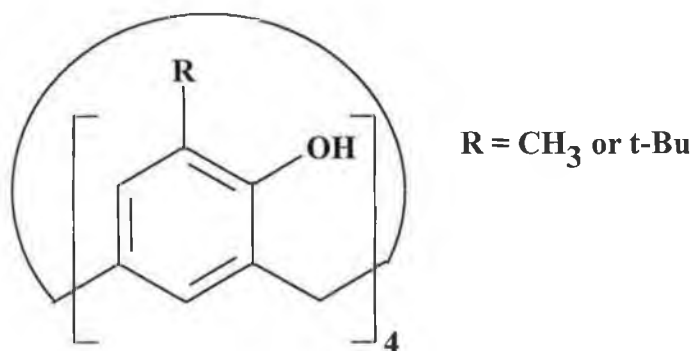
C 1-28

According to Böhmer,[23] the spectra of the calix[5]arenes and higher oligomers exhibit a singlet for the methylene protons when the solution temperature is sufficiently high (e.g., 50 °C). At lower temperatures (e.g., -40 °C) this singlet splits into a pair of doublets, suggesting that as with the calix[4]arenes, interconversion between the different conformers ceases to take place as the temperature decreases. In the case of the calix[6]arenes and calix[7]arenes, three and seven pairs of doublets are observed, respectively, indicating disordered conformations.[30] Remarkably, the temperature dependence of the NMR spectrum of the calix[8]arene, **C 1-16,** in CDCl$_3$ corresponds very closely to that of the calix[4]arene, **C 1-1**. The greater flexibility that would be expected of the larger calixarene is noticeable in a solvent such as deuterated pyridine which breaks down the intramolecular hydrogen bonds in the calix[8]arene; here, a singlet is observed for the methylene protons down to -53 °C and -93 °C in a mixture of deuterated pyridine and CS$_2$.[26] Thus, in the presence of hydrogen bonding solvents, **C 1-16** is conformationally mobile. A necessary corollary to this postulate is that the methylene carbons are equivalent at temperatures above the coalescence point, i.e.,
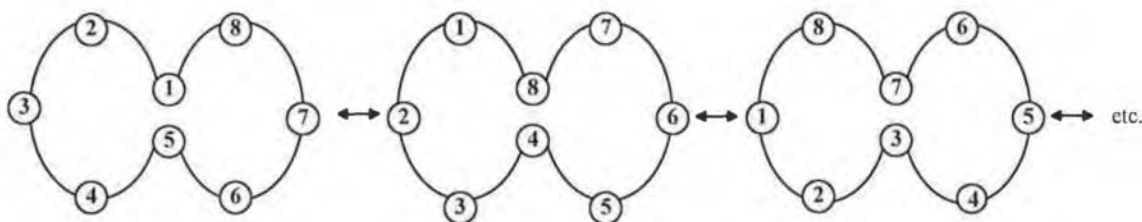
Otherwise, several CH$_2$ peaks would be expected to be observed at these temperatures.

13

As was found with calix[4]arenes, the effect of the interplay between intramolecular hydrogen bond attractions and the steric hindrances are also observed with calix[6]arenes. For example, the ^{1}H NMR spectra of **C 1-13**, **C 1-25** and **C 1-26** showed that these compounds were found to be conformationally mobile at ambient temperatures in CDCl$_3$ solutions.[31] In contrast, the ^{1}H NMR spectrum of **C 1-27** shows doublets for the bridging CH$_2$ protons at temperatures up to ca. 100 °C, at which point they start to broaden.[31] Such evidence is consistent with a fixed cone conformation at room temperature, i.e., the steric hindrance of the *p*-cyano group in **C 1-27** prevents conformer interconversion at room temperature. Down to -60 °C, the ^{1}H NMR spectrum of **C 1-29** shows a pair of doublets and singlet that is characteristic of the 1,2,3-alternate conformation. By 100 °C, the methylene pattern has changed to three broad singlets, possibly the result of partial inversion involving the ArOMe moieties swinging through the annulus.[31]
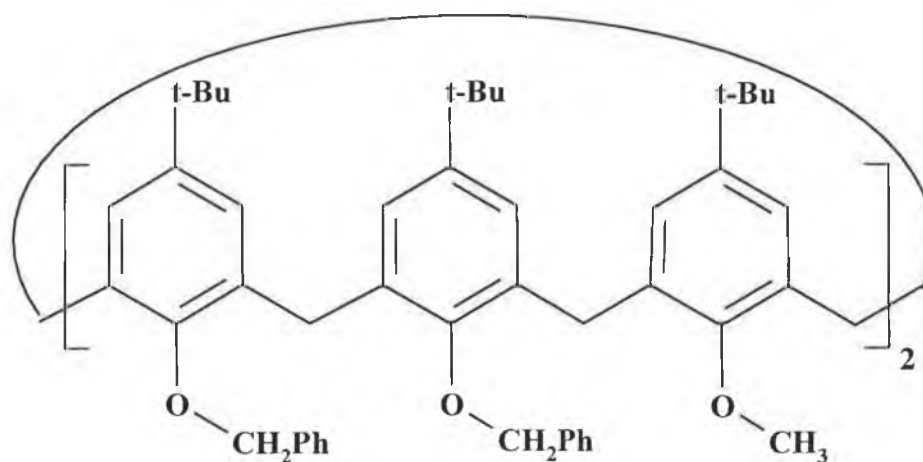
C 1-29

A very interesting paper is that by Inokuchi and Shinkai,[32] who report that mass spectrometric measurements has provided conclusive evidence that the calix[8]arene, **C 1-16**, aggregates to form dimers and trimers in solution, presumably through the partial cleavage of some of the *intramolecular* hydrogen bonds and the formation of *intermolecular* hydrogen bonds. Evidence of dimer formation was observed for the calix[5]arene, **C 1-11**, the calix[6]arene, **C 1-13**, and the calix[7]arene, **C 1-15**, evidence of formation of the dimers only was obtained. No such evidence was

14

obtained in the case of the calix[4]arene, **C 1-1**. However, evidence of dimer formation was obtained in the case of the calix[4]arene, **C 1-30**. A possible explanation for this is that, the stability conferred upon the monomer of **C 1-1** by intramolecular hydrogen bonding between the four hydroxyl groups is so great that there is no incentive to form aggregates but that the monomer of **C 1-30** does not have this great stability.
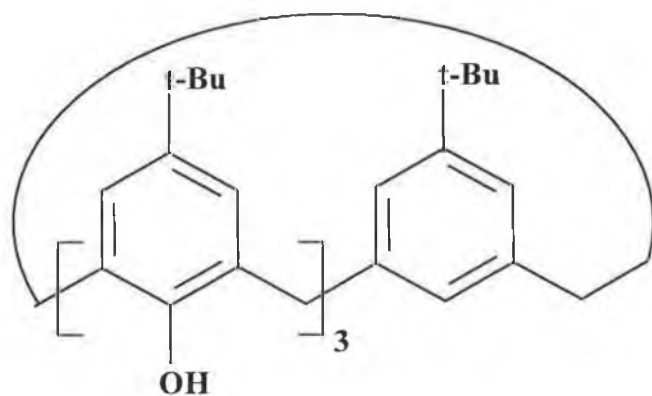
C 1-30

1.3. Calixarenes as Host Molecules

The ability of calixarenes to complex with metal ions has been studied[25,33] and the following conclusions have been reached:

- Esters and ketones complex Group 1 cations in preference to Group 2 cations.[33a]

- Selectivity depends on ring size and in the case of the calix[4]arenes, on conformation also. For example, tetraester calix[4]arenes in the cone conformation are selective for Na^+, while the other conformers favour K^+.[34] The 1,3-alternate conformer of **C 1-31** is more selective for Cs^+ and exhibits a lower limit of detection, than any of the other possible conformers.[35]

- Pentaesters in a cone-like conformation complex have a preference for the larger cations without making any particular distinction between K^+, Rb^+, and Cs^+.[33c]

- Hexaesters prefer Cs^+, while octaesters exhibit no complexing ability of note.[36]

- Tertiary amides bind Group 1 cations with much greater strength than esters.[43]

15

- Calixarenes with mixed functionalities are another method for tailoring the complexing abilities of the ionophores.[36,37]

- Calixarenes with 'soft' donor atoms have been used to complex transition metal complexes. For example, **C 1-32** has been used to complex Pt^{2+}.[38] Pb^{2+} [39] and Ag^{+} has been bound with **C 1-33**.[40] **C 1-34** and **C 1-35** have been found to be effective extractants for Au^{3+}.[41]

C 1-31

C 1-32

16
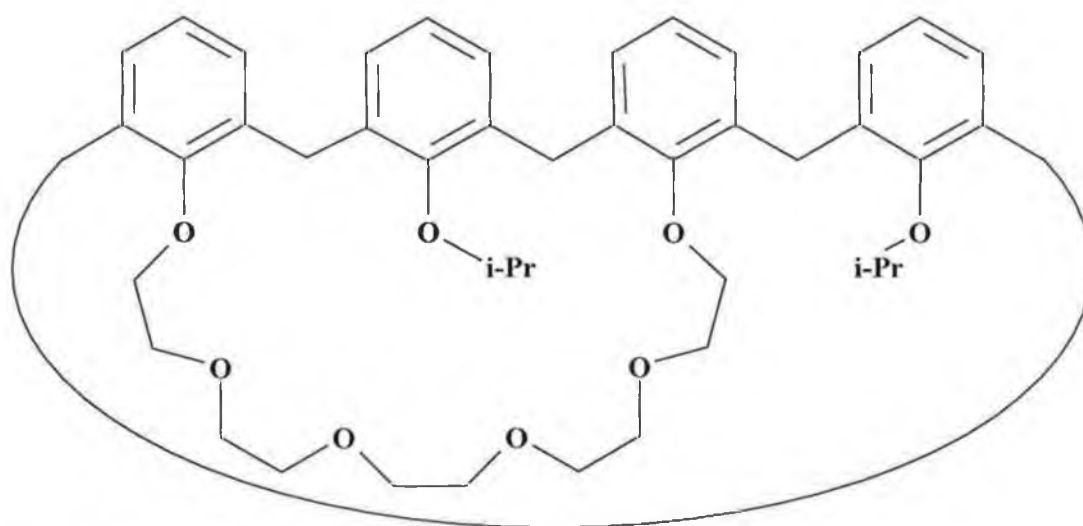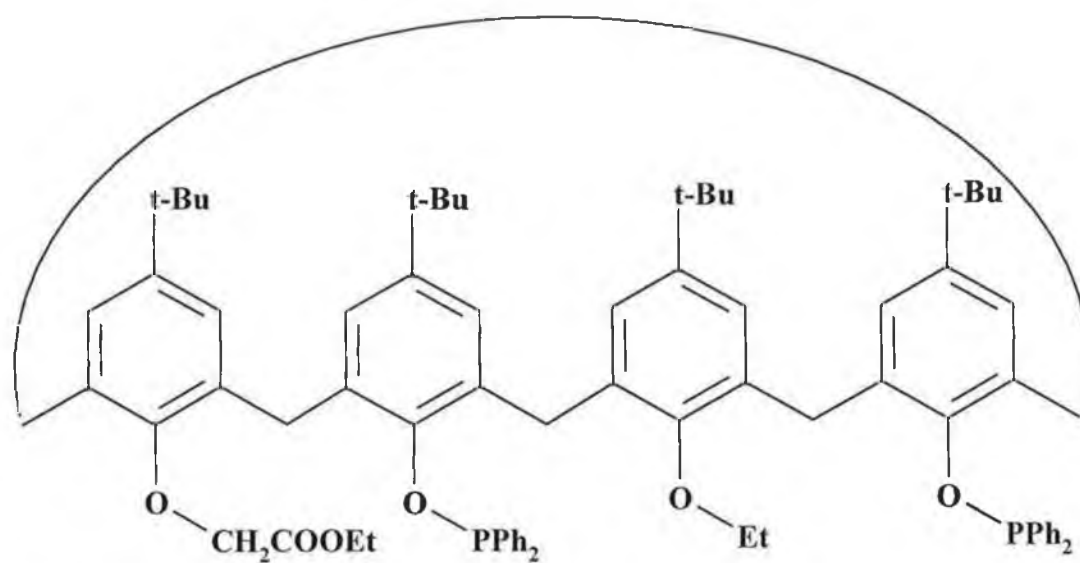
1.3.1.   ***Structure of Cation Complexes***

Calix[4]arenes such as **C 1-20**, **C 1-36**, **C 1-37** and **C 1-38** form 1:1 complexes with cations with fourfold symmetry. Conclusive evidence for the 1:1 stoichiometry of such complexes was obtained from a ^{1}H NMR titration of **C 1-20**, where the addition of NaSCN to a solution of the calixarene in $CDCl_3$ caused changes in the spectrum of **C 1-20** (as described below for the complex formed between **C 1-37** and Na^+) but that no further changes were observed when the salt/ligand ratio was increased beyond 1.[25]

It has been reported that the report that X-ray structure of the K^+ complex of **C 1-38** shows the complex has a fourfold symmetry.[42,43] Molecular modelling, albeit of the Na^+ complex of **C 1-36**, confirms this. For example, both pairs of aryl rings on opposite sides of the macrocycle are inclined at virtually equal angles (46.72° for rings **A** and **C** and 46.75° for rings **B** and **D**). See Figure 1-1.

As stated in Section 1.2.2, the uncomplexed form of ligands such as **C 1-20** and **C 1-36** have a structure in which the pairs of aryl rings on opposite sides of the macrocycle are inclined at very different angles. The carbonyl groups also point outwards. Upon complexation with a Group 1 cation, the carbonyl groups rotate inwards and the ligand structure takes on C_{4v} symmetry.[23] This increase in symmetry has been shown to occur in solution by ^{1}H NMR spectroscopy.[25] For example, *one* peak was observed the for the *t*-butyl protons in the ^{1}H NMR spectrum of the Na^+ complexes formed with **C 1-48**[44] and **C 1-49**,[45] (compared to *two* peaks in the free form of these ligands), indicating that upon complexation, the *t*-butyl groups and therefore, the aryl rings on opposite sides of the macrocycle become equivalent. See Footnote [a].

---

[a] The free calixarene ligands usually exhibit *one* peak for the *t*-butyl protons because of the C_{2v} to C_{2v} interconversion discussed previously.
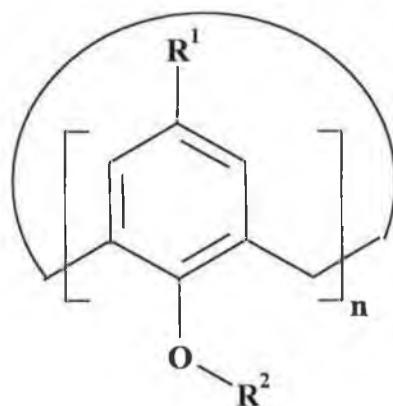
	n	R^1	R^2
C 1-33	4	t-Bu	$CH_2C(S)N(C_2H_5)_2$
C 1-34	4	t-Bu	$(CH_2)_2C(S)N(CH_3)_2$
C 1-35	4	t-Bu	$(CH_2)_2SH$
C 1-36	4	t-Bu	$CH_2CO_2CH_3$
C 1-37	4	t-Bu	$CH_2CO_2CH_2CH_3$
C 1-38	4	t-Bu	$CH_2C(O)N(CH_3)_2$
C 1-39	4	H	$CH_2CH_2CH_3$
C 1-40	4	t-Bu	$CH_2CO_2(CH_2)_2OCH_3$
C 1-41	6	t-Bu	CH_2CO_2Et
C 1-42	6	H	CH_2CO_2Et
C 1-43	4	t-Bu	$CH_2CO_2(CH_2)_2SCH_3$
C 1-44	4	t-Bu	$CH_2CO_2(CH_2)_2$—N (azepanone ring with =O)
C 1-45	6	H	$CH_2CO_2C_{10}H_{21}$
C 1-46	6	t-Bu	H
C 1-47	4	t-Bu	$CH_2C(S)N(CH_3)_2$

18
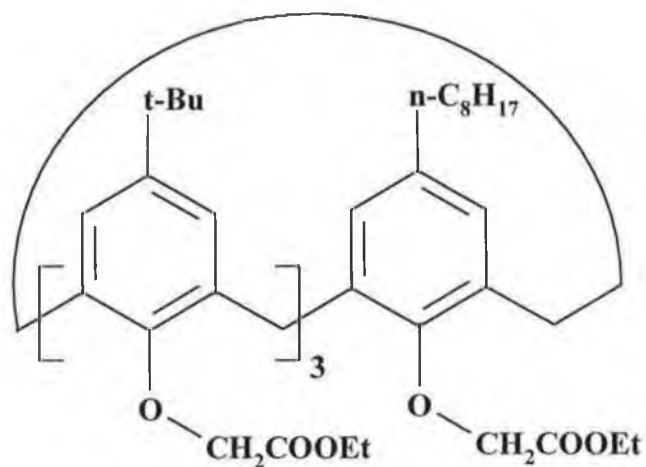
C 1-48
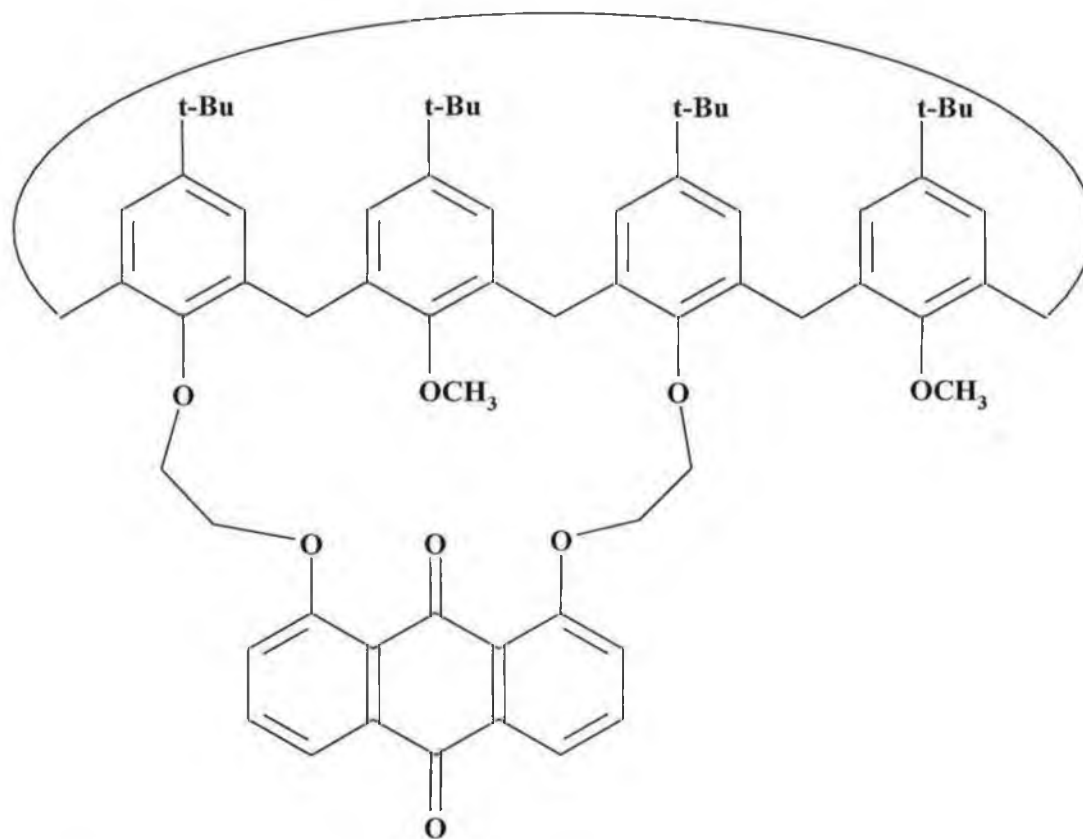
C 1-49

The resonance of the methylene protons of both the bridging groups and in the pendant groups of calixarenes such as **C 1-20**, **C 1-36**, **C 1-37** and **C 1-38** change upon complexation. Furthermore, these changes occur for a greater number of

complexes than the changes in the number of the peaks due to the *t*-butyl groups. These change are listed in Table 1-1 for the complexation of **C 1-37** with Na^+.[46] Most of the resonances are shifted to a lower magnetic field and this is due to the electron-withdrawing effect of the Na^+ ion and the resultant deshielding of the protons.   Two more important differences between the spectra of the free and complexed forms of the ligand are:

(i) the methylene protons of the OCH_2CO moieties (the *c* protons) are shifted upfield by 0.21 ppm upon complexation

(ii) the equatorial protons, H_{eq}, (the *e* protons) are shifted upfield by 0.54 ppm. while the axial protons, H_{ax}, (the *f* protons) are shifted downfield by 0.28 ppm

The occurrence of change (i) can be accounted for by assuming that the pendant groups adopt a *trans* conformation upon complexation as this conformation is found in the solid state for the K^+ complex of **C 1-38** and the molecular model of Na^+ complex of **C 1-37**, as described above.   This conformational change causes the protons in the OCH_2CO moieties to move out of the polar cavity and closer to the aryl rings of the macrocycle. The π electron clouds shield them from the magnetic field of the spectrometer to a greater extent than in the case of the free ligand causing the frequency of their resonance to be shifted upfield.

That the ligand geometry in such complexes has a C_{4v} symmetry upon complexation is also suggested by change (ii). On the basis of the discussion in Section 1.2.1 of the assignments made in relation to the ^{1}H NMR spectrum of the free form of **C 1-20**, it can be said that the spectrum of the free ligand of **C 1-37** consists of a doublet at 3.14 ppm due to the H_{eq} protons and that the H_{ax} protons give rise to the other doublet at 4.94 ppm. This is because of the proximity of the H_{ax} protons to the phenoxy oxygen atoms and the deshielding effect of these oxygen atoms.[24,25] Molecular models (not shown) indicate upon complexation, that both the H_{ax} and H_{eq} protons are closer (by ca. 0.1 Å) to these oxygen atoms. While this would explain the upfield shift of 0.28 ppm experienced by H_{eq} protons, it would not explain the 0.54 ppm downfield shift of the H_{ax} protons. However, molecular models of the **C 1-36**:Na^+ complex show that the axial protons are closer to the aryl rings in the macrocycle than in the free ligand. Thus, in the complex, the shielding effect of these aryl rings on the H_{ax} protons must

be a greater influence on the resonance frequency of these protons than in the free ligand. Therefore, changes (i) and (ii) are evidence that in solution, the aryl rings become more, but not necessarily completely equivalent.

It is important to note that molecular dynamics simulations of calixarene:metal complexes in solution have indicated that the conformation shown in Figure 1-1 is in equilibrium with other conformations where the carbonyl groups are not twisted inwards to the same extent.[47] Therefore, while the evidence available for the geometry of the ligand in such complexes when in solution is not as conclusive as X-ray structural analysis, the fact that such changes in the ^{1}H NMR spectra are observed to a lesser extent with the calix[6]arene and calix[8]arene analogues of **C 1-37** and not at all with its acyclic analogues, upon addition of Na$^+$,[46] is a very strong indication of the level of preorganization of **C 1-37**.

Table 1-1. ^{1}H NMR Chemical Shifts, σ, of C 1-37 and its Na$^+$ Complex.[46]

Proton	σ (C 1-37) / ppm	σ (C 1-37:Na$^+$) / ppm	
a	1.26	1.36	
b	4.17	4.36	
c	4.78	4.57	
d	1.09	1.16	
eq	3.14	3.42	
ax	4.94	4.40	
f	6.81	7.23	
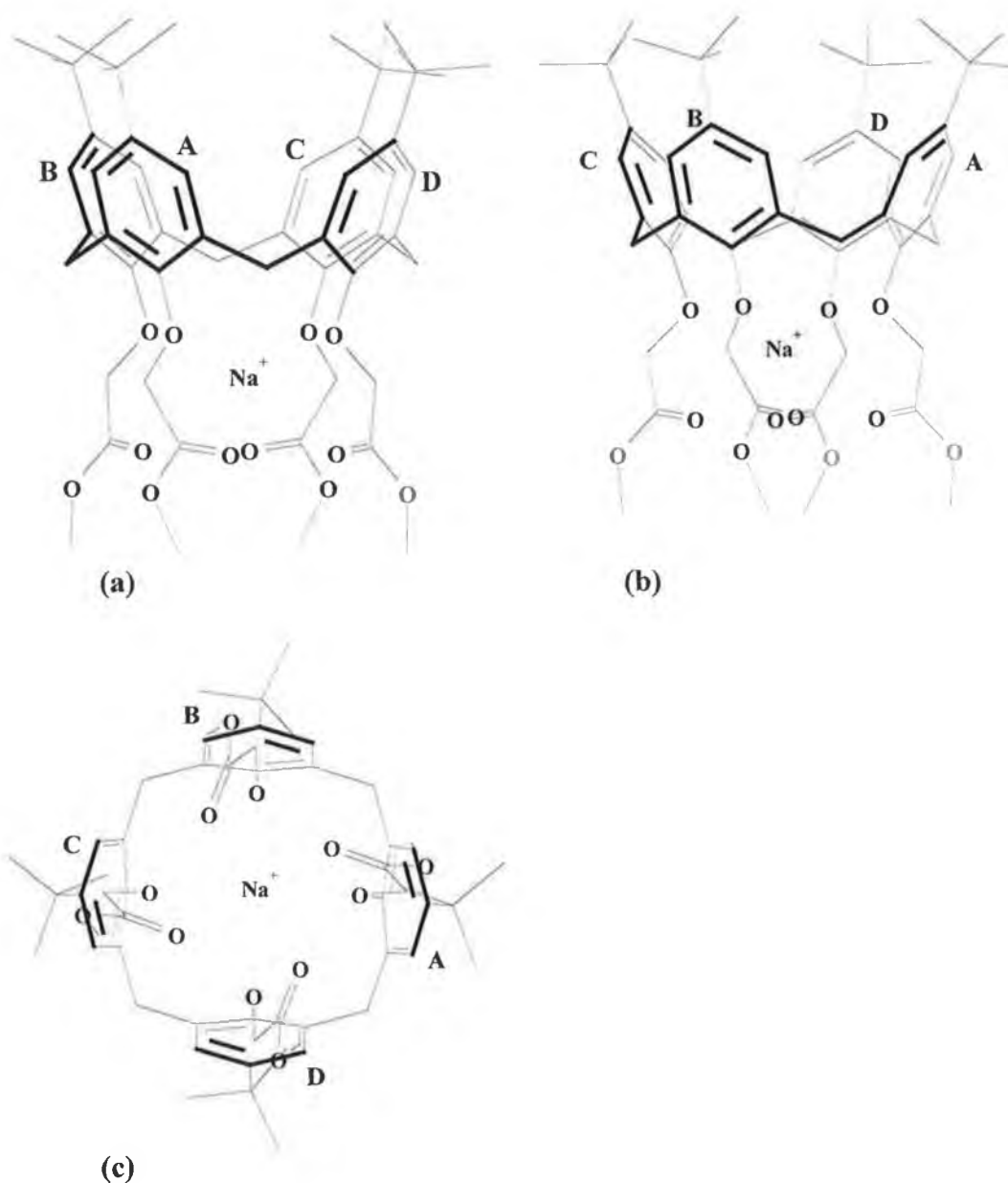
Figure 1-1. *Molecular models of the Na$^+$ complex of C 1-36. Side on views, (a) and (b) and view through cavity, (c). Details of the molecular modelling are given in Chapter Two.*

The ligand in such complexes exhibit different geometries. For example, the X-ray structure of the Na$^+$ complex of **C 1-37** in its 1,3-alternate form, show that the carbonyl groups point *directly* at the ion.[48] In contrast, molecular models of the *cone* **C 1-37**:Na$^+$ complex (not shown, but the ligand geometry and the ion position in the models are virtually identical to that of the Na$^+$ complex of *cone* **C 1-36**, given in

22

Figure 1-1) show that the pendant groups on opposite sides of the macrocycle adopt a *trans* conformation and the carbonyl groups do *not* point *directly* at the ion. The difference in ligand geometry is reflected in the fact that the 1,3-alternate complex has a higher formation constant than that of the cone complex (the log values are 4.10 and 3.95 respectively).[34] That the four-fold interaction of the 1,3-alternate complex results in a higher formation constant than that for the cone complex where the interaction is eight-fold, must be due to the fact that ion-dipole interactions are most effective when they are directional. This property is explained in Figure 1-2. As the angle ϕ becomes closer to 180° the interaction between the cation and atom with a slight negative charge becomes stronger, the ion is drawn closer to this negatively charged atom and therefore (from Coulomb's Law), the resultant force of attraction increases..
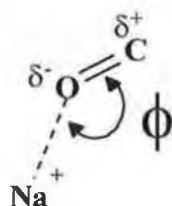
Figure 1-2. *Explanation of the directional nature of cation-dipole bonds. The interaction between the Na^+ ion and a carbonyl group is used as an example.*

A factor which inhibits the formation of these complexes is the reduction in entropy as a result of the symmetrical arrangement of the ligand in the complex. However, this would not appear to be a controlling factor as the thermodynamics of formation of complexes between **C 1-36** and Group 1 cations (in benzonitrile at least) as studied by Danil de Namor and co-workers,[49] suggest that the complexation is enthalpically controlled. For further details, see Ref. 49.

Complexation can occur in different regions of calixarenes. For example, in the Ag^+ complex formed by **C 1-39**, the ion is complexed in the macrocyclic ring cavity in both the solid state and also in solution, because of cation-π interactions.[40] Evidence for the solution conformation is the fact the *m-* and *p-* hydrogen atoms of the aryl rings experience large downfield shifts upon complexation with the Ag^+ ion. In

23

contrast, the shifts experienced by the protons in the pendant groups are relatively small, indicating that complexation does not occur in this latter region. Yet another mode of complexation has been observed in the case of the Pt^{2+} complex formed with **C 1-32**.[39] In this complex the ions are 'sandwiched' between two calixarene molecules, in a square planar, *trans*, geometry with a phosphorous atom on each calixarene and two chlorine atoms occupying the co-ordination sites. That the complex consists of two calixarene molecules was inferred from the results of molecular weight determination by vapour-phase osmometry and IR spectroscopy. The IR absorption at 346 cm^{-1} [ν (Pt-Cl)] and P-Pt coupling constant of 3026 Hz was the evidence to support the *trans* nature of the geometry of the complex about the Pt^{2+} ion.

Redox-active calixarenes are interesting from two points of view. Firstly, they allow one to study electron transfer in systems (such as proteins) where the geometry is constrained and/or which contain multiple redox active sites. Secondly, their use as electrochemical sensors is discussed in Section 1.4.2. **C 1-49** is interesting in that upon one-electron electrochemical reduction in the presence of K^+, Bethell *et. al.* found that evidence (from cyclic voltammetry) was obtained that the binding process is enhanced.[45] ^{1}H NMR spectra indicated that the conformation of the ligand in the complex changed from cone to partial cone when reduction took place, emphasising the importance of ligand conformation in designing redox-active ionophores.

However, it must be pointed out that Bethell *et. al.* found (with *two* different software packages) that the molecular model of the cone **C 1-49**:K^+ complex was lower in energy than that of the partial cone **C 1-49**:K^+ complex by ca. 1 kcal mol^{-1}. The authors do not state that this is in contradiction with the ^{1}H NMR spectral evidence which indicates that **C 1-49** is present mainly as the partial cone conformer when complexed with potassium. The molecular model of the sodium complex of **C 1-49** in its cone form was also found to be lower in energy than that of partial cone sodium complex by more than 3 kcal mol^{-1} and this *is* in agreement with the evidence from ^{1}H NMR spectra.

Another way in which the ligand conformation can change is exhibited by **C 1-50** whose conformation is reported as changing from 'open' to 'closed' forms upon

24

complexation with Na$^+$.[50] The IR spectrum of **C 1-50** gave two N-H bands at 3275 and 3310 cm^{-1} and these bands were hardly affected by a 2 to 5 mmol dm^{-3} change in concentration. In contrast, the fact that IR spectrum of the reference compound, **C 1-51**, shows two N-H bands at higher frequency (3400 and 3420 cm^{-1}) which were also concentration independent. This evidence indicates that intramolecular bonds are present in the uncomplexed form of **C 1-50**. Further support for this conclusion was obtained from ^{1}H NMR spectra: two singlet resonances were observed for **C 1-50** at σ 9.22 and 10.24 ppm, and at σ 8.05 and 8.79 ppm for **C 1-51**.

Upon addition of NaClO$_4$, the ^{1}H NMR spectrum of **C 1-50** gave new N-H signals in comparison to the ^{1}H NMR spectrum of the uncomplexed form of **C 1-50**. Significantly, these signals are *upfield* by 0.57-0.80 ppm from that of the uncomplexed form, indicating that some factor is affecting the chemical shifts of these protons other than the electron withdrawing effect of the Na$^+$ ion as complexation with a cation normally results in *downfield* shifts of the proton signals in such complexes. Murakami and Shinkai,[50] propose that the additional factor is the destruction of the intramolecular hydrogen bonds in **C 1-50** as a result of the addition of Na$^+$ since for **C 1-50** to bind with Na$^+$, the two pendant groups containing the carbonyl groups must rotate inwards and this forces the diamidopyridine groups apart. They support this claim by showing that when **C 1-52** (which has a pteridine moiety complementary to the diaminopyridine groups in the calixarene) was added to the **C 1-50**:Na$^+$ complex, the N-H signals are upfileld by 0.33-0.49 ppm from that of the uncomplexed form. The deshielding of the N-H protons is presumably due to the formation of hydrogen bonds between **C 1-50** and **C 1-52**. In contrast, the chemical shifts of the N-H protons of the free form of **C 1-50** were scarcely affected by the addition of **C 1-52**.   These facts indicate that the conformation of the diaminopyridine groups in the free form of **C 1-50** is significantly different to that in the **C 1-50**:Na$^+$ complex.   These proposed conformational changes are given in Figure 1-3. One would have expected that the IR spectra of the **C 1-50**:Na$^+$ complex and the **C 1-50**:Na$^+$:**C 1-52** aggregate would have confirmed the destruction of the intramolecular hydrogen bonds as a result of Na$^+$ addition, but unfortunately, such IR spectra were not reported.

25

C 1-50

C 1-51

C 1-52

26
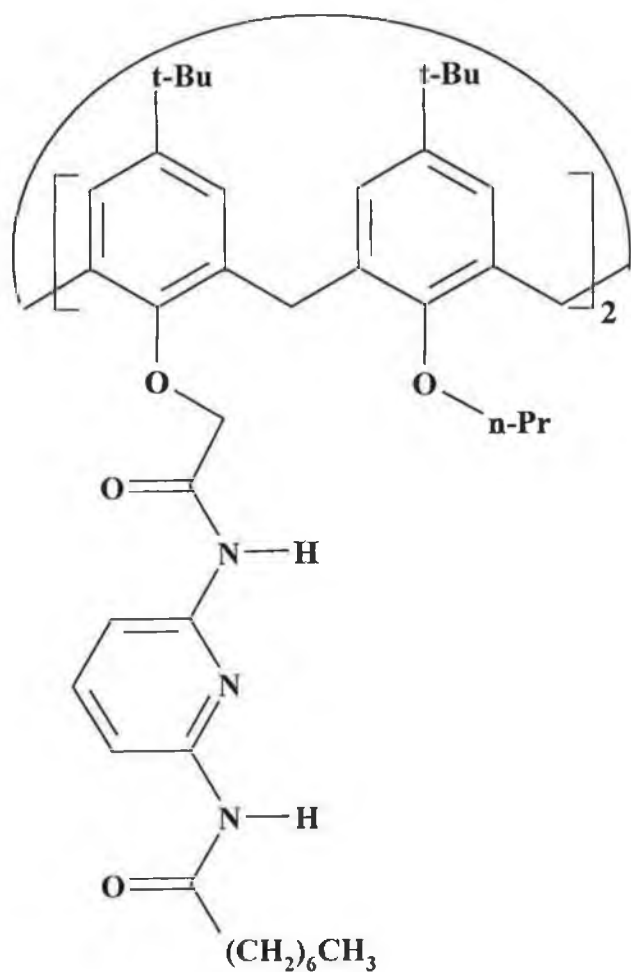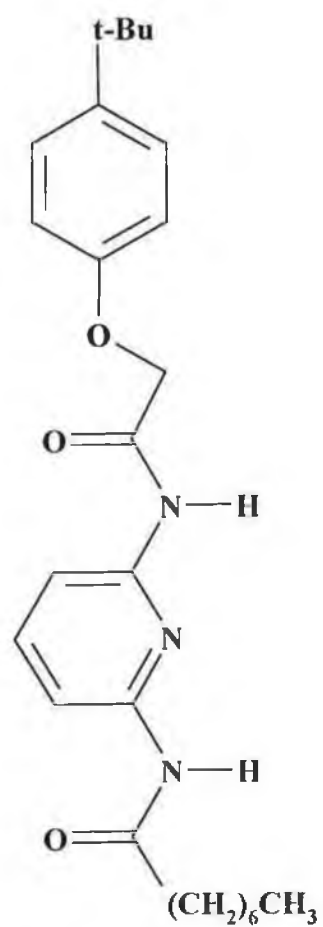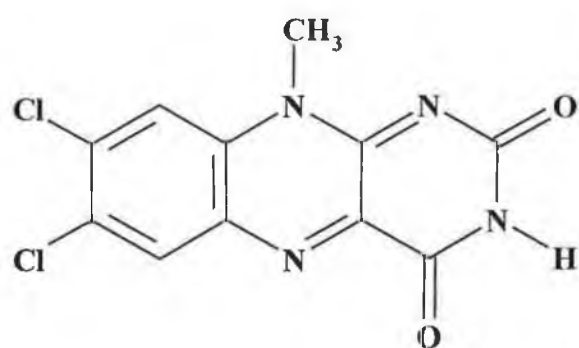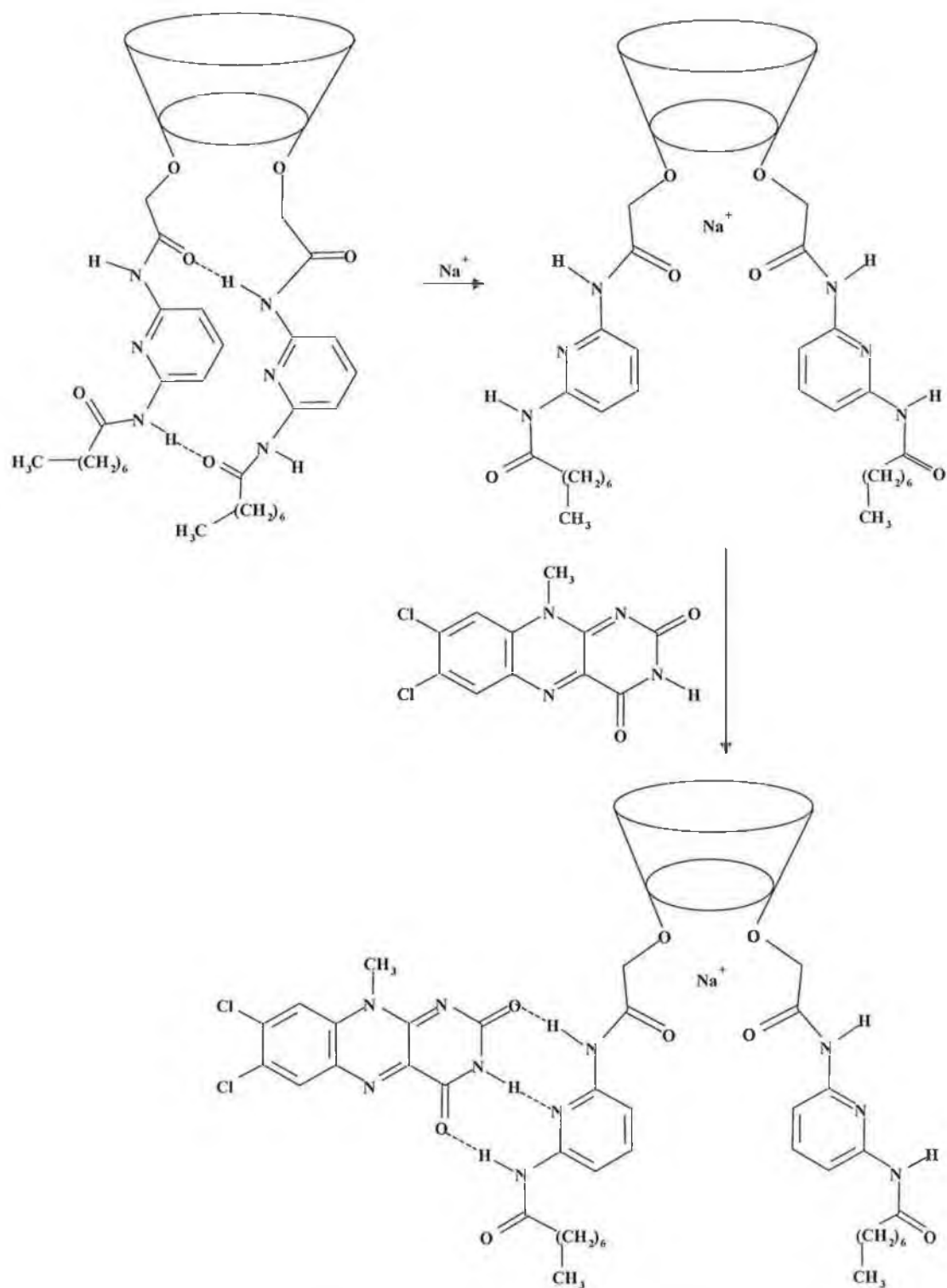
Figure 1-3. *Structures of C 1-50, C 1-50:Na⁺ and C 1-50:Na⁺:C 1-52, as proposed by Murakami and Shinkai.[50] The i-propoxy pendant groups of C 1-50 and the binding of C 1-50 with a second C 1-52 molecule have been omitted for the sake of clarity.*

27

Similarly, evidence from ^{1}H NMR spectra is provided that the Na^{+}-induced conformational changes in **C 1-53** cause its binding abilities to change.[51] It was propose that the binding of 1,3,5-trinitrobenzene by the pyrene groups of **C 1-53** is destroyed in an allosteric or 'tweezing' effect by the addition of the Na^{+} ion. It is disappointing that the conformational changes in **C 1-50** and **C 1-53** that are proposed as taking place upon complexation with Na^{+} were not confirmed by molecular modelling while the energies obtained from molecular modelling of the **C 1-49**:K^{+} complex contradicts the evidence obtained from ^{1}H NMR spectra. The X-ray structures of these compounds and their metal complexes, which would have confirmed or denied that the aforementioned conformational changes take place, have not been reported Nonetheless, these three compounds (**C 1-49**, **C 1-50** and **C 1-53**) have potential for application in sensors as it may be possible to control the complexation process externally.
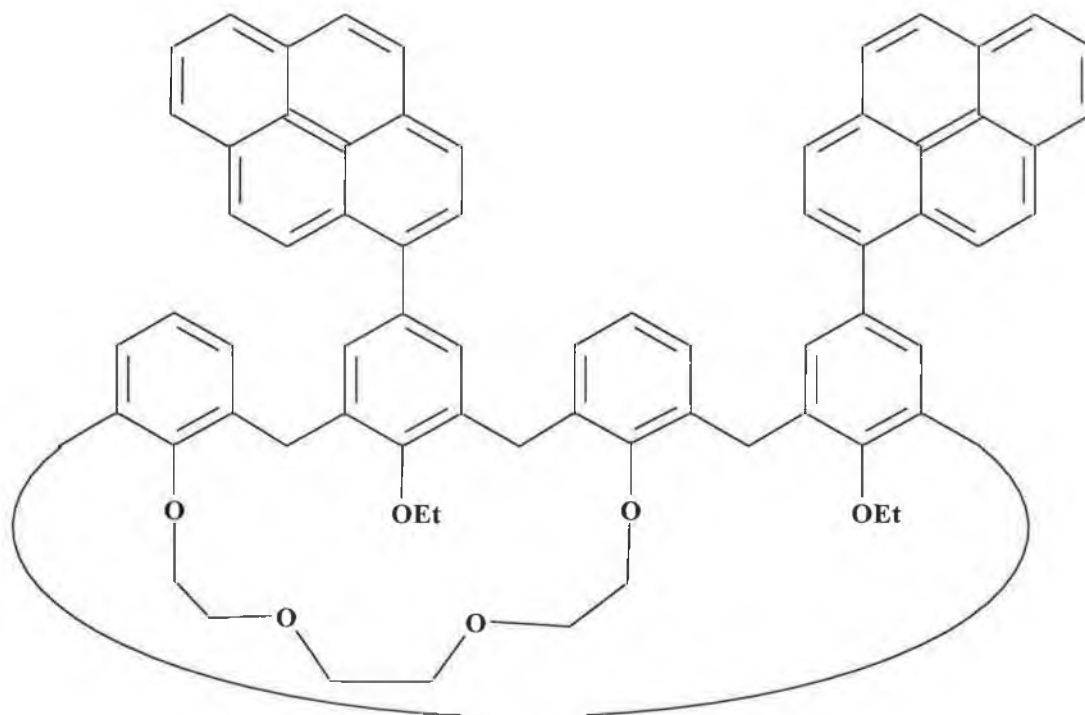
C 1-53

1.4. Sensor Applications of Calixarenes

1.4.1. Ion-Selective Electrodes

Probably the most common analytical application of calixarenes is their use as ionophores in ion-selective electrodes (ISE's). This steady-state method involves measuring the potential between the ISE and a reference electrode (whose potential is effectively constant over a wide range of conditions) when both electrodes are in contact with an electrolyte. Such measurements are made over a wide range in concentration for electrolytes containing the ion of interest (the primary ion) and/or several interfering ions. The use of a calixarene in the construction of an ISE was first reported in 1986[52] and numerous papers have been published since in this area. **C 1-36,**[53,54] **C 1-37**[55,56] and **C 1-38**[57] have been used to produce the best Na^+-selective electrodes, even in comparison to commercially available Na^+ ISE's or the ETH neutral carrier based electrodes.[58] **C 1-36** has been found to be particularly useful for the analysis of Na^+ in blood.[59] .

Diamond and McKervey[60] report that drift in the readings during the calibration and sample measurements is a problem, especially in the case of the determination of sodium in blood because the concentration range of sodium in blood is very small (typically 0.12-0.15 mol dm^{-3}). Flow-injection analysis (FIA) has been found to be an effective method of reducing drift. **C 1-36** was found to be a very useful ionophores in an FIA system for blood sodium analysis.[61,62]. More recently, Na^+-selective electrodes have been assessed using batch injection analysis (BIA),[63] which offers similar advantages to FIA but without the problems associated with valves, tubing, detector flow cells and pumps encountered in FIA.[64]

The calix[4]arene, **C 1-54**, has been found to show selectivity for K^+.[65] This can be understood by considering the size of the cavity. Most of the known calix[4]arenes have a cavity suitable for complexation with Na^+. Complexation with K^+ requires a larger cavity and in **C 1-54**, this is achieved by the increasing the size of the bridge between the aromatic rings. The ISE with **C 1-54** has good sensitivity but has a narrow working range and its selectivity is limited, especially in comparison to valinomycin for example, which is well established as a ionophore for K^+.[66]
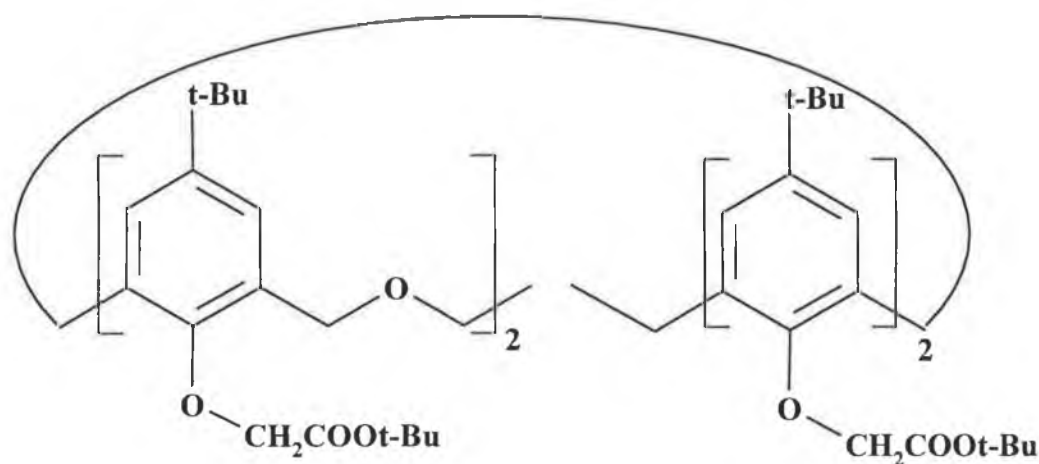
C 1-54

As might be expected, calixarenes with larger cavities are selective for large cations. For example, the calix[6]arenes, **C 1-41** and **C 1-42**,[67] and the calix[4]arene, **C 1-31**, in its 1,3-alternate form, have been found to be selective for Cs^+.[35]

C 1-33, **C 1-43**, **C 1-44** and **C 1-55** have been used to construct Ag^+-selective ISE's.[68] The order of degree of linearity in the response was found to be **C 1-43** > **C 1-55** > **C 1-33** > **C 1-44**, with **C 1-44** giving the lowest response of 38.26 mV decade^{-1} in the rather limited range of -3.8 to -1.8 log activity (Ag^+) units. This trend may be attributed to the number and type of 'soft' donor atoms in each ionophore. For example, **C 1-43** contains an S atom and no N atoms in each of the pendant groups whereas in **C 1-44**, the opposite is true. The potentiometric selectivity coefficients obtained show that the greatest interference is caused by Na^+ and Hg^{2+} ions. That **C 1-55** should show the greatest Na^+ interference is not surprising considering the presence of two ethyl ester pendant groups, since this group is known to be selective for Na^+, as discussed previously, while the Hg^{2+} interference can be attributed to the presence of the S atoms in the ionophores.
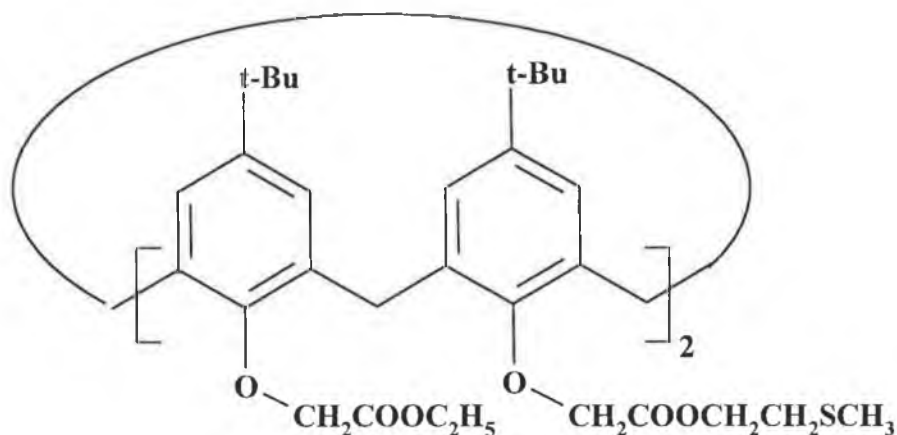
C 1-55

1.4.2.   *Calixarenes and Voltammetry*

In voltammetry, electrolysis takes place at a working electrode when a current is applied from an external source. Depending on the way in which the potential is changed (positively or negatively), reduction or oxidation respectively takes place. This reaction produces a current which is proportional to the concentration of electroactive species if it is due to diffusion only (electric migration is prevented by using an excess of inert background electrolyte, while convection is prevented by ensuring that the solution is free of stirring or any other mechanical vibration).

During the past twenty years much effort has gone into the examination of the effect of immobilisation of reagents at electrodes to produce chemically modified electrodes (CME's). The advantages of CME's include the ability to accumulate trace analyte from the solution, resulting in an increased concentration of analyte at the electrode surface, as happens in anodic and cathodic stripping voltammetry, except that the CME accumulation is governed by selectivity for the target analyte on the part of the immobilised receptor.

The polymeric calixarene, **C 1-56**, has been used for the voltammetric analysis of Pb^{2+}, Cu^{2+} and Hg^{2+} in dilute aqueous solution.[69] The method consisted of binding of the ions by the calixarene, electroreduction and anodic stripping measurement. Coating the electrode with a polymer has the advantage that accumulation of the ions at the electrode takes place easier than with a monolayer because of the greater thickness of the polymeric layer. However, the use of a tetraester calix[4]arene

31

meant that interference from Group I cations, notably Na$^+$, was a problem. This is attributed to the 'hard' nature of the oxygen donor atoms in the calixarene. This led to the use of **C 1-33** when using the same method for the analysis for Ag$^+$. This calixarene had already been used in potentiometric Ag$^+$ ISE's.[68] However, its incorporation into a CME inhibited rather than enhanced the uptake of Ag$^+$.[69b]
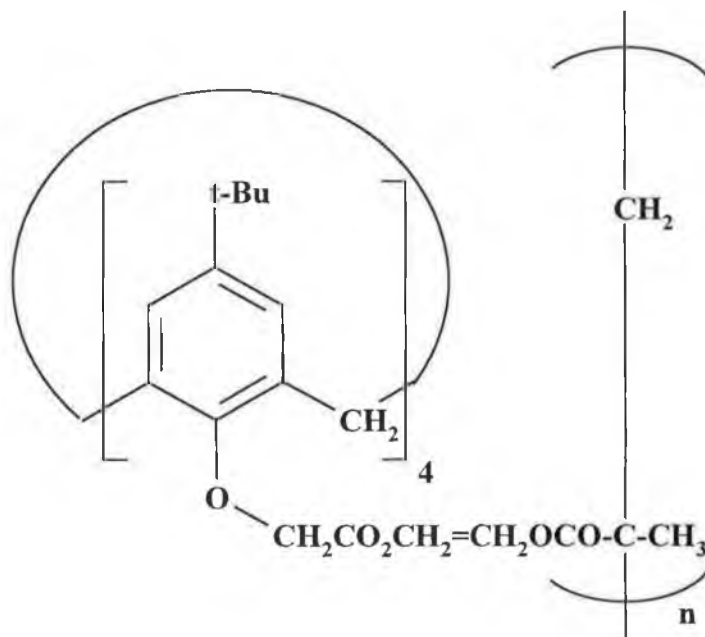
C 1-56

Cyclic voltammetry has also been used to investigate the electrochemical properties of the diquinones **C 1-57**, **C 1-58**, and **C 1-57** in various dichloromethane / acetonitrile mixtures.[70] It was found in general, that these species undergo three distinct electron transfer processes (two one-electron and a two-electron transfer) and that the potentials of these reductions in the presence of Group 1, Group 2, ammonium and alkylammonium cations are significantly anodically shifted to enable these compounds to act as cation sensing devices.

32
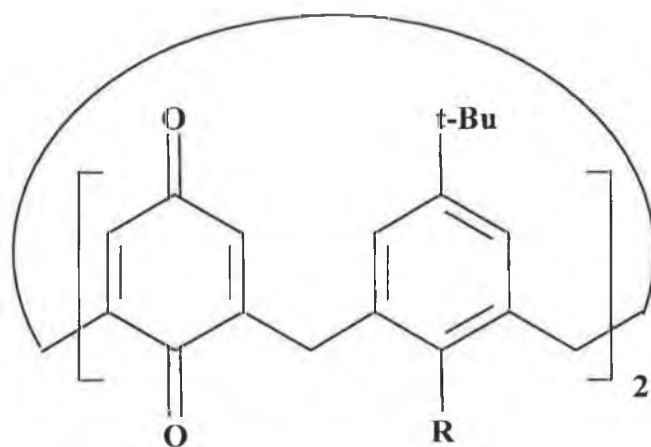
R

C 1-57 $CH_2(CO)OC_2H_5$

C 1-58 $CH_2(CO)N(C_2H_5)_2$

C 1-59 CH_3

1.4.3.   Calixarenes and Optical Methods of Detection

A trend in sensor research in recent years has been the development of chromophores and fluorophores which produce an optical response, for example, a colour change, in the presence of a cation. The advantages of this method include safety, less noise and no drift. Acidic chromophores, for example, azophenols and nitrophenols, are popular. In the presence of a suitable cation and a base (a base which, in the absence of a cation, is unable to deprotonate the chromophore and has no effect on the absorption spectrum of the chromophore), a complex is formed between the anion of the chromophore and the cation. The electron distribution in chromophore is delocalised more than that of the free ligand and the absorption maximum in the spectrum shifts to a longer wavelength. If the change in wavelength of maximum absorption is large enough, a colour change should also be observed. **C 1-60** in the presence of triethylamine, has been found to be Li^+-selective.[71] **C 1-62** and **C 1-61** have been found to show a 10-40-fold selectivity for Li^+ over Na^+ when the base morpholine is present.[72]

33
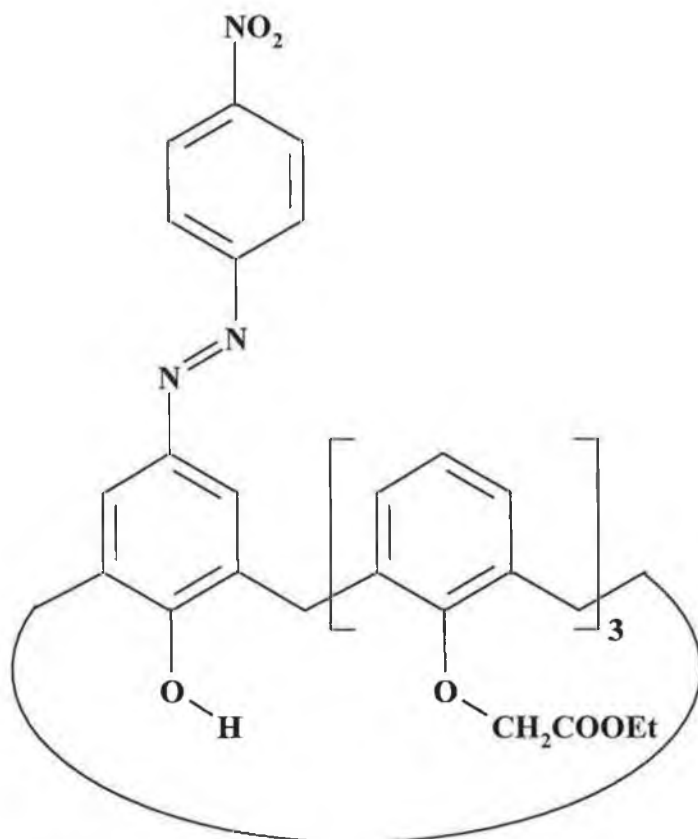
C 1-60
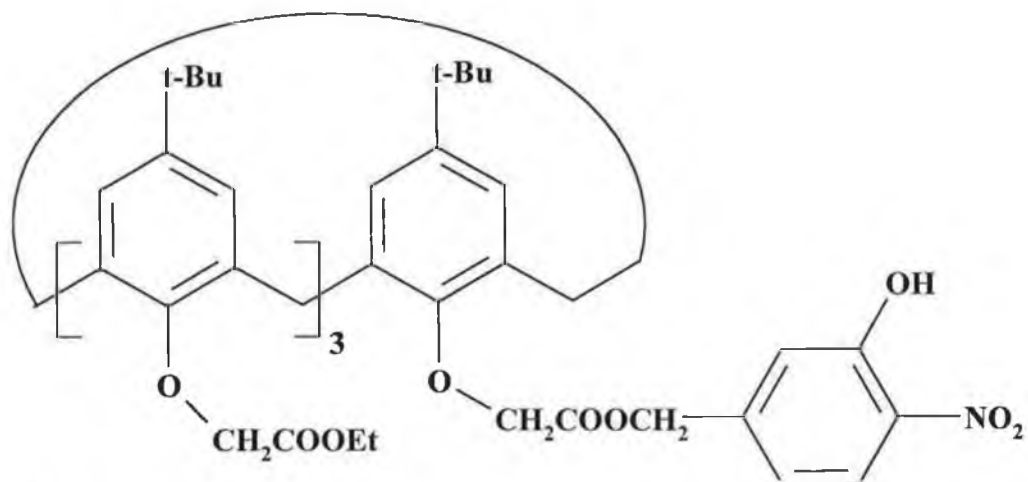
C 1-61
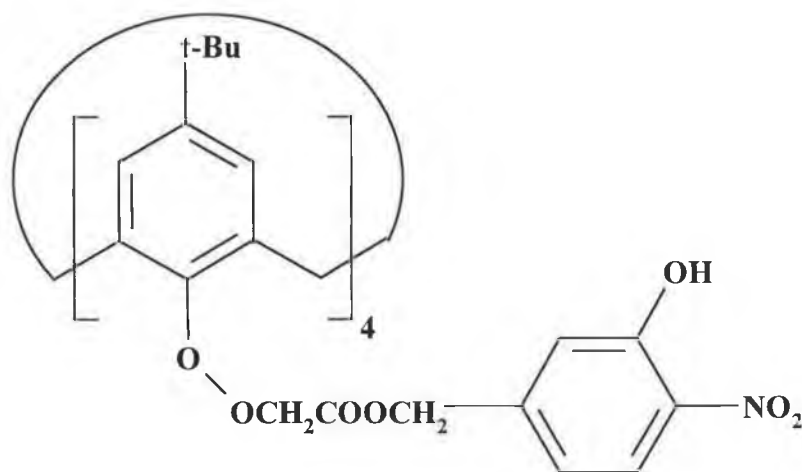
C 1-62

The wavelength of maximum absorption of **C 1-63** in 99 % ethanol increases by ca. 100 nm upon addition of Ca^{2+}.[73] The intensity at maximum absorption also increases. Addition of Na^+, K^+ or Mg^{2+} produces minor changes in the absorption spectrum. The selectivity of **C 1-63** for Ca^{2+} is confirmed by the fact the formation constant for the complex formed between it and Ca^{2+} is least ca. 250 times greater than those values obtained for other interfering ions. The H^+-selective chromophore, ETH 5294 (abbreviated as **CI**), has been used with **C 1-36** and **C 1-41**, to construct ion-selective optodes which are selective for Na^+ and K^+ respectively.[74] These devices work on the basis of a cation-exchange system as described in Scheme 1-1 for the equilibrium between the polymeric membrane (**p**) and aqueous phases. The formation of a complex between the calixarene (**C**) and the metal (**M**) complex induces changes in the absorbance due to the protonated and deprotonated forms of ETH 5294.

$$M^+_{(aq)} \ + \ CIH^+_{(p)} \ + \ C_{(p)} \qquad MC^+_{(p)} \ + \ CI_{(p)} + \ H^+_{(aq)}$$

Scheme 1-1

35
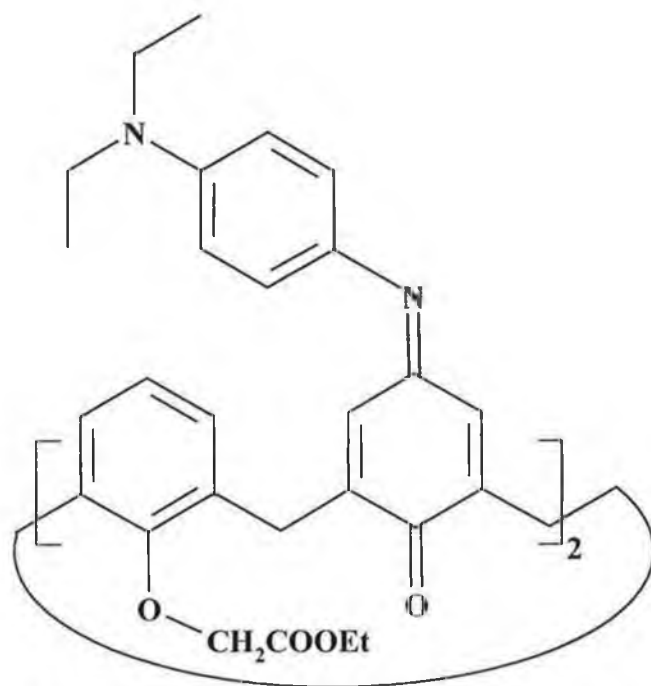
C 1-63

C **1-64** (chromogenically active due to the presence to the phenolic group in conjugation with the dinitrophenyl substituent) in chloroform extracts K^+ from aqueous solution, in preference to Na^+ in the pH range 7-9 (extraction coefficient is 1000) and no extraction of Mg^{2+} or Ca^{2+} was observed.[75] C **1-65**, has been used to complex UO_2^{2+} and the absorbance of the complex at 449 nm permitted analysis for UO_2^{2+} at the ppm level, even in the presence of interfering ions.[76]
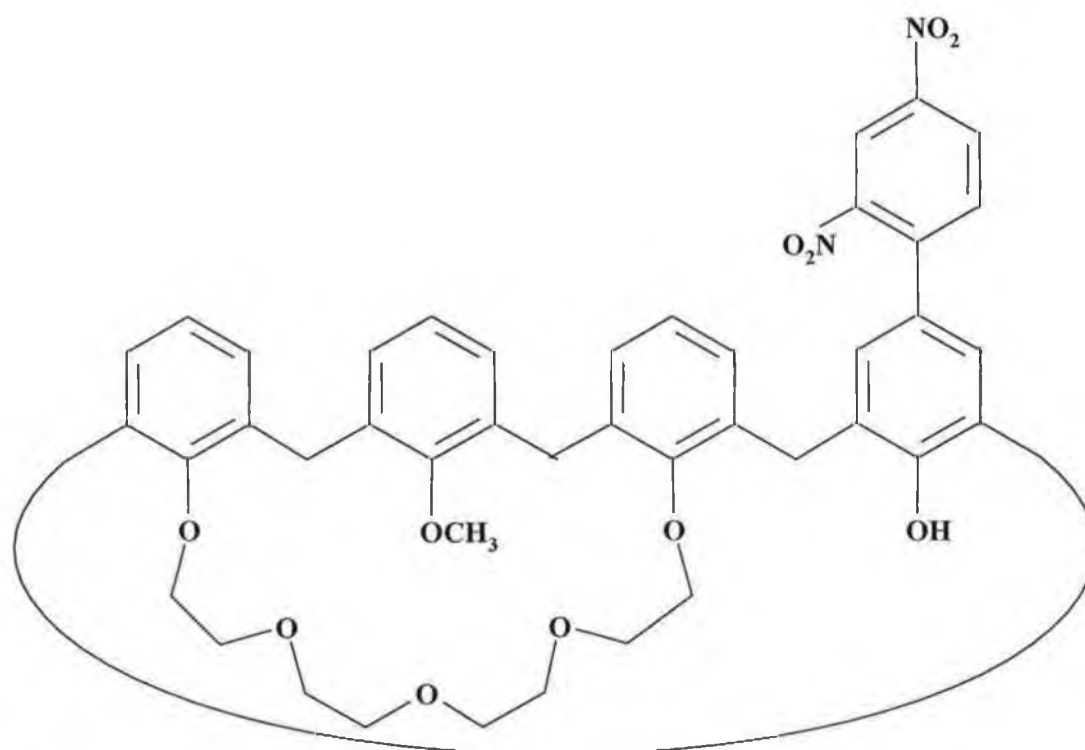
C 1-64
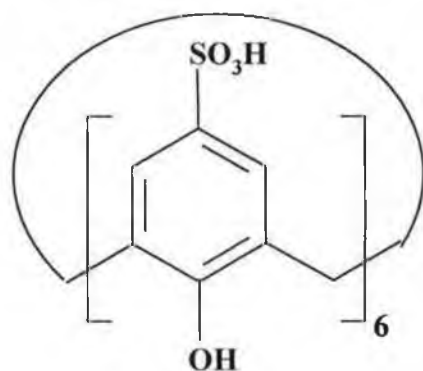
C 1-65

Optical transduction is also possible through the use of fluorescent calixarenes. Complexation between the calixarene and a cation invariably leads to conformational changes in the calixarene and this can effect the emission spectrum of the calixarene fluorophore. As with absorption spectra, the emission spectrum can be related to the cation concentration. **C 1-66** has been described as having 'perfect selectivity' for

Li$^+$.[77] Na$^+$ selectivity has been observed with calix[4]arene esters and amides with anthryl groups on the lower rim, for example, the fluorophore, **C 1-67**.[78]

C 1-66

C 1-67

Li$^+$.[77] Na$^+$ selectivity has been observed with calix[4]arene esters and amides with anthryl groups on the lower rim, for example, the fluorophore, **C 1-67**.[78]
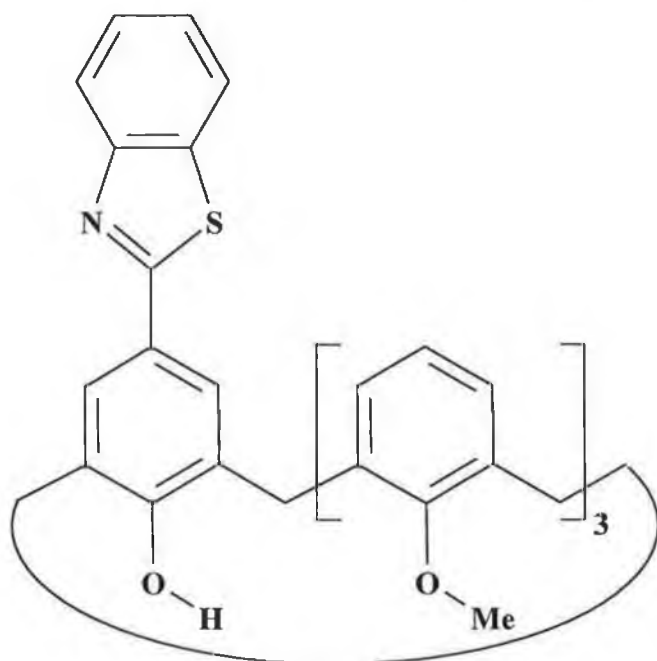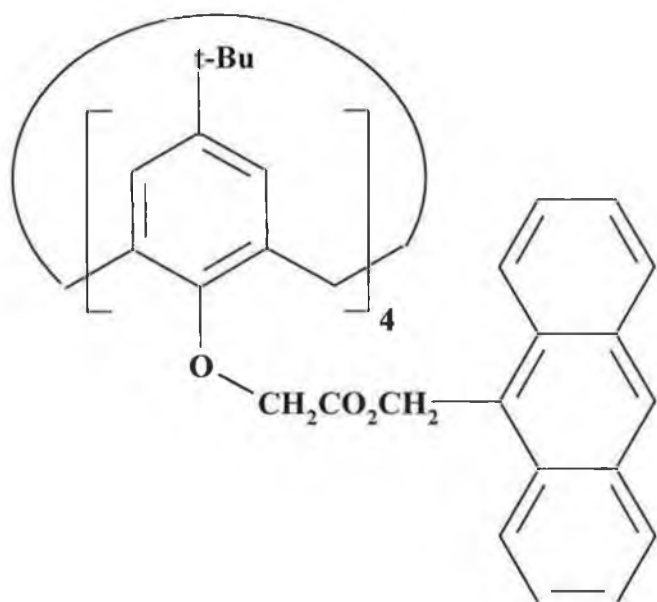
1.4.4.   Calixarenes as Sensors For Organic Guests

Using a calixarene to bind with an organic guest poses a new problem. Organic guests, unlike simple inorganic cations, are not normally spherical and it is more difficult to find a ligand which has the appropriate three-dimensional structure to form a complex.

Odashima *et.al.*[79] Chan and *et.al.*[80] used **C 1-42** and **C 1-45** to construct ISE's which are especially selective for primary amines. A formaldehyde-selective electrode has been designed based on the interaction between the tetraester, **C 1-36**, and an ionic hydrazone, generated in situ.[81] At pH 5.4, the electrode exhibits a diionic hyper Nernstian response of 32.4 mV per decade in the range 4×10^{-5} to 0.1 mol dm^{-3} formaldehyde. However, at pH 9.2, the electrode shows a near Nernstian response of 50.3 mV per decade over a narrower concentration range. Carboxylic acids have been determined by in-situ conversion to amines and quantification of the amines by an ISE with **C 1-41** as the ionophore.[82] Cyclic voltammetry has been used to the study the complexes formed by **C 1-68** with protonated amines and neutral ferrocene derivatives.[83] **C 1-68** is notable for the fact that it is water-soluble as this is unusual for calixarenes. **C 1-41** and **C 1-46** have been used to develop sensors for 2-phenylethylamine.[84] The dye Acridine Orange was immobilised in membranes constructed with each of these calixarenes and the fluorescence was found to decrease in the presence of 2-phenylethylamine.

C 1-68

39
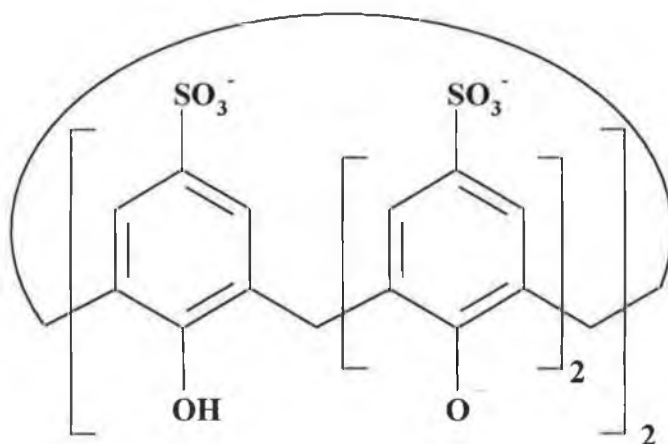
One of the most exciting challenges in sensor is the development of hosts capable of chiral recognition. This has obvious applications in the pharmaceutical industry as many drugs are chiral. Grady *et. al.*[85] describes a system where the recognition of 1-phenylethylamine (PEA) by the fluorogenic calixarene, (*S*)-**C 1-69**, quenches the fluorescence of these calixarenes because they contains fluorescent groups in its binding cavity. More importantly, the quenching occurs to a greater extent with the (*S*)- form of PEA than for the (*R*)- form. Just as importantly, it was found that the fluorescence of tetraester calix[4]arenes, such as **C 1-36**, was insignificant, while the non-macrocyclic compound, (*S*)-**C 1-70**, was found to be incapable of distinguishing between the enantiomers of PEA. Thus, it is the unique combination of pendant groups which are both chiral and flourescent, with the calixarene macrocyclic cavity which results in the chiral discriminatory ability of the (*S*)-**C 1-69**. It was demonstrated that is possible to determine the composition of a mixture of enantiomers of the substrate if the total concentration of both enantiomers is known. Kubo *et. al.*[86] describe a system, where the UV-visible absorbance of **C 1-71** was used for the detection of phenylglycinol. The addition of (R)-phenylglycinol resulted in a shift (of 23 nm) of the band at 515.5 nm and the appearance of new absorption band at ca. 650 nm. Subsequent additions of (R)-phenylglycinol caused the absorbance at both wavelengths to increase with isobestic points at 416 and 505 nm. The advantage of using spectral methods to develop chiral sensors is that they are amenable to real-time analysis, unlike the methods commonly employed in the pharmaceutical industry - circular dichroism, specific rotation and liquid and gas chromatography.[85] Furthermore, the separation methods are more expensive in terms of reagent consumption and cost of instrumentation, and they generate more waste than the spectral methods. Of the two spectroscopic methods discussed here, fluorescence methods are more sensitive and the dynamic range is wider than those based on UV-visible absorption.[87]
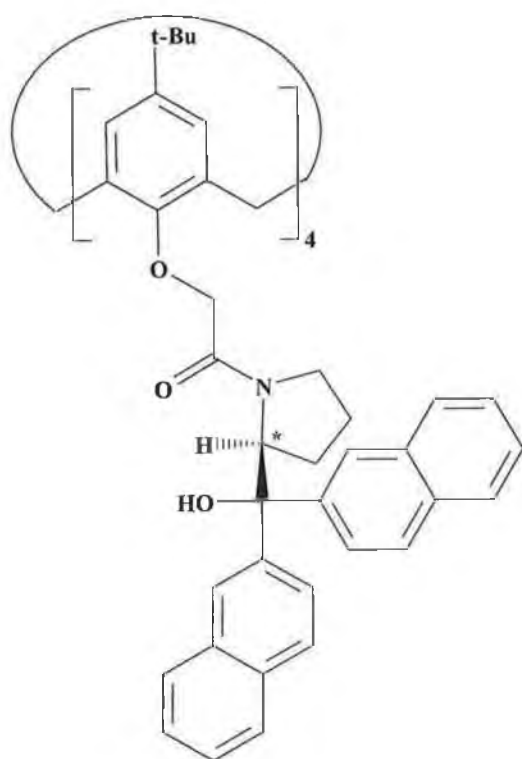
C 1-69
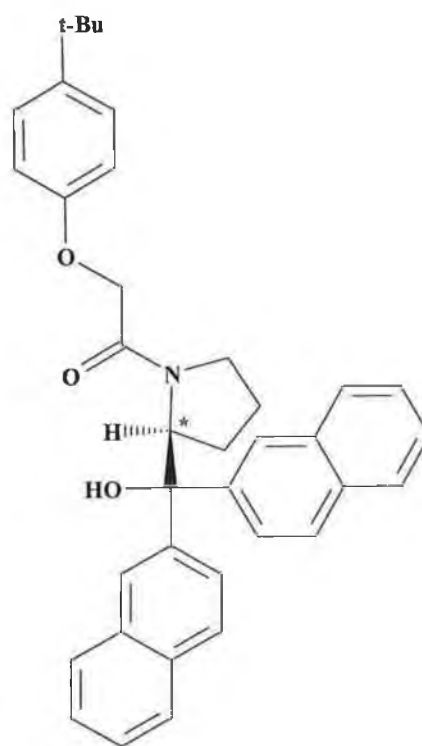
C 1-70
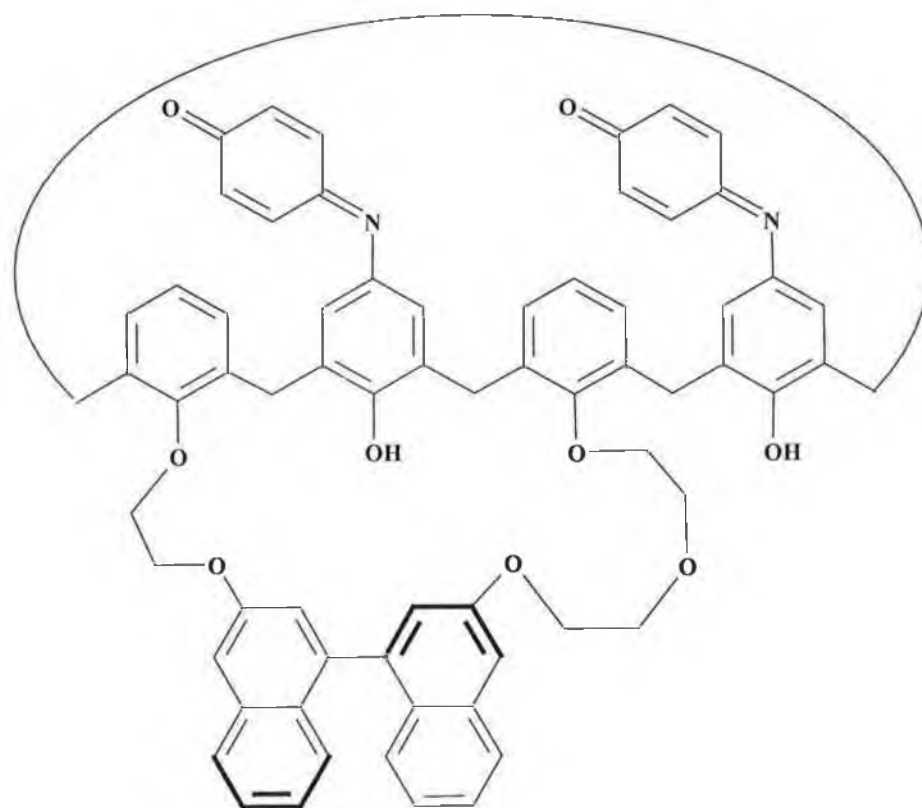
C 1-71

1.4.5.   *Sensors for Anions*

The development of calixarenes for use as sensors for anions is still in its infancy. **C 1-72** has been used, with cyclic voltammetry, to quantitatively detect $H_2PO_4^-$ and in the presence of HSO_4^- and Cl^-.[88] Similarly, **C 1-73** has been shown, again with cyclic voltammetry, to exhibit excellent selectivity for carboxylate anions and in particular the acetate anion, over common anions.[89] Furthermore, the complexes formed by **C 1-73** have much greater formation constants than those complexes formed by the non-macrocyclic ligand, **C 1-74**, and this emphasises the rigidity with which the Co^+ 'sandwich' unit is held in **C 1-73**, thus creating an ideal binding site for anions. ClO_4^- has been determined using an ISE based on the Hg^{2+} complex of **C 1-47**.[90] High selectivity was shown towards common anions except I^-.
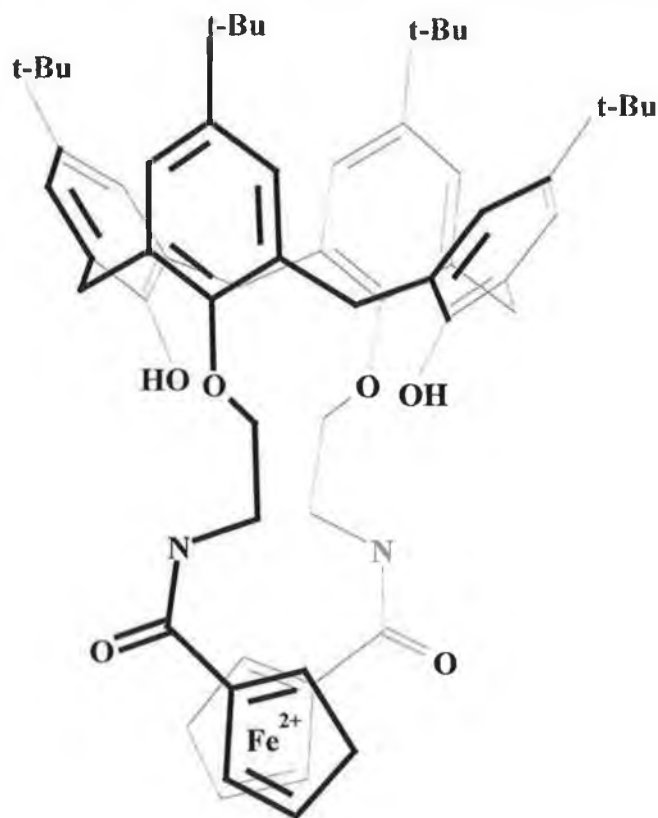
C 1-72
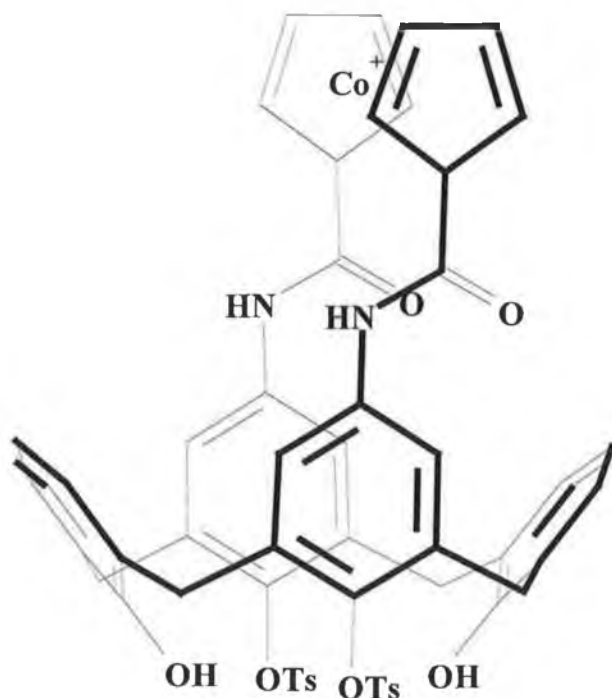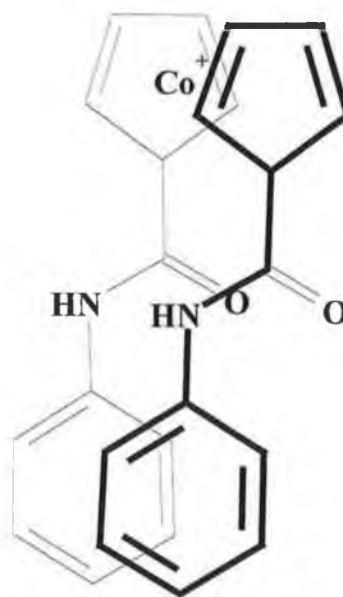
C 1-73   C 1-74

1.4.6.   Patents

Diamond and McKervey[60] state that almost 100 patents which include 'calixarenes' as a keyword have been filed. Some of these patents refer to the synthesis of calixarene derivatives. However other patents refer to the use of calixarenes in applications as varied as fuel additives, hair dyes, rubber stabilisers and corrosion inhibitors. Four of the patents relate to the use calixarenes as sensors, as developed by Diamond, Harris, McKervey and Svehla and co-workers. For example, two patents describe the use of ionophores such as **C 1-36** and **C 1-37** in the construction of ISE's.[91,92] Another patent refers to the creation of optical sensors with calixarenes such as **C 1-60, C 1-62** and **C 1-61**.[93]

1.5.   Future Applications of Calixarenes

The use of calixarenes as sensors is just beginning to develop. They have they already been used to detect a wide range of species but their is potential for the development of calixarenes which can operate in a novel way leading to novel applications. There is potential for the development of calixarenes as sensors for toxic vapours and molecules of biological importance. Binding of molecules of

biological importance, requires that the host and the guest have complementarity in both their shape and functional groups and both aspects of calixarenes can be modified.

1.6. Location Of Files

Description	Computer	Directory	File Name	Comment(s)
This thesis	Gateway	C:\	PK-Thesis	
	P5-100	__Paddy\	4p0.doc	
		There will never...		

44

1.7. References

1. C. D. Gutsche, *Calixarenes*, Royal Society of Chemistry, Cambridge, England, 1989.

2. J. Vicens and V. Böhmer, *Eds., Calixarenes, A Versatile Class of Macrocyclic Compounds*, Kluwer, Dordrecht, 1990.

3. C. D. Gutsche, B. Dhawam, J. A. Levine, K. H. No and L. J. Bauer, *Tetrahedron*, **1983**, 39, 409.

4. M. Perrin and D. Oehler, *Conformations of Calixarenes in The Crystalline State* in ref. 2, p. 65.

5. F. Grynszpan, Z. Goren and S. E. Biali, *J. Org. Chem.,* **1991**, 56, 532.

6. F. Grynszpan and S. E. Biali, *Tetrahedron Lett.,* **1991**, 32, 5155.

7. C. G. Gibbs and C. D. Gutsche, *J. Am. Chem. Soc.,* **1993**, 115, 5338.

8. X. Delaigue, J. M. Harrowfield, M. W. Hosseini, A. De Cian and N. Kyritsakas, *J. Chem. Soc., Chem. Commun.,* **1994**, 1579.

9. Y. Morita, T. Agawa, Y. Kai, N. Kaneshia, N. Kasai, E. Nomura and H. Taniguchi, *Chem. Lett.,* **1989**, 1349.

10. Y. Morita, T. Agawa, E. Nomura and H. Taniguchi, *J. Org. Chem.,* **1992**, 57, 3658.

11. G. Ferguson, J. F. Gallagher, Y. Li, M. A. McKervey, E. Madigan, J. F. Malone, M. B. Moran and A. Walker, *Supramol. Chem.,* **1996**, 7, 223.

12. a) M. Coruzzi, G. D. Andreeti, V. Bocchi, A. Pochini, and R. Ungaro, *J. Chem. Soc., Perkin Trans.* 2, **1982**, 1133; b) M. Perrin, and S. Lecocq, *J. Incl. Phenom. Mol. Recog.* **1991**, 11, 171; c) R. K. Juneja, K. D. Robinson, G. W. Orr, R.H. Dubois, K. A. Belmore, J. L. Atwood, J. M. Ripmeester and C. I. Ratcliffe, *J. Incl. Phenom. Mol. Recog.,* **1992**, 13, 93; d) J. F. Gallagher,

G. Ferguson, V. Böhmer and D. Kraft, *Acta Cryst. C*, **1994**, 50, 73; e) S. Papparaldo and G. Ferguson, *J. Org. Chem.,* **1996**, 61, 2407.

13. M. Halit, D. Oehler, M. Perrin, A. Thozet, R. Perrin, J. Vicens and M. Bourakhouadar *J. Incl. Phenom.,* **1988**, 6, 613.

14. G. D. Andreeti, F. Uggozoli, A. Casnatti, E. Ghidini, A. Pochini and R. Ungaro, *Gazz. Chim. Ital.,* **1989**, 119, 47.

15. R. G. Janssen, J. P. M. van Duynhoven, W. Verboom, G. J. van Hummel, S. Harkema and D. N. Reinhoudt, *J. Am. Chem. Soc.,* **1996**, 118, 3666.

16. J. L. Atwood, D. L. Clark, R. K. Juneja, G. W. Orr, K. D. Robinson and R. L. Vincent, *J. Am. Chem. Soc.,* **1992**, 114, 7558.

17. W. J. Wolfgong, L. K. Talafuse, J. M. Smith, M. J. Adams, F. Adeogba, M. Valenzula, E. Rodriguez, K. Contreras, D. M. Carter, A. Bacchus, A. R. McGuffey and S.G. Bott, *Supramol. Chem.,* **1996**, 7, 67.

18. M. A. McKervey, E. M. Seward, G. Ferguson, B. Ruhl and S. J. Harris, *J. Chem. Soc., Chem. Commun.,* **1985**, 388.

19. G. D. Andreeti, F. Uggozoli, Y. Nakomoto and S.-I. Ishida, *J. Incl. Phenom. Mol. Recog.,* **1991**, 10, 241.

20. C. D. Gutsche, A. E. Gutsche and A. I. Karaulov, *J. Incl. Phenom.,* **1985**, 3, 447.

21. M. Czugler, S. Tisza and G. Speier, *J. Incl. Phenom. Mol. Recog.,* **1991**, 11, 323.

22. T. Hareeda and S. Shinkai, *J. Chem. Soc., Perkin Trans. 2,* **1995**, 2231.

23. V. Böhmer, *Angew. Chem., Int. Ed. Engl.,* **1995**, 34, 713.

24. A. Arduini, A. Pochini, S. Reverberi, and R. Ungaro, *J. Chem. Soc., Chem. Commun.,* **1984**, 981.

25.   A. Arduini, A. Pochini, S. Reverberi, R. Ungaro, G. D. Andreeti and F. Uggozoli, *Tetrahedron,* **1986**, 42, 2089.

26.   C. D. Gutsche and L. J. Bauer, *Tetrahedron Lett.,* **1981**, 22, 4763.

27.   Ref. 1, p.91.

28.   E. Dahan and S. Biali, *J. Org. Chem.,* **1991**, 56, 7269.

29.   K. Iwamoto, K. Araki and S. Shinkai, *J. Org. Chem.,* **1991**, 56, 4955.

30.   C. D. Gutsche, in "Single Step Syntheses and Properties of Calixarenes", ref. 2, pp. 3-37.

31.   S. Kanamathareddy and C. D. Gutsche, *J. Org. Chem.,* **1994**, 59, 3871.

32.   F. Inokuchi and S. Shinkai, *J. Chem. Soc., Perkin Trans. 2,* **1996**, 601.

33.   a) D. M. Roundhill, *Metal-Complexes of Calixarenes*, in K. D. Karlin, Ed., "Progress in Inorganic Chemistry", John Wiley & Sons Inc., New York, 1995, Vol. 43, pp. 533-592; b) F. Arnaud-Neu, M.-J. Schwing-Weill, K. Ziat, S. Cremin, S. J. Harris and M. A. McKervey, *New J. Chem,* **1991**, 15, 33; c) G. Barrett, M. A. McKervey, J. F. Malone, A. Walker, F. Arnaud-Neu, L. Guerra, M.-J. Schwing-Weill, C. D. Gutsche and D. R. Stewart, *J. Chem. Soc., Perkin Trans. 2,* **1993**, 1475.

34.   K. Iwamoto and S. Shinkai, *J. Org. Chem.,* **1992**, 57, 7066.

35.   C. Bocchi, M. Careri, A. Casnati and G. Mori, *Anal. Chem.,* **1995**, 67, 4234.

36.   F. Arnaud-Neu, E. M. Collins, M. Deasy, G. Ferguson, S. J. Harris, B. Kaitner, A. J. Lough, M. A. McKervey, E. Marques, B. Ruhl, M.-J. Schwing-Weill and E. M. Seward, *J. Am. Chem. Soc.,* **1989**, 111, 8681.

37.   a) E. M. Collins, M. A. McKervey and S. J. Harris, *J. Chem. Soc., Perkin Trans. 1,* **1989**, 372; b) E. M. Collins, M. A. McKervey, E. Madigan, M. B. Moran, M. Owens, G. Ferguson and S. J. Harris, *J. Chem. Soc., Perkin Trans.*

1, 1991, 3137;   c) K. Kimura, T. Matsuba, Y. Tsujimura and M. Yokoyama, *Anal. Chem.* **1992**, 64, 2508.

38.   C. Loeber, D. Matt, P. Briard and D. Grandjean, *J. Chem Soc., Dalton Trans,* **1996,** 513.

39.   F. Arnaud-Neu, G. Barrett, D. Corry, S. Cremin, G. Ferguson, J. F. Gallagher, S. J. Harris, and M.-J. Schwing-Weill, *J. Chem. Soc., Perkin Trans. 2,* **1997,** 575.

40.   A. Ikeda, H. Tsuzuki and S. Shinkai, *J. Chem. Soc., Perkin Trans. 2,* **1994,** 2073.

41.   A. T. Yordanov, B. R. Whittlesey and D. M. Roundhill, *Inorg. Chem.*, **1998,** 3526.

42.   G. Calestani, F. Uggozoli, A. Arduini, E. Ghidini and R. Ungaro, *J. Chem. Soc., Chem. Commun.,* **1987,** 344.

43.   A. Arduini, E. Ghidini., A. Pochini, R. Ungaro, G. D. Andreeti, G. Calestani and F. Uggozoli, *J. Incl. Phenom.,* **1988,** 6, 119.

44.   L. Zetta, A. Wolff, W. Vogt, K.-L. Platt and V. Böhmer, *Tetrahedron,* **1991,** 47, 1911.

45.   D. Bethell, G. Doughertry and D. C. Cupertino, *J. Chem. Soc., Chem. Commun.,* **1995,** 675.

46.   A. Yamada, T. Murase, K. Kikukawa, T. Arimura and S. Shinkai, *J. Chem. Soc., Perkin Trans. 2,* **1991,** 793.

47.   P. Guilbaud, A. Varnek and G. Wipff, *J. Am. Chem. Soc.,* **1993,** 115, 8298.

48.   A. Ikeda, H. Tsuzuki and S. Shinkai, *Tetrahedron Lett.,* **1994,** 35, 8417.

49.   A. F. Danil de Namor, M. C. Cabaleiro, B. M. Vuano, M. Salomon, O. I. Pieroni, D. A. Pacheco Tanaka, C. Y. Ng, M. A. Llosa Tanco, N. M.

Rodriguerez, J. D. Cárdenas Garcia and A. R. Casal, *Pure Appl. Chem.*, **1994**, 66, 435.

50.   H. Murakami and S. Shinkai, *J. Chem. Soc., Chem. Commun.,* **1993**, 1537.

51.   H. Matsumoto and S. Shinkai, *Tetrahedron Lett.,* **1996**, 37, 77.

52.   D. Diamond, *Anal. Chem. Symp. Ser.,* **1986**, 25, 155.

53.   D. Diamond, G. Svehla, E. M. Seward and M. A. McKervey, *Anal. Chim. Acta,* **1988**, 204, 223.

54.   A. M. Cadogan, D. Diamond, M. R. Smyth, M. Deasy, M. A. McKervey and S. J. Harris, *Analyst*, **1989**, 114, 1551.

55.   D. Diamond and G. Svehla, *Trends, Anal. Chem.* **1987**, 6, 46.

56.   K. M. O' Connor, M. Cherry, G. Svehla, S. J. Harris and M. A. McKervey, *Talanta*, **1994**, 41, 1207.

57.   K. Cunningham, G. Svehla, S. J. Harris and M. A. McKervey, *Analyst*, **1993**, 118, 341.

58.   P. Anker, H.-B. Jenny, U. Wuthier, R. Asper, D. Ammann, and W. Simon, *Clin. Chem.*, **1983**, 29, 1508.

59.   M. Telting Diaz, D. Diamond and M. R. Smyth, *J. Pharm. Biomed. Anal.*, **1990**, 8, 695.

60.   D. Diamond and M. A. McKervey, *Chem. Rev.* **1996**, 15.

61.   M. Telting Diaz, F. Regan, D. Diamond and M. R. Smyth, *Anal. Chim. Acta,* **1991**, 251, 149.

62.   D. Diamond and R. J. Forster, *Anal. Chim. Acta*, **1993**, 276, 75.

63.   D. Diamond, J. Lu and Q. Chen, *Anal. Chim. Acta,* **1993**, 281, 629.

64.   J. Wang and Z. Taha, *Anal. Chem.* **1991**, 63, 1053.

65.   A. Cadogan, D. Diamond, S. Cremin, M. A. McKervey, E. M. Seward and S. J. Harris, *Anal. Proc.*, **1991**, 28, 13.

66.   D. Ammann, W. E. Morf, P. Anker, P. C. Meier, E. Pretsch and W. Simon, *Ion-selective Revs.*, **1983**, 5 (3), 38.

67.   A. Cadogan, D. Diamond, M. R. Smyth, G. Svehla, M. A. McKervey, E. M. Seward and S. J. Harris, *Analyst*, **1990**, 115, 1207.

68.   K. O' Connor, G. Svehla, S. J. Harris and M. A. McKervey, *Talanta,* **1992**, 39, 1549.

69.   a) D. W. Arrigan, G. Svehla, S. J. Harris and M. A. McKervey, *Anal. Proc.*, **1992**, 29, 27; b) D. W. Arrigan, G. Svehla, S. J. Harris and M. A. McKervey, *Electroanalysis*, **1994**, 6, 97.

70.   P.D. Beer, P. A. Gale, Z. Chen, M. G. B. Drew, J. A. Heath, M. I. Ogden and H. R. Powell, *Inorg Chem*, **1997**, 5880.

71.   H. Shimizu, K. Iwamoto, K. Fujimoto and S. Shinkai, *Chem. Lett.,* **1991**, 2147.

72.   M. McCarrick, S. J. Harris, D. Diamond, G. Barrett, and M. A. McKervey, *J. Chem. Soc., Perkin Trans. 2*, **1993**, 1963.

73.   Y. Kubo, S. Hamaguchi, A. Niimi, K. Yoshida and S. Tokita, *J. Chem. Soc., Chem. Commun.,* **1993**, 305.

74   a) W. H. Chan, A. W. M. Lee, C. M. Lee, K. W. Yau, and K. M. Wang, *Analyst,* **1995**, 120, 1963; b) W. H. Chan, A. W. M. Lee, D. W. Kwong, W. L. Tam and K. M. Wang, *Analyst,* **1996**, 121, 531.

75.   A. M. King, C. P. Moore and K. R. A. Samankumara Sandanayake, *J. Chem. Soc., Chem. Commun.,* **1992**, 582.

76.   J. A. Liyanage, D. M. Taylor and D. R. Williams, *Anal. Proc.* **1995**, 32, 217.

77. K. Iwamoto, K. Araki, H. Fujimoto and S. Shinkai, *J. Chem. Soc., Perkin Trans. 1*, **1992**, 1885.

78. C. Perez-Jiminez, S. J. Harris and D. Diamond, *J. Chem. Soc., Chem. Commun.,* **1993**, 480.

79. K. Odashima, K. Yafi, K. Tohda and Y. Umezawa, *Anal. Chem.* **1993**, 65, 1074.

80. W. H. Chan, K. K. Shiu and X. H. Gu, *Analyst*, **1993**, 118, 863.

81. W. H. Chan and R. Yuan, *Analyst,* **1995**, 120, 1055.

82. A. W. M. Lee, W. H. Chan and Y. S. Tam, *Analyst,* **1995**, 120, 2841.

83. L. Zhang, A. Macias, T. Lu, J. I. Gordon, G. W. Gokel and A. E. Kaifer, *J. Chem. Soc., Chem. Commun.,* **1993**, 1017.

84. Y. Kawabata, T. Yamashiro, Y. Kitazaki, and T. Imasaka, *Sens. Actuators B,* **1996**, B29, 135.

85. T. Grady, S. J. Harris, M. R. Smyth, D. Diamond, and P. Hailey, *Anal. Chem.* **1996**, 68, 3775.

86. Y. Kubo, S. Maeda, S. Tokita and M. Kubo, *Nature*, **1996**, 382, 522.

87. G. D. Christian, "Analytical Chemistry", 5th ed., Wiley and Sons, New York, 1994, p. 449.

88. P. D. Beer, Z. Chen, A. Goulden, A. Graydon, S. E. Stokes and T. Wear, *J. Chem. Soc., Chem. Commun.,* **1993**, 1834.

89. M. G. B. Drew, D. Hesek and K. C. Nam, *Chem. Commun.,* **1997**, 107.

90. W. Wroblewski, E. Malinowska, and Z. Brzozka, Electroanalysis, **1996**, 8, 75.

91. S. J. Harris, M. A. McKervey, G. Svehla and D. Diamond. Received notification that European Patent Office is prepared to grant a patent on 22nd October, 1996. No. is 91311462.5.

92. S. J. Harris, M. A. McKervey, G. Svehla and D. Diamond, U.S. Patent Application, filed on 10th December, 1990.

93. Private communication with D. Diamond, School of Chemical Sciences, Dublin City University.

2. Modelling of Calixarene Cation Complexes With Molecular Mechanics

2.1. Introduction

Molecular modelling is a rapidly advancing and exciting field. The complexity of the phenomena under investigation and the power of the hardware and software used to carry out such investigations are constantly growing.

2.1.1.   *Molecular Mechanics*

Molecular mechanics is a method used to study the three-dimensional structure of molecules, which is conceptually simple and compared to quantum mechanical methods, it requires little computing power to implement. It should be pointed out that molecular mechanics and quantum mechanics complement each other in that an molecular mechanics optimised structure can be used as input for a quantum mechanical calculation.

Molecular mechanics considers that the energy (sometimes called the "steric" energy) of a molecule is the difference in potential energy between the real molecule and a hypothetical molecule, the structural features (bond lengths and bond angles, etc.,) of which are at their ideal values. For example, the ideal value of a C-C-C bond angle is 109.471°. The energy of the molecule, E, is the sum of these differences:

$$ E \;=\; E_s \;+\; E_b \;+\; E_\omega \;+\; E_{nb} \;+\ldots \qquad\qquad \text{Eqn. 2-1} $$

where: E_s is the energy of the bonds as they are stretched from their ideal lengths

E_b is the energy resulting from bending bond angles from their ideal values

E_ω is the torsional energy resulting from the rotating or twisting of bonds

E_{nb} is the energy of (intramolecular or intermolecular) nonbonded interactions

If other terms such as electrostatic interactions or hydrogen bonding have to be considered, then extra terms must be added to Eqn. (2-1). It is important to recognise that E has meaning only when compared to other geometries of the same molecule.

Strictly speaking, each molecule will have its own particular combination of potential energy functions (known as a force field). In practice however, force fields are defined for particular classes of compounds or for elements in general, as is the case with the MM2 force field, developed by Allinger's research group.[1,2] Force fields are parameterised to make the properties (for example, geometries, enthalpies of formation and dipole moments) of the predicted structure correlate with that of the actual structure.

In modelling the molecular structure of a compound, a trial geometry is initially constructed using the force field and E is calculated. Then, using a gradient search method (see Section 2.1.1.2), the geometry is systematically adjusted until the gradient of the potential energy is less than or equal to a specified value. The structure of the molecule is then said to be optimised.

Constructing A Force Field

Most of what is to be discussed in this section applies to the MM2 force field. If a bond is stretched or compressed, it is assumed that Hooke's law applies (see Eqn. (2-2)). A similar relationship applies to bending angles (see Eqn. (2-3).

$$ E_s \;=\; \sum \frac{k_s}{2}\left(l - l_0\right) \qquad\qquad \text{Eqn. 2-2} $$

$$E_b = \sum \frac{k_b}{2}(\theta - \theta_0)$$ Eqn. 2-3

where: k_S and k_θ are the stretching and bending the force constants respectively

l and θ are the actual bond length and bond angle, respectively

l_0 and θ_0 are the ideal bond length and bond angle, respectively.

The expressions for the torsional and non-bonded energies are more complicated, suffice to say that the expression for the torsional energy is a Fourier series, while the for the non-bonded energy is calculated from two expressions, one for short distances (see footnote [a]) and one for longer distances. Both expressions involve the use of r^* (a measure of van der Waals' radius) and a hardness parameter which is a measure of the depth of the potential well.

The collection of force constants, r^* values and hardness parameters for a given element in a given chemical environment define an atom type. A parameter **set** is a collection of atom types for different elements in various chemical environments. Different parameter sets may be used in combination with a given force field.

Gradient Search Methods

In the optimisations discussed in this chapter, three search methods are used:

1. **Steepest Descent**

    This method moves down the steepest slope (of interatomic forces) on the potential energy surface. If the energy of the molecular system decreases, it continues in the same direction and by a larger step (1.2 times larger); if it decreases the next step size is half that of the previous step. The method is useful for correcting poor starting geometries but is slow (relative to other methods) to converge and can oscillate.

---

[a] A distance is said to be short if the sum of the van der Waals' radii parameters for the two atoms involved is less than 3.311.

2. Polak-Ribiere

This is a conjugate gradient method which means that it chooses a conjugate direction h_i, initially the steepest descent direction, and thereafter according to:

$$\mathbf{h}_i \quad = \quad \mathbf{g}_i \quad + \quad \gamma_i \mathbf{h}_{i-1} \qquad\qquad \text{Eqn. 2-4}$$

where g_i is the current gradient and

h_{i-1} is the previous conjugate direction and, using the previous gradient, g_{i-1}:

$$\gamma_i \quad = \quad \frac{\left(g_i - g_{i-1}\right) \bullet g_{i-1}}{g_{i-1} \bullet g_{i-1}} \qquad\qquad \text{Eqn. 2-5}$$

There are at least two evaluations (points) for each direction (cycle). This method converges quicker than the steepest descent method.

3. Block Diagonal Newton-Raphson

This is the only method that calculates second derivatives which indicate the degree of curvature in the potential energy surface. Of the three search methods, it is the most efficient in converging but it does require a reasonable starting geometry. The *full* Newton-Raphson method computes the Hessian matrix, *A*, of second derivatives. For example, if the surface is quadratic, then:

$$\mathbf{A}_{jk} \quad = \quad \delta^2 \mathbf{E}/\delta \mathbf{X}_A \, \delta \mathbf{Y}_B \qquad\qquad \text{Eqn. 2-6}$$

The method estimates at the 3 co-ordinate vector, *x*, according to:

$$\mathbf{x}_i \quad = \quad \mathbf{x}_{i-1} \quad + \quad \mathbf{A}^{-1} \bullet \mathbf{g}_i \qquad\qquad \text{Eqn. 2-7}$$

The procedure calculates *A* for one atom at a time. *A* is then inverted and the new co-ordinates of the atom are calculated according to Eqn. 2-7.

For the software used in this investigation, HyperChem,[3] this method can be used with one of the force fields available - MM+. This force field is derived from Allinger's MM2 force field.[1,2] The Newton-Raphson method employed here neglects coupling between different atoms and oscillation is possible as a result.

The procedure adopted was to use the steepest descent method initially to eliminate instability in the starting geometry, then the Polak-Ribiere method to

further refine the geometry and finally the Newton-Raphson method to achieve convergence.

The Pitfalls of Molecular Mechanics

The first disadvantage of molecular mechanics, as with all methods of molecular modelling, is that if the potential energy surface of a molecule consists of many local minima, then finding the global minimum (the usual objective in molecular modelling) can be very difficult.   In general, one must start optimisations with structures which are near each likely local minimum, i.e., the user must guess or predict these likely structures.   Some force fields consist of a dihedral angle driver which allows the user to let the program scan part of the potential energy surface and then optimise the structure at each of the local minima found can be optimised.

A second drawback is that where there are no force field parameters available for an element in a given chemical environment, the user must make estimates of the likely values of these parameters and this may lead to inaccuracies.

2.1.2.   *Semi-empirical Quantum Mechanics*

To study the interaction between a ligand and a cation, it is necessary to know the electron distribution in the ligand, and the cation, if it is polyatomic.   Quantum mechanics can be used for this purpose.   The functions describing the electron distribution in molecules the size of calixarenes cannot be solved analytically and this has led to the development of, among other things, semi-empirical (SE) quantum mechanical methods which describe the electron distribution in terms of partial charges on each atom.

There are several SE methods available which differ theoretically or in their parameters for the elements available. Limitations on time have meant that three SE methods - MNDO, AM1 and PM3 - only were used as these are probably the most popular SE methods.

SE methods can be classed according to how they treat interaction between the electrons.   Electrostatic repulsion between electrons is referred to as coulombic interaction. The identical nature of electrons requires that a correction be made for

electrons of the same spin and the contribution to the calculation made by this correction is known as an exchange interaction.

The Neglect of Differential Overlap (NDO) methods neglect many of the exchange integrals. With Complete NDO (CNDO), for example, electron repulsion depends on the nature of the atoms involved and not on the particular orbitals. In the Intermediate NDO (INDO) method and other variations on it, exchange integrals between electrons on the same atom need not be equal, but can depend on the orbitals involved.

In addition to the integrals used in the INDO methods, the Neglect of Diatomic Differential Overlap (NDDO) methods (MNDO, AM1 and PM3) have an additional class of integrals which take into account the overlap density between two orbitals centred on the same atom interacting with the overlap density between two orbitals also centred on a single (but possibly different) atom.

MNDO

This method was devised and developed by Dewar and co-workers,[4] and has been reviewed by Thiel.[5] While it successful in reproducing molecular properties such as bond angles and macroscopic properties such as enthalpies of formation, it is not without its weaknesses. In particular, it fails to reproduce energies for compounds containing hydrogen bonds or four membered carbon rings or for molecules which are sterically crowded, for example, neopentane.

AM1

Austin Model 1 (AM1) is a modified MNDO method proposed and developed by Dewar and co-workers[6,7] and Stewart.[8] The basic difference between the two methods is the addition of Gaussian functions to some of the core repulsion functions (CRF's) for certain elements. They were used as 'patches' for specific types of systems that could not be handled in general parameterisation without disrupting other chemically important items.[9]

Problems still exist with AM1. For example, the treatment of phosphorous-oxygen bonds is inaccurate, nitro-containing compounds are too positive in energy and the peroxide bond is too short.

PM3

PM3, developed by Stewart, is a reparameterisation of AM1 and it differs only in the values of the parameters.[10,11] The parameters for PM3 were derived by using a larger number and wider variety of comparisons between experimental and computed molecular properties. In practice, it results in non-bonded interactions being less repulsive than in AM1.

2.1.3.   Using Molecular Mechanics To Model of Calixarene-Metal Complexes

Molecular mechanics calculations are already well established in the field of calixarene chemistry. Up to this point their primary use has been in exploring the conformations of the metal-free calix[n]arenes (n=4-6),[12] although the results of very detailed molecular dynamics calculations on calix[4]arene:metal complexes which also included solvent molecules have been published.[13] Numerous studies have shown that most of the widely available molecular mechanics force-fields can be used to give very reasonable molecular structures for the various conformations available to calix[n]arenes (n=4-6) but the methods are rather less successful in predicting the energy ordering of the conformations which can be adopted by any given molecule.[14]

Since one of the main driving forces for studies of this class of compounds is their ability to coordinate metal ions, in some cases with a high degree of selectivity, it is important to understand the structure of the metal complexes that they form. The complexes typically have contain more than 30 heavy atoms so that *ab-initio* methods with large basis sets are prohibitively expensive in terms of computational time for routine studies. While it is possible to carry out semi-empirical studies, the need for large concerted motions of the aryl rings during geometry optimisation makes these calculations rather lengthy. Moreover, it is not established that semi-empirical methods are significantly better than molecular mechanics methods even for studies of the metal-free calixarenes.[14] For these reasons the structures of calixarene:metal complexes have been modelled using a simple molecular mechanics force field (MM+), testing the optimised geometries against known crystal structures. This geometrical information should be useful not only in guiding the synthesis of

59

new calixarenes but also should provide a method of generating reasonable input geometries for more sophisticated modelling techniques.

Unfortunately, although there is a very extensive database of metal-free calixarene single-crystal X-ray structures, the data set for calixarene:metal complexes is much more limited. Moreover, the compounds span calix[4]arenes and calix[5]arenes which bind through the oxygen atoms of alcohols, ethers, esters or amides. A method which successfully reproduces the geometries of all the above, such as one described below, could be regarded as of general utility.

Bell and co-workers have modelled complexes of calixarenes with Group 1 metals, using crystal structures of calixarenes with encapsulated Na^+, K^+, Rb^+ and Cs^+ ions as reference data.[15] This gave a reasonable range of Group I metal ions with which to test the modelling procedure. The study involved using molecular mechanics to optimise the geometry of such complexes *in vacuo* after partial charges (calculated with the AM1 semi-empirical method) had been placed on the ligand. The resulting structures fitted the X-ray structures well when superimposed. It gave metal ion positions within calix[n]arenes in the solid state which, in the worst cases, were up to 0.5 Å in error, although the average error was considerably less. Solvent molecules and counterions were included where appropriate- i.e. in crystal structures.

The calixarenes studied in the investigation described above were in the so-called 'cone' conformation. In contrast, in the study described in this chapter, molecular mechanics was used to model the geometry of the sodium complex of a calix[4]arene tetraester, in the 1,3-alternate conformation.[16] In **C 2-1**, there is the possibility that complexation of the cation can take place at several sites within the calixarene. Therefore, it is of interest to determine what effect varying the initial position of the cation has on the optimised geometry of the complex.

2.2. Experimental

Optimisations were carried out using the HyperChem[3] molecular modelling package (version 4) running on a 180 MHz Pentium Pro PC with 32 MB RAM.

60

Tetraester calix[4]arenes, in the cone conformation, such as **C 2-2,** are well established as ionophores for the Na^+ ion[17]. It is known, from NMR spectroscopy, that **C 2-2**, upon complexation with Na^+, remains in a 'cone' conformation but (unlike the free ligand) has a four-fold symmetry and that the ion is coordinated by the four phenoxy oxygen atoms and the four carbonyl oxygen atoms [18]. This eight-fold coordination is found in the energy-minimised model of the complex (see Figure 2-1) and in the X-ray structure of the complex formed between the tetraamide analogue of **C 2-2** and K^{+}[19]. Thus, it is clear that Na^+ ion can be complexed by **C 2-2** and other, similar calixarenes in one region only. (In the cone conformation, the carboxylate oxygen atoms of **C 2-2** do not have the correct orientation to interact with the Na^+ ion collectively, either on their own or with the other types of oxygen atoms in **C 2-2**).

Examination of the total charge density contour plot for **C 2-2,** given in Figure 2-2b, identifies the phenoxy, carbonyl and carboxylate oxygen atoms as giving regions of high electron density (a very similar plot would be obtained if the contour plot were taken in a plane approximately containing the '2' and '4' pendant groups). The contour plot for **C 2-1**, shown in Figure 2-3b, indicates that although the same types of atoms give regions with high electron density, these atoms are dispersed over the entire molecule, rather than clustered in a single obvious binding site. Thus, the 1,3-alternate conformation of **C 2-1** creates several possible complexation sites and this is in contrast to the number of sites available in the case of **C 2-2**. (It is important to note that model in Figure 2-2a and Figure 2-2b was obtained by rearranging, for illustration purposes, the ligand geometry in the optimised structure of **C 2-2**:Na^+, so that the phenoxy and carbonyl oxygen atoms of the two pendant groups on opposite sides of the cavity were approximately in the same plane. However, for Figure 2-3a and Figure 2-3b, no such rearrangement of the geometry of **C 2-1** structure was not necessary.)

The X-ray structure of the **C 2-1**:Na^+ complex is given in Figure 2-4a and Figure 2-5a[18], (the Cambridge Crystallographic Data Centre[20] reference is YERFIK). This complex was chosen for further modelling studies because its structure suggests that there is the possibility of migration of the cation. Furthermore, the apparent multiple

binding sites allow one to test the extent to which the modelling procedure can find the global minimum (in terms of energy) of an optimised structure more rigorously than is possible in the case of the 'cone' calix[4]arenes. In this work, it is assumed that the global minimum corresponds to the X-ray structure.

The modelling procedure uses electrostatic interactions to bind the metal ion within the calixarene, which means that partial charges must be calculated for the ligand. In this work three methods were used to calculate these charges. The first method was to use a single point, semi-empirical calculation (AM1[4]) on a compound similar to **C 2-1** (one full aryl ring and its substituents plus ethyl groups substituted at the bridging positions on the ring (see Figure 2-6)). These charges (Method 1) were then transferred, with averaging and rounding off, to the entire molecule of **C 2-1**, meaning that chemically equivalent atoms were assigned the same charge. The transferring of charges is a labour-intensive process and consequently, partial charges were also calculated on the full ligand with the AM1, MNDO[4,5] and PM3[10,11] semi-empirical methods (Method 2), which was a less laborious process. Another advantage of the latter method is that the effect on the optimised geometry of the complex, of assigning slightly different partial charges to atoms that are chemically equivalent but conformationally different, can be seen. This is relevant to the modelling of **C 2-1**:Na$^+$, as the geometry of the pendant groups in the '2' and '4' positions of **C 2-1** is different to that of the pendant groups in the '1' and '3' positions. However, Methods 1 and 2 both suffer from the disadvantage that because the calculations are carried out on the free ligand, they do not take into account withdrawal of electron density from the ligand when it binds with a cation. Accordingly, partial charges were also determined by carrying semi-empirical calculations on the full metal complex using those methods which have parameters for sodium - INDO[21], CNDO[22] and ZINDO/1[23] (Method 3).

The molecular mechanics MM+ force field available with the HyperChem software (and indeed, the other force fields available in HyperChem) contain no parameters for Group 1 metal ions and therefore, as in previous studies[15], the atom type for neon was used for the sodium ion since neutral neon is isoelectronic with Na$^+$. The ion was assigned a formal charge of +1 in the case of Methods 1 and 2.

The starting geometry used for the ligand for both the molecular mechanics and semi-empirical calculations was that of the ligand as in the X-ray structure of **C 2-1**:Na$^+$ (see Figure 2-4a). Hydrogen atoms needed to be added, as the X-ray structure did not contain them. With Methods 1 and 3, the ion was initially placed in Position 2 only - the position it occupies in the X-ray structure (see Figure 2-4a and Figure 2-7). When partial charges were assigned with Method 2 the initial position of the Na$^+$ ion was varied as shown in Figure 2-7. The geometry of the structure was subsequently optimised using the MM+ force field within HyperChem, which is a modified version of the MM2 force field developed by Allinger *et. al.*[24] A combination of three algorithms were used: steepest descent initially, then Polak-Ribiere and finally, Newton-Raphson. The atomic charges electrostatic interaction option was used without any artificial distance cut-off. The terminating gradient was 0.001 kcal mol^{-1} Å^{-1}.

The quality of fit of the structure to the X-ray structure was assessed by superimposing each optimised structure upon it and calculating the Root Mean Square (RMS) Overlay Error.

2.3. Results and Discussion

Molecular mechanics optimisations of **C 2-1**:Na$^+$ (partial charges assigned with Methods 1 and 2), produced structures (see Figure 2-4b and Figure 2-5b) that closely match the X-ray structure (shown in Figure 2-4a and Figure 2-5a), as judged by the smallness of the RMS Overlay Errors, given in Table 2-1. Of these structures, that produced using the combination of the PM3 semi-empirical method and Method 2 of assigning partial charges gave the best results, as judged by the error in the cation positions in the X-ray and optimised structures (see Table 2-1) and by examination of the geometry of the complex in the region of the cation (compare Figure 2-8 (the X-ray structure) with Figure 2-9 (AM1/Method 1) and Figure 2-10 (PM3/Method 2)).

63

Table 2-1. *RMS Overlay Error and distances of the optimised Na$^+$ position from its X-ray position, following the superimposition of optimised structures upon the X-ray structure of C 2-1:Na$^+$ for five different starting positions of the Na$^+$ ion.*

Semi-Empirical Method	Method of Assigning Partial Charges	Na$^+$ Starting Position [a]	RMS Overlay Errors / [b]	Separation Of The Optimised and X-ray Positions of Na$^+$ / Å [b]
AM1	1	2	0.733	0.45
AM1	2	2	0.734 [c]	0.46 [c]
MNDO	2	2	0.731 [c]	0.33 [c]
PM3	2	2	0.731 [c]	0.32 [c]
INDO	3	2	0.951	0.34
CNDO	3	2	0.942	0.32
ZINDO/1	3	2	0.981	0.54

[a] *See Figure 2-7.*

[b] *These distances were measured after superimposing three of the methylene bridging carbons of the optimised structure on those of the X-ray structure.*

[c] *In these cases, virtually identical results (the values differ in the third decimal place only) were obtained when the Na$^+$ ion was placed in different starting positions.*

It is worth noting that virtually identical structures were obtained when the AM1, MNDO and PM3 semi-empirical methods were used to determine partial charges with Method 2 and also when the AM1 method was used to assign charges with Method 1 (see Figure 2-9 and Figure 2-10, where partial charges were assigned with AM1/Method 1 and PM3/Method 2 respectively). The former result would suggest that the optimised structure of this complex is independent of the semi-empirical method used to assign partial charges to the ligand, while the latter result indicates

that (albeit slightly) different initial conformations of the pendant groups in the ligand and any resultant differences in partial charge between chemically equivalent atoms in the pendant groups with different conformations, have a small effect on the optimised structure of the ligand in the complex.

A very encouraging result is the fact that, when Method 2 was used to assign partial charges, the geometries of the optimised structures of the complex (both in terms of the conformation of the ligand and the position of the ion) are almost identical, regardless of the initial position of the ion, for each of the three semi-empirical methods used (see Table 2-1 and Table 2-2).

It is very interesting to note that though the conformation of the ligand initially used was that of the X-ray structure, the two pendant groups most involved in the binding of the ion as indicated by the X-ray structure (the '1' and '3' pendant groups), are the least involved according to the optimised structures, regardless of the initial position of the ion, i.e., when, for example, the ion was placed initially placed in Position 2 - its position in the X-ray structure - its optimised position was that of Position 3 with the corresponding rearrangement of the both pairs of pendant groups. It is important to realise that in the X-ray structure, the '1' and '3' pendant groups of the ligand have a geometry that is very well suited to complexation with the Na^+ ion as the ion is approximately equidistant from the carbonyl and phenoxy oxygen atoms of these pendant groups, and the two carbonyl groups and the Na^+ ion are approximately in the same plane. This movement of the ion from Position 2 to Position 3 suggests that the energy barrier to the migration is relatively small. This is supported by evidence, obtained from dynamic ^1H NMR measurements,[25] that the Na^+ ion oscillates rapidly (163 s^{-1}) across the hydrophobic arene cavity in an intramolecular fashion.

A very noticeable difference between the optimised structures (when partial charges were assigned with Methods 1 and 2) and the X-ray structure of **C 2-1**:Na^+ concerns the final position of the Na^+ ion. In those optimised structures where partial charges were assigned with Methods 1 and 2, it is nearer to the phenoxy oxygen atoms than the carbonyl oxygen atoms, whereas in the X-ray structure (see Figure 2-4a and Figure 2-8), the Na^+ ion is positioned lower in the cavity, by 0.32 to 0.46 Å, as is shown in Table 2-1. Furthermore, as illustrated in Figure 2-9, Figure 2-10 and

65

Figure 2-11, the optimised structures produced using Methods 1 and 2 give the impression that the Na^+ ion is bound mainly by the two phenoxy oxygen atoms of the pendant groups in the '1' and '3' positions, whereas the X-ray structure (see Figure 2-4a and Figure 2-8) indicates that the carbonyl oxygen atoms in these pendant groups are involved in the complexation to a very similar degree as the phenoxy oxygen atoms. However, as might be expected for a complex containing 154 atoms, the difference in position of the ion in the X-ray and optimised structures has little effect on the RMS overlay error; when the ligand from the optimised and X-ray structures (i.e., *without* the ion) are superimposed on each other, the RMS overlay error changes little from that obtained with the ion present, typically by ca. 0.03 Å.

In molecular modelling, differences in the ion position between X-ray and optimised structures can arise because a counterion and/or solvent molecule(s) were not included in the modelling. Preliminary work (results not shown) in which a perchlorate ion (sodium perchlorate was used to prepare the **C 2-1**:Na^+ complex[18]) was initially placed just below the '1' and '3' pendant groups of the ligand resulted in an optimised position of the perchlorate ion which was in the cavity created by the '1' and '3' pendant groups, with an distance of 3.65 Å between the Na^+ ion and the nearest chlorine atom. This result is clearly at variance with the X-ray structure because the latter structure indicates that the perchlorate counterion is outside both cavities of the calixarene. I feel justified in excluding solvent molecules from these modelling studies because they are not part of the X-ray structure.

The part of the complex where the X-ray and optimised structures match least, and therefore, presumably the main reason for the magnitude of the RMS Overlay Error, is in the conformation of the pendant groups not involved in the complexation of the sodium (compare Figure 2-4a with Figure 2-4b and Figure 2-5a with Figure 2-5b). For example, Figure 2-5a clearly shows that the orientation of the one of the carbonyl groups of the pendant group in the '3' position of the X-ray structure is very different to that in the optimised structure, shown in Figure 2-5b. The same feature was also present in the optimised structures obtained for the AM1 and MNDO semi-empirical methods and also when Method 1 was used to assign AM1 partial charges.

When Method 3 was used to assign partial charges, the quality of fit was poorer than when Methods 1 and 2 were used (see the RMS values in Table 2-1 and compare Figure 2-8 with Figure 2-11). A possible reason for this is the fact that the use of Method 3 resulted in partial charges on the sodium of typically +0.3, which is in contrast to the charge of +1 which was formally assigned to the sodium ion with Methods 1 and 2. Thus, it is possible that the greater magnitude of the partial charges on the ligand atoms generated by Method 3 caused intra-ligand attractive and repulsive forces to be greater than with Methods 1 and 2, leading to a poorer quality fit with the X-ray structure. The Na^+ ion in these optimised structures is approximately equidistant from the phenoxy and carbonyl oxygen atoms, as in the X-ray structure, but the ligand geometry in the region of the cation is noticeably different to that shown by the X-ray structure. This leads to a RMS Overlay Error which is significantly larger than that found when partial charges were assigned with Methods 1 and 2. In particular, the distances between the phenoxy oxygen atoms and between the carbonyl oxygen atoms diagonally across the cavity differ from the corresponding distances in the X-ray structure to a much greater extent than when Methods 1 and 2 were used to assign partial charges (compare Figure 2-8 with Figure 2-11). Also, the carbonyl and phenoxy oxygen atoms of one pendant group which bind with the Na^+ ion are not in the same plane as those atoms of the pendant group on the opposite side of the cavity. This feature is also present in the X-ray structure and those optimised structures where partial charges were assigned with Methods 1 and 2 but to a lesser extent (see Table 2-2).

Table 2-2. *Critical Distances and Angle For The X-ray and Optimised Structures of*
C 2-1:Na$^+$ in the region of the Na$^+$ ion.

Semi-Empirical Method / X-ray	Method of assigning / Partial Charges	O2-O3 / Å	O1-O4 / Å	Mean of O2-Na$^+$ and O3-Na$^+$ / Å	Mean of O1-Na$^+$ and O4-Na$^+$ / Å	O1-C1-C2-O4 Improper Torsional Angle / ^{o}
X-ray [a]	N/A	3.29	4.39	2.33	2.39	-6.14
AM1 [b]	1	2.98	4.57	2.55	2.32	-7.94
AM1	2 [e]	2.96	4.56	2.54	2.32	-8.22
MNDO	2 [e]	2.99	4.51	2.46	2.32	-8.02
PM3 [c]	2 [e]	3.06	4.61	2.42	2.38	-7.83
INDO [d]	3	4.36	4.81	2.59	2.74	-11.04
CNDO	3	4.30	4.80	2.60	2.70	-10.94
ZINDO/1	3	4.91	5.06	3.00	2.75	-9.41

N/A Not applicable

[a] *These values are also given in Figure 2-8.*

[b] *These values are also given in Figure 2-9.*

[c] *These values are also given in Figure 2-10.*

[d] *These values are also given in Figure 2-11.*

[e] *The results, for Method 2, are almost identical for the five starting Na$^+$ positions.*
For the distances quoted, variation occurs in third decimal place, while the range
over which the improper torsional angle varies is ca. 0.10^O.

A possible source of inaccuracy in the modelled structures is the use of the neon
atom type for the sodium ion. In HyperChem, the atom type for an element that does
not form covalent bonds, consists of just two parameters r* and ε. For neon, r* = 1.60
Å and ε = 0.09 kcal mol^{-1}. For example, the parameters used by Grootenhuis and

Kollman[26] in studies of Na^+ binding to crown ethers ($r^* = 1.60$ Å and $\varepsilon = 0.01$ kcal mol^{-1}) were also applied by us, resulting in slightly poorer RMS overlay errors, differing typically by 0.05 Å, i.e., the use of an ε value whose magnitude was nine times smaller than that used to define the atom type for neon in HyperChem, made little difference to the result. It should be possible to adjust these parameters to give better agreement between the modelled and X-ray structures and work in this area is ongoing.

While it is likely that the atom type that they developed was suited to crown ethers more than to calixarenes, it is also possible that the different result obtained was due to the use of a different force field (that found in AMBER[27] which was the software package used) by Grootenhuis and Kollmann. In general, good results are not expected when an atom type, developed for use with one force field, is used with another on[28]. I also wish to explore the extent to which the initial conformation of the ligand affects the geometry of the optimised structure of the complex.

2.4.   Conclusion

In summary, this straightforward and computationally undemanding method is surprisingly good at reproducing the structures of a range of calixarene:metal complexes.[15,16] This implies that the force field employed is at least reasonably good at balancing the conflicting demands of the electrostatic interactions between the ligating oxygen atoms and the encapsulated metal ions with the stretching/bending forces induced in the calixarene by the metal ion inclusion. There is clearly potential for refining the method as more crystallographic data becomes available, indeed it was found that the metal ion parameters could be adjusted to make near-perfect fits to the crystallographic data[15]. However, the method, as it stands, already provides a simple and inexpensive visualisation tool, which should be useful for the design of new calixarene derivatives.

This chapter demonstrates that in some calixarenes at least, the optimised geometry of the ligand in the complex and the final position of the ion is independent of the initial position of the ion and this is a very encouraging result. I have also demonstrated that improved results are obtained when cations (of Group 1 and Group

2, at least) are assigned formal charges than when partial charges are calculated for both the ligand and the metal ion.

2.5. Figures
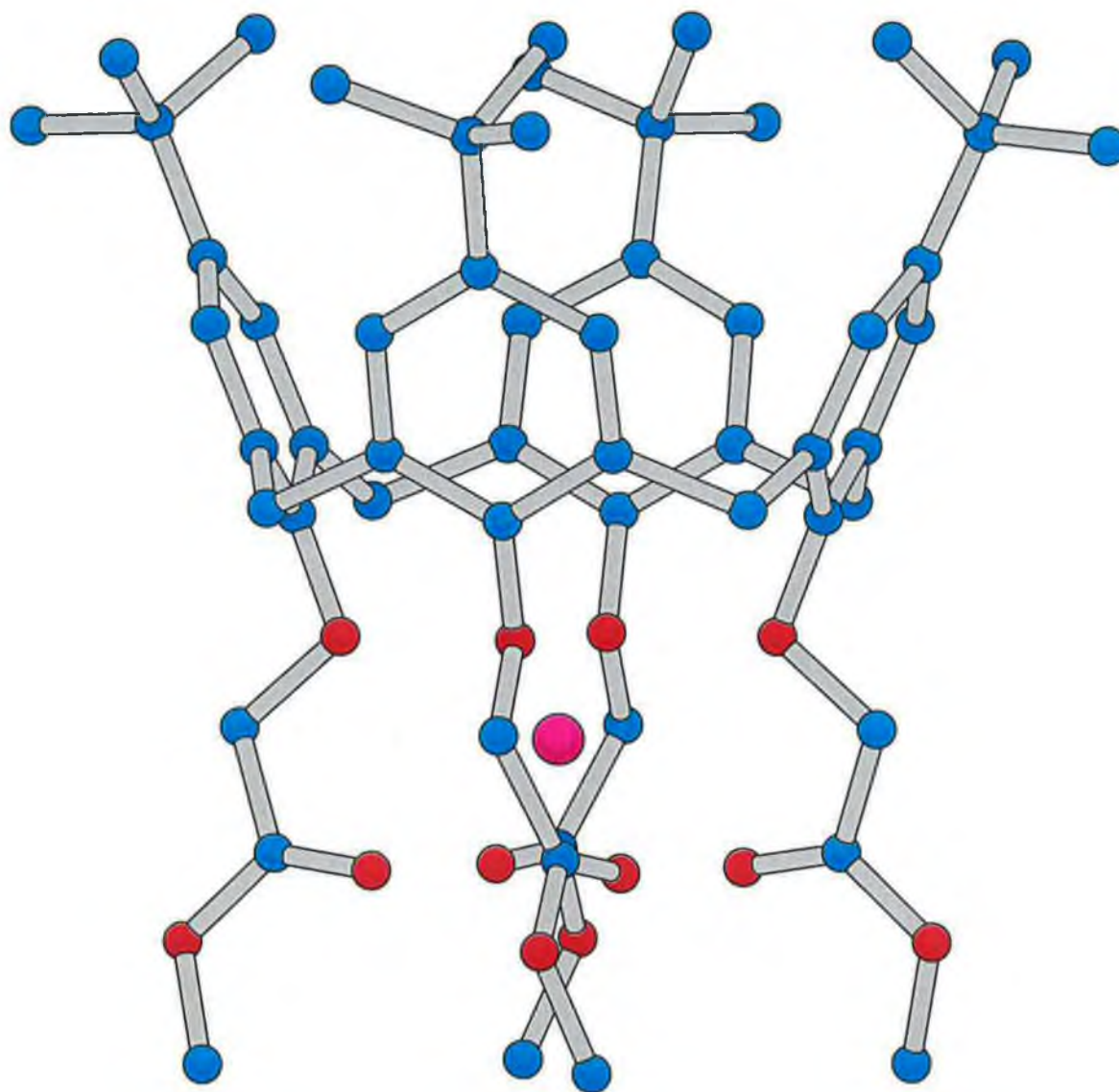
Figure 2-1. *Ball and tube rendering of the side-on view of the optimised structure of*
C 2-2:*Na⁺.   PM3 partial charges were placed on the ligand with Method 2 and by
initially placing the ion close to the optimised position.   The initial geometry used for
the ligand was that of the optimised structure of the free ligand. Colour code: cyan -
carbon, red - oxygen, magenta - sodium.*
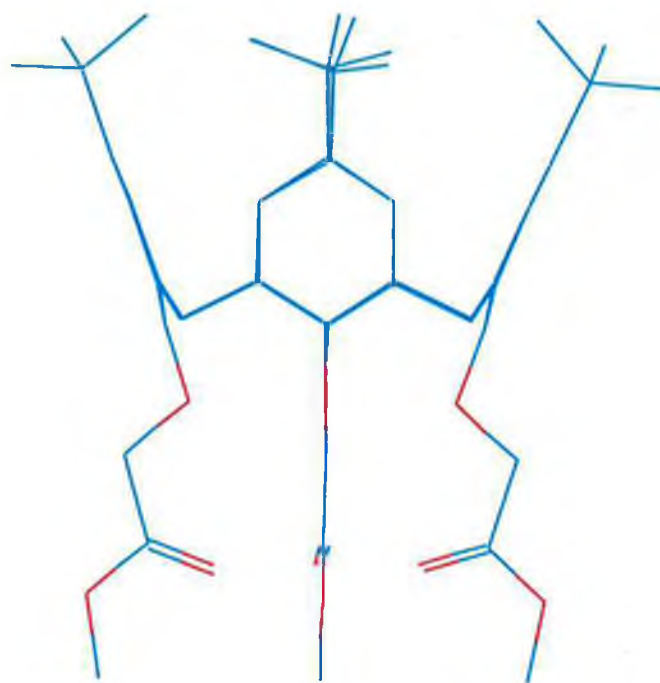
(a)
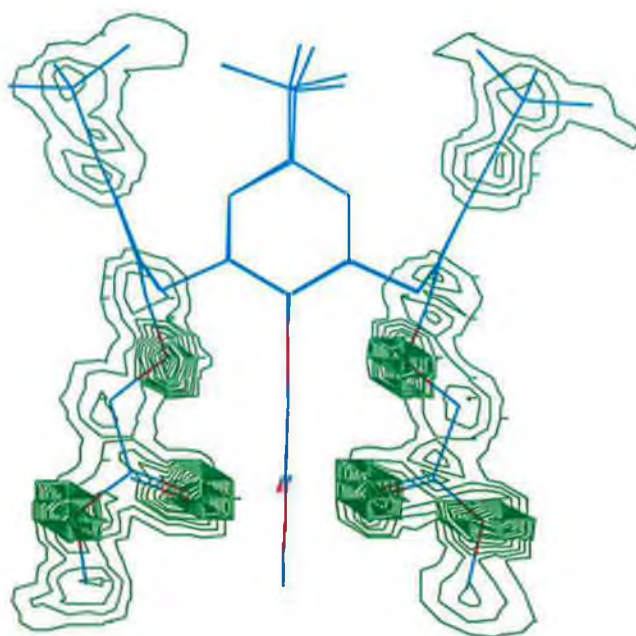
(b)

Figure 2-2. *Stick rendering of the structure of **C 2-2**, without, (a) and with, (b) the total charge density contour plot superimposed.   The contour plots were determined using PM3 partial charges, assigned with Method 2 and they apply to a plane which is parallel to the plane of the page and which contains the centre of mass of the molecule.*

72
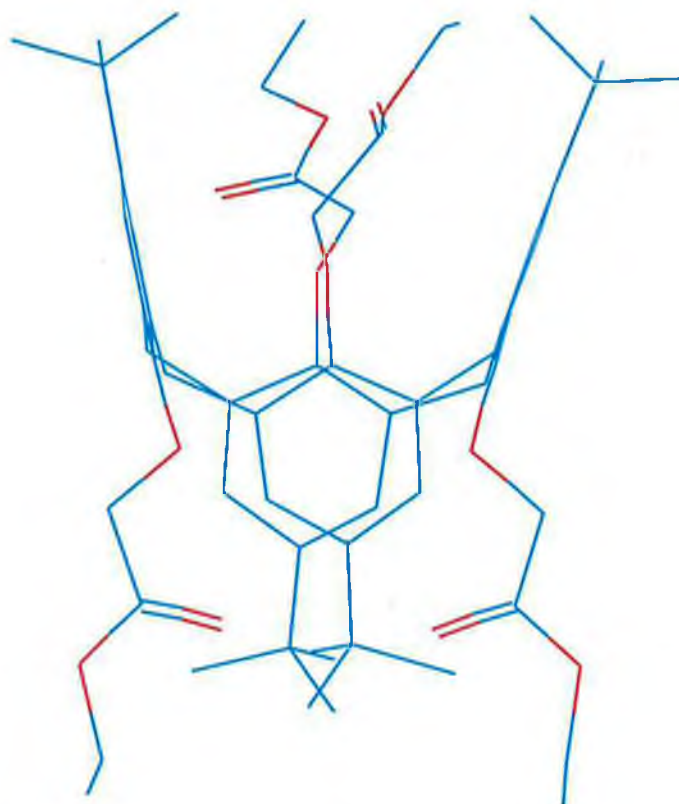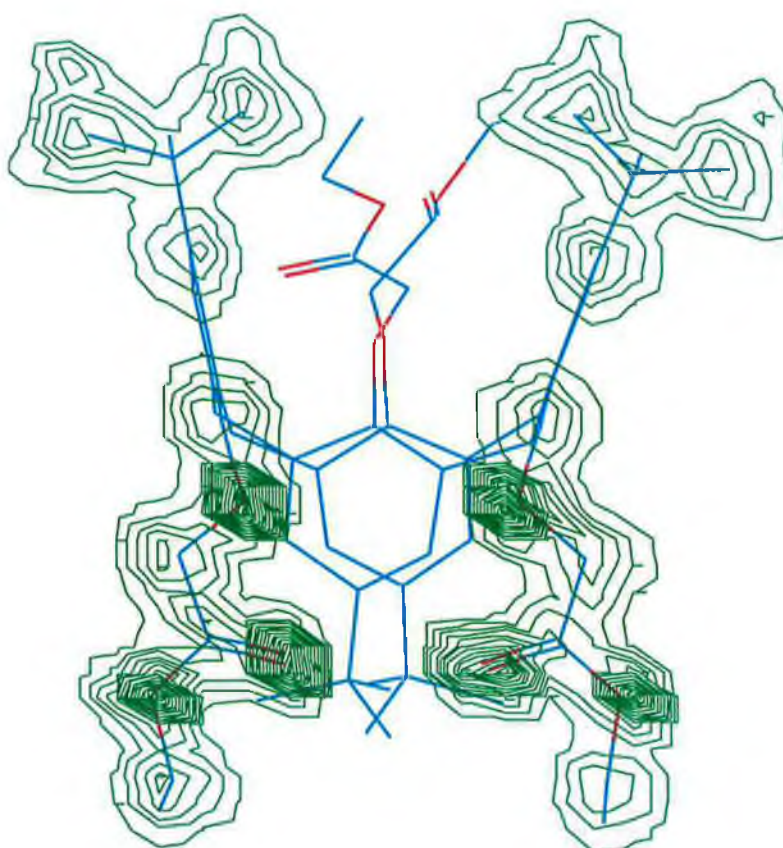
Figure 2-3. *As for Figure 2-2, except that **C 2-1** is shown.*

(a)

(b)

73
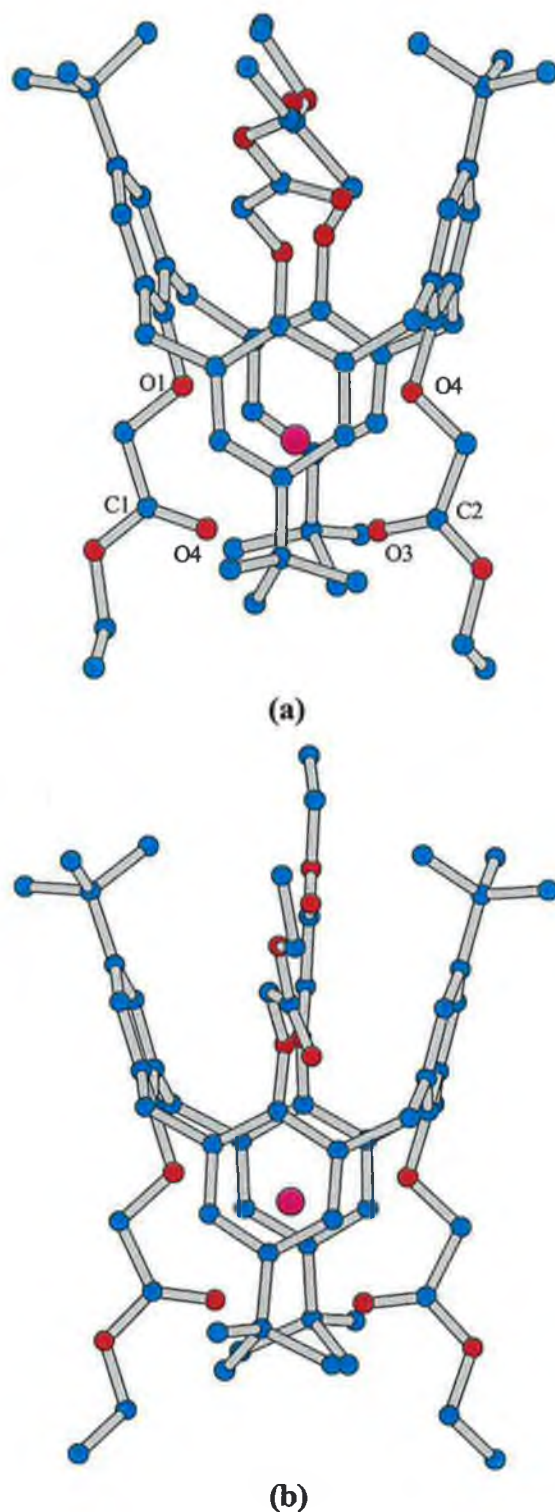
Figure 2-4. *Ball and tube rendering of the side-on views of the X-ray, (a) and optimised, (b) structures of **C 2-1**:Na⁺. The optimised structure was obtained by placing PM3 partial charges with Method 2 and by initially placing the ion in Position 2. The atom labels in (a) are used to define the region of the cation and are also used in Table 2-2 and in Figure 2-9 to Figure 2-11, inclusive. Colour code: cyan - carbon, red - oxygen, magenta - sodium.*

74
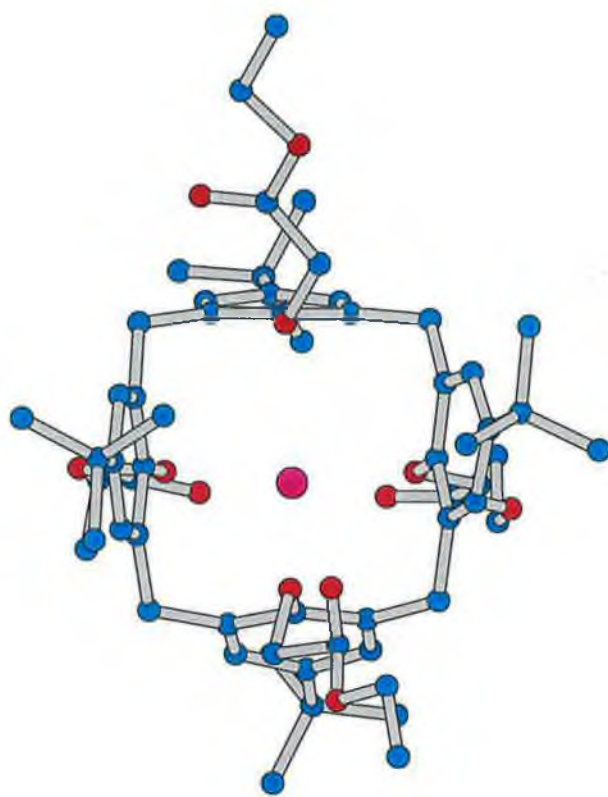
(a)
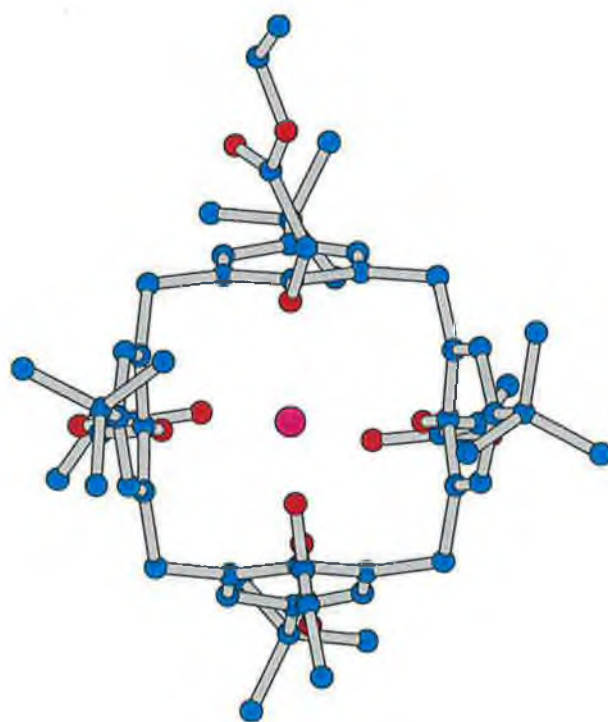
(b)

Figure 2-5. *As for Figure 2-4, except that the view through the cavities are shown.*
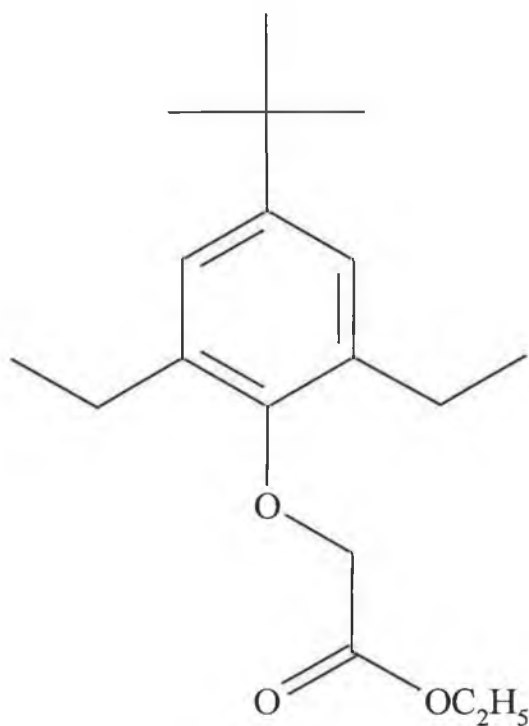
Figure 2-6. *Line rendering of the compound used to assign partial charges to **C 2-1** by Method 1.*
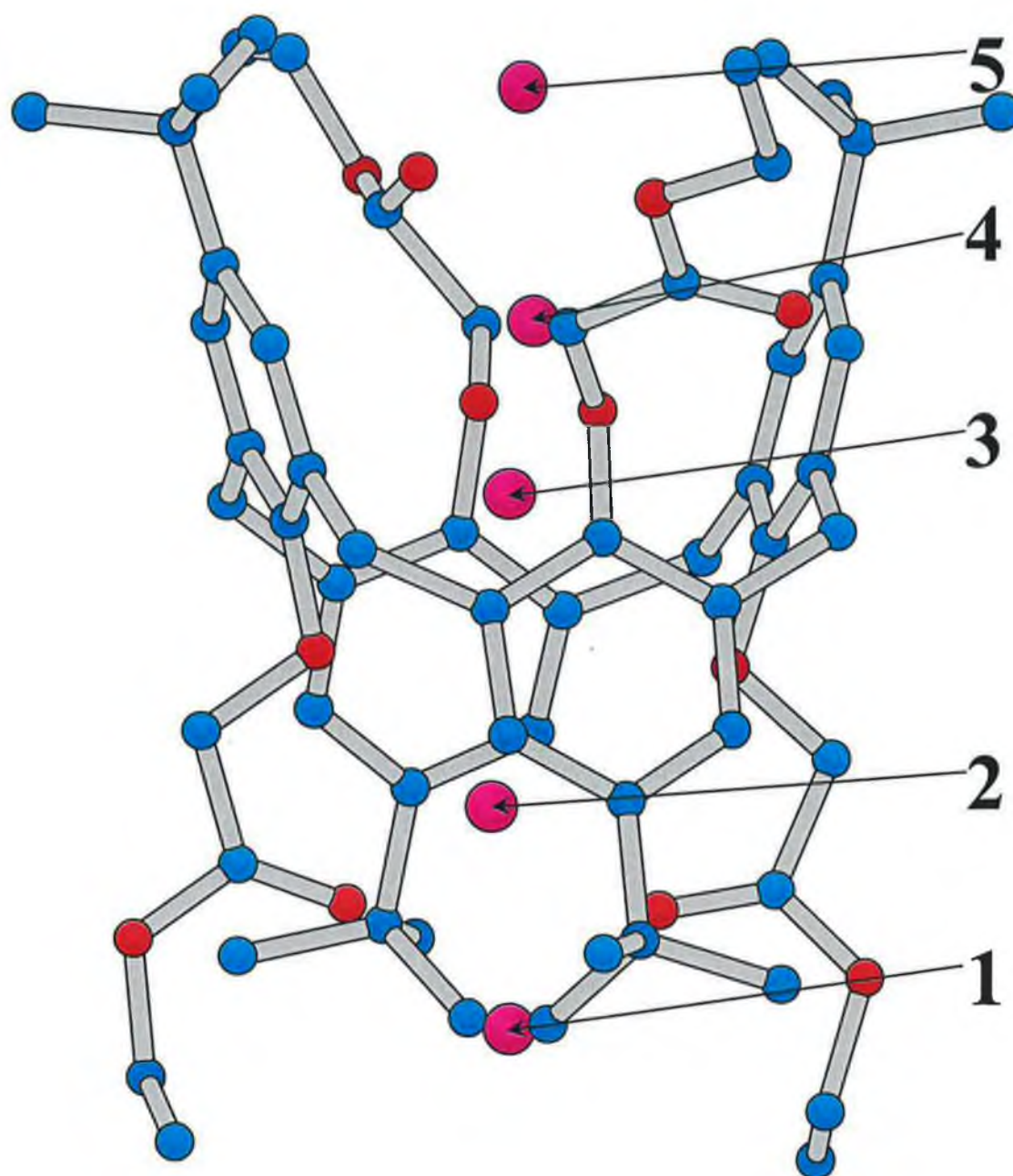
Figure 2-7. *Ball and tube rendering of the side-on view of the X-ray structure of C 2-1:Na⁺, showing the different positions in which the Na⁺ ion was initially placed when carrying out the optimisations. In the X-ray structure, the Na⁺ ion is in Position 2.*
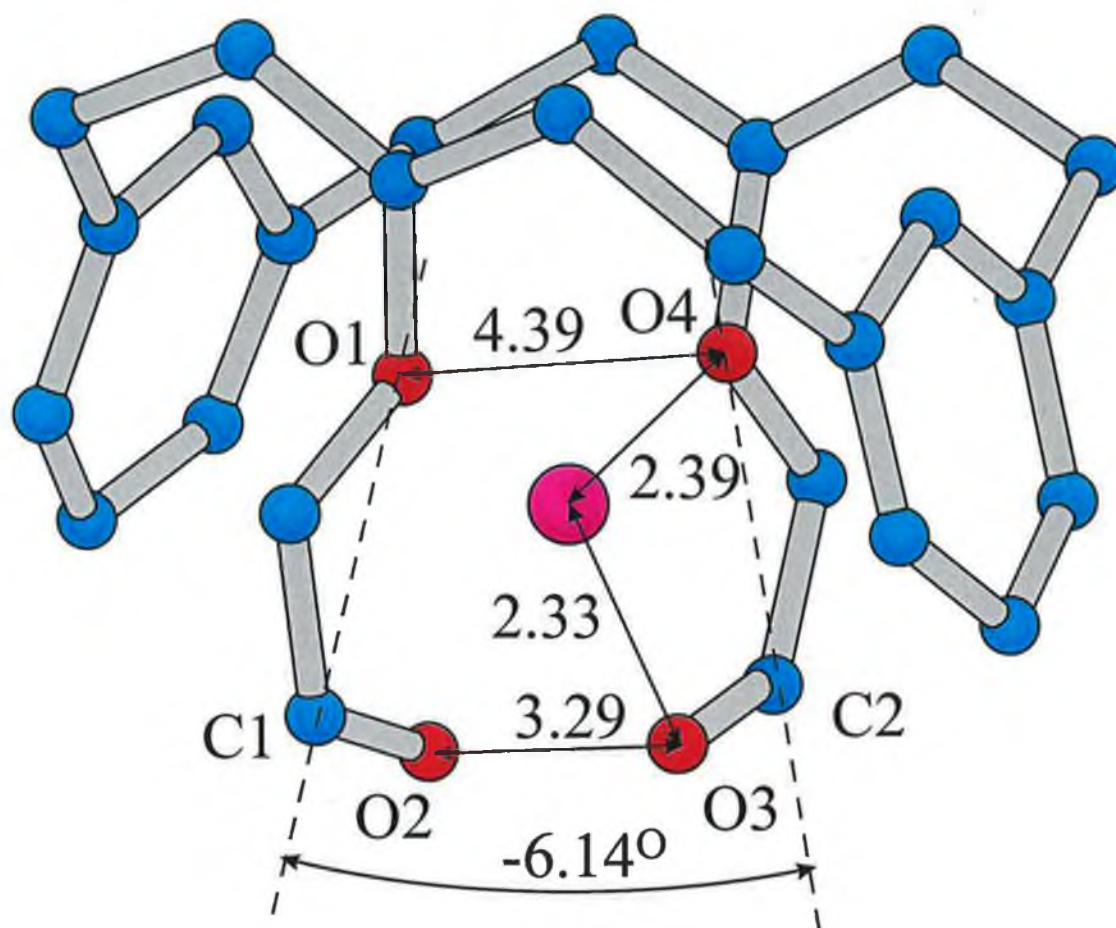
Figure 2-8. *Ball and tube rendering of the side-on view of the X-ray Structure of C 2-1:Na⁺, showing the geometry of the complex in the region of the cation. The metal to ligand distances shown, given in Angstroms, are mean distances, for oxygen atoms of a given type. The measurements shown are also given in Table 2-2. Colour code: cyan - carbon, red - oxygen, magenta - sodium.*
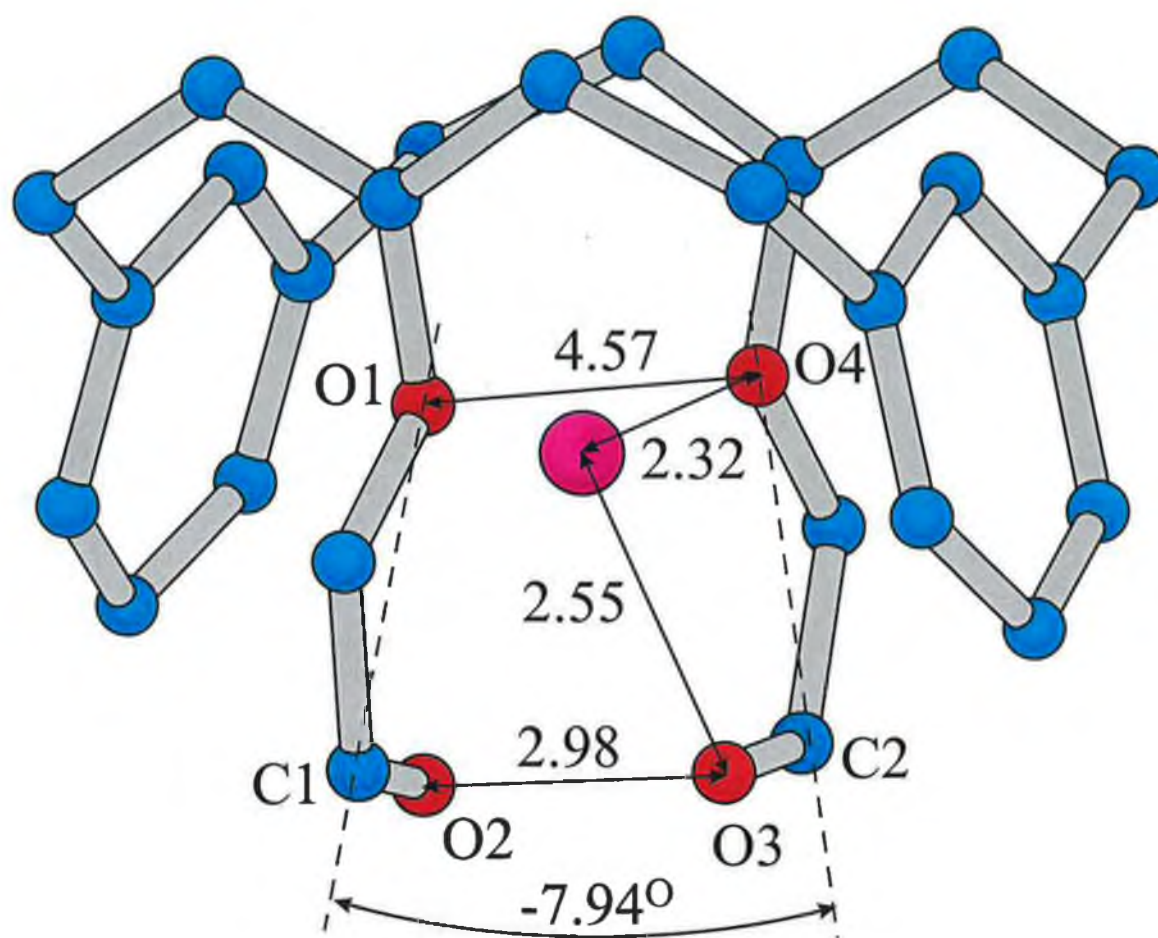
Figure 2-9. *As for Figure 2-8, except that the optimised structure of C 2-1:Na⁺ is shown, in the region of the cation. The ion was initially placed in Position 2 and AM1 partial charges were assigned to the ligand with Method 1.*
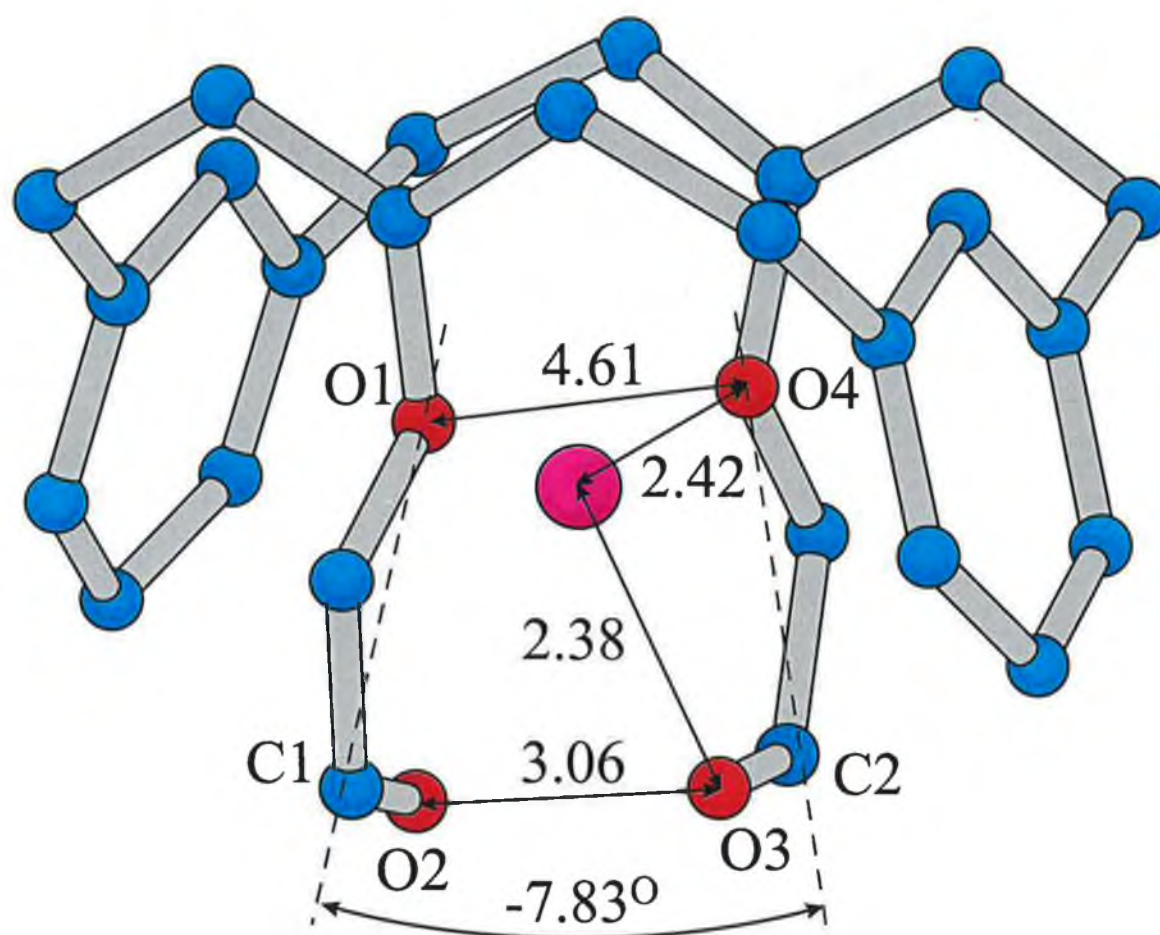
Figure 2-10. *As for Figure 2-9, except that the optimised structure shown has PM3 partial charges assigned with Method 2.*
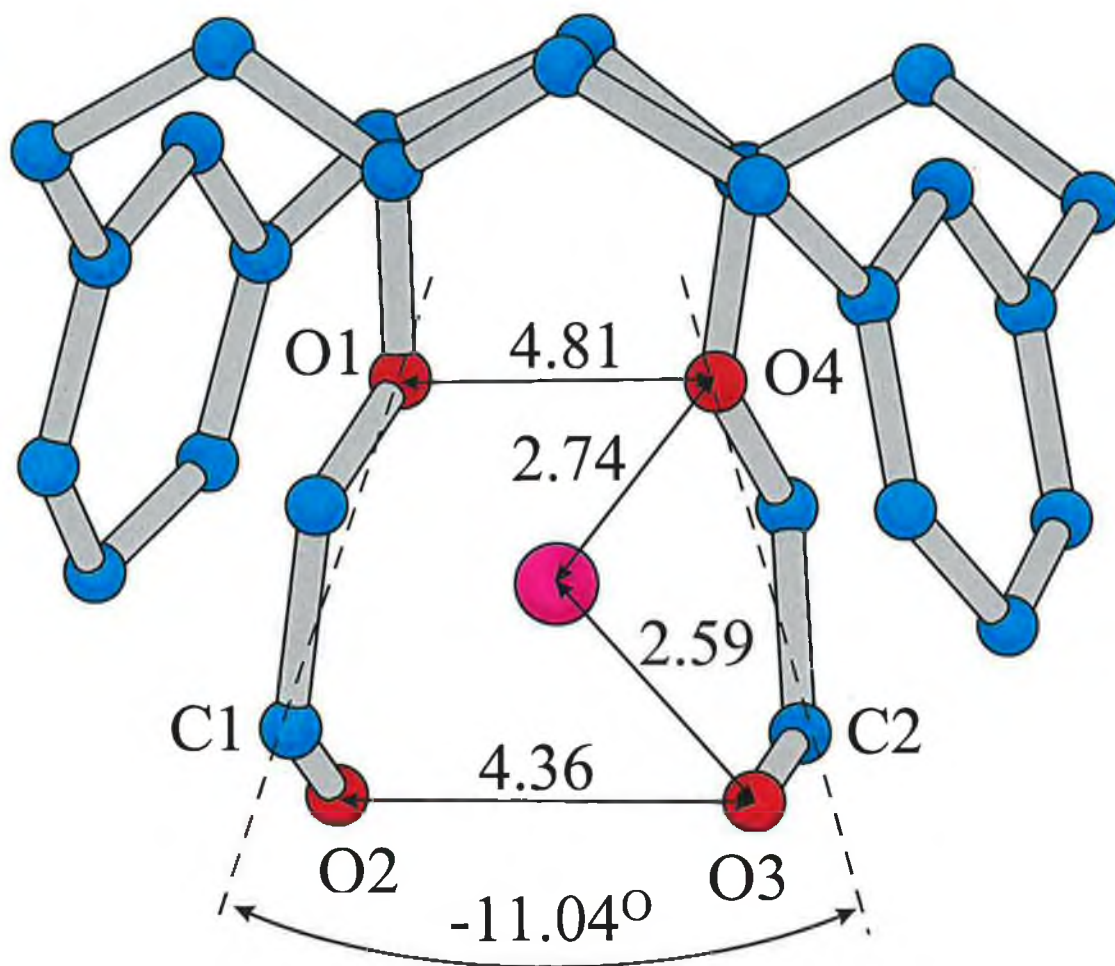
Figure 2-11. *As for Figure 2-10, except that the optimised structure shown has INDO partial charges assigned with Method 3.*

2.6.   Compounds

t-Bu   t-Bu

OR^1 OR^1

O1   O4

C1   C2

OC$_2$H$_5$ O2   t-Bu   t-Bu   O3   OC$_2$H$_5$

$$R^1 \quad = \quad CH_2 \overset{\overset{\displaystyle O}{\|}}{} \!\!\!\!-OC_2H_5$$

C 2-1

t-Bu   t-Bu   t-Bu   t-Bu

OR^2 OR^3 OR^3 OR^2

$$R^2 \quad = \quad R^3 \quad = \quad CH_2 \overset{\overset{\displaystyle O}{\|}}{} \!\!\!\!-OCH_3$$

C 2-2
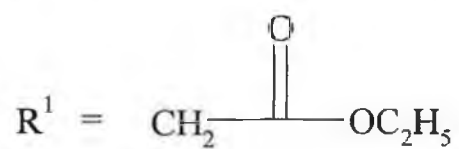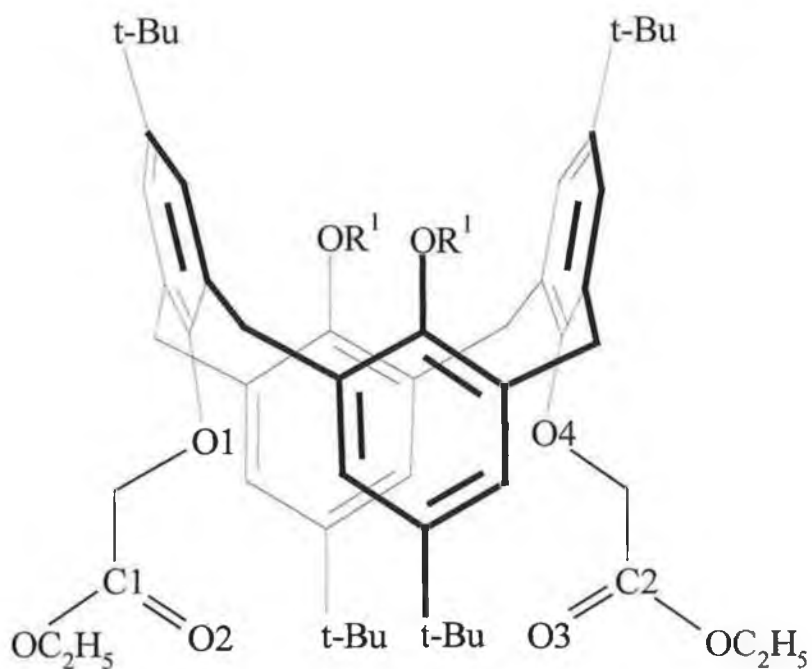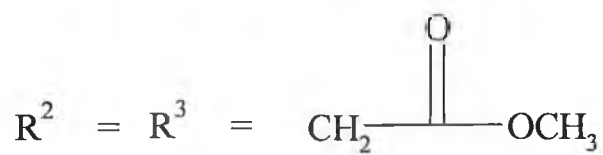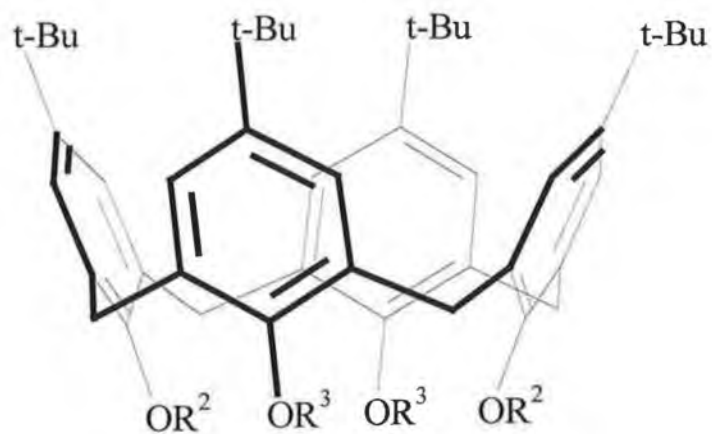
82

2.7. Location Of Files

Description	Computer	Directory	File Name	Comment(s)
HyperChem files	Dell Pentium Pro 180 PC	C:\ _Paddy\ Mol Mod\ All Parallel Start\ Yerfik\ Last Bloody Attempt	*.hin (structures) and *.log (record of optimisations)	
Reprint of Paper (in Adobe Acrobat format): *Modelling ... Conformation*"				

2.8. References

1.   N. L. Allinger, *J. Am. Chem. Soc.*, **1977**, 99, 8127.

2.   N. L. Allinger and U. Burkert, "*Molecular Mechanics*", American Chemical Society, 1982.

3.   Hyperchem is available from Hypercube, Inc., 1115 N.W. 4th Street, Gainesville, Florida, 32601 U.S.A.

4.   a) M. J. S. Dewar and W. Thiel, *J. Am. Chem. Soc.*, 1977, **99**, 4899; b) M. J. S. Dewar and M. L. McKee, *ibid.*, 5231; c) M. J. S. Dewar and H. Rzepa, *J. Am. Chem. Soc.*, **1978**, 100, 58.

5.   W. Thiel, *Tetrahedron*, **1988**, 44, 7393.

6.   M. J. S. Dewar, E. G. Zoebisch, E. F. Healy and J. J. P. Stewart, *J. Am. Chem. Soc.*, **1985**, 107, 3902.

7.   M. J. S. Dewar and K. M. Dieter, *J. Am. Chem. Soc.*, **1986**, 108, 8075.

8.   J. J. P. Stewart, *J. Comp. Aided Mol. Design*, **1990**, 4, 1.

9.   Private communication with A. J. Holder, Dept. of Chemistry, University of Missouri-Kansas City, Kansas City.

10.   J. J. P. Stewart, *J. Comp. Chem.*, 1989, **10**, 209.

11.   J. J. P. Stewart, *ibid*, 221.

12.   a) L. C. Groenen, J.-D. van Loon, W. Verboom, S. Harkema, A. Casnati, R. Ungaro, A. Pochini, F. Ugozzoli and D. N. Reinhoudt, *J. Am. Chem. Soc.*, **1991**, 113, 2385; b) P. D. J. Grootentuis, P. A. Kollman, L. C. Groenen, D. N. Rienhoult, G. J. van Hummel, F. Uggozoli and G. D. Andreeti, *J. Am. Chem. Soc.*, **1990**, 112, 4165; c) D. L. Stewart, M. Krawiec, R. P. Kashyap, W. H. Watson and C. D. Gutsche, *J. Am. Chem. Soc.*, **1995**, 117, 586; d) P. Nieri, M. Foti, G. Ferguson, J. F. Gallagher, B. Kaitner, M. Pons, M. Antonia Molins, L. Giunta and S. Pappalardo and P. D. J. Grootentuis, *J. Am. Chem. Soc.*, **1992**, 114, 7814.

13.   a) P. Guilbaud, A. Varnek and G. Wipf, *J. Am. Chem. Soc.*, **1993**, 115, 8298; b) P. Guilbaud and G. Wipf, *J. Mol. Struct., (Theochem)*, **1996**, 366, 1,55.

14.   K. B. Lipkowitz and G. Pearl, *J. Org. Chem.*, **1993**, 58, 6729 and references contained therein.

15.   S. E .J. Bell, M. A. McKervey, D. Fayne, P. Kane and D. Diamond, *J. Mod. Model.*, **1998**, 4, 44.

16.   P. Kane, D. Fayne, D. Diamond, S. E .J. Bell and M. A. McKervey, , *J. Mod Model.*, **1998**, in press.

17.   a) D. Diamond, G. Svehla, E. M. Seward, M. A. McKervey, *Anal. Chim. Acta*, **1988**, *204*, 223p; b) A. M. Cadogan, Diamond, D. Smyth, M. R. Deasy, M. M. A. McKervey and S. J. Harris, *Analyst*, **1989**, *114*, 1551.

18.   A. Ikeda, H. Tsuzuki, S. Shinkai, *Tetrahedron Lett.*, **1994**, 35, 8417.

19.   a) G. Calestani, F.Uggozoli, A Arduini, E. Ghidini and R. Ungaro, *J. Chem. Soc., Chem. Commun.*, **1987**, 344. b) A. Arduini, E.Ghidini., A.Pochini, R. Ungaro, G. Andreeti, G. D. Calestani and F. Uggozoli, *J. Incl. Phenom.*, **1988**, *6*, 119.

20.   a) This crystal structure is available from the Cambridge Crystallographic Data Centre, 12 Union Road, Cambridge CB2 1EW, UK, e-mail: deposit@ccdc.cam.ac.uk b) F. H. Allen and O. Kennard, *Chem. Des. Auto. News*, **1993**, *8*, 1 & 31-37.

21.   J. A. Pople, D. P. Santry and G. A. Segal, *J. Chem. Phys.*, **1967**, *47*, 2026.

22.   a) J. A. Pople, D. P. Santry and G. A. Segal, *J. Chem. Phys.*, **1965**, *43*, S129; b) J. A. Pople, D. P. Santry and G. A. Segal, *ibid.*, S136. c) J. A. Pople, D. P. Santry and G. A. Segal, *J. Chem. Phys.*, *ibid*, 3289.

23.   W. D. Anderson, W. P. Edwards and M. C. Zerner, *Inorg. Chem.*, **1986**, *28*, 2732.

24.   N. L. Allinger, *J. Am. Chem. Soc.*, **1977**, *99*, 8127.

25.   A. Ikeda and S. Shinkai, *J. Am. Chem. Soc.* **1994**, *116*, 3102.

26.   P. D. J. Grootenhuis and P. A. Kollmann, *J. Am. Chem. Soc.* **1989**, *111*, 2152.

27.   AMBER, v. 5 is available from Oxford Molecular. In the USA: e-mail: products@oxmol.com. In the UK: e-mail: products@oxmol.co.uk. More information on AMBER can be found at: http://www.amber.ucsf.edu/amber/ and http://www.oxmol.co.uk/prods/amber/.

28.   P. Komba and T. W. Hambley, "Molecular Modelling Of Inorganic Compounds", VCH, Weinheim, 1995.

3. Conformational Analysis of Complexes of Calix[4]arenes with Group 1 and Group 2 Cations

3.1. Introduction

Ever since the discovery of calixarenes,[1] much interest has focussed on exploiting the structural features which allow them to act as potential hosts for guest molecules. This feature is extremely important in sensors, where the ability to selectively bind one particular molecule or ion over another is extremely important. Several sensors and separation processes have successfully utilised calixarenes in this regard.[2]

The ability to predict the selectivity of as yet unknown calixarenes for certain ions or molecules has an enormous advantage over the intuitive approach currently used in designing new receptors, as this is hugely inefficient, because of the time and effort involved. Understanding the interactions and type of complexation which occur in a calixarene complex is of great assistance in predicting the selectivity of a calixarene.

The use of phosphine oxides for use as extractants has been long established.[3] Potentiometric studies on **C 3-1** (see Figure 3-2), presented in this chapter, indicate that it has a poor ability to discriminate between the ions investigated. In contrast,

87

the tetraphosphine oxide calix[4]arene, **C 3-2**, is known by potentiometric and optical studies to be selective for Ca^{2+} in the presence of Na^+, Li^+ and Mg^{2+}.[4] Potentiometric studies have also been used to establish that the tetraester calix[4]arenes, **C 3-3**[5] and **C 3-4**,[6] are known to selectively bind Na^+ in the presence of several common interfering ions such as Li^+, Na^+, K^+ and Mg^{2+}.

The study described here uses Monte Carlo conformational searches in combination with molecular mechanics to model the complexation of the four calixarenes mentioned above with several Group 1 and Group 2 cations, specifically Li^+, Na^+, K^+, Mg^{2+} and Ca^{2+}. Conformational searching is very relevant to the modelling of **C 3-1** and **C 3-2** because of the possibility that the bulky phenyl groups could prevent simple geometry optimisations from finding new, lower-energy minima. The difference in molecular structure between **C 3-3** and **C 3-4** lies *outside* the calixarene cavity (where cations are usually bound) and thus, it would be of interest to determine if conformational searching can provide one with information on any differences in how these two ligands bind with cations.

In general, conformational searches are conducted as described in the flowchart given in Figure 3-1. The purpose of constraint tests is to eliminate conformers that have inverted chiral centres or which have two or more pairs of atoms that are too close to one another.

The various methods used to carry out conformational searches can be classified in a number of ways. Firstly, in the way they sample the conformational space available - systematically or randomly. Although the systematic searches guarantee to cover all regions of the conformational space, the amount time required to do so is prohibitive for many molecules if it is desired to cover the space at a high resolution.

Another way of classifying conformational searches is according to the type of variable used to generate starting geometries. Methods based on varying torsional angles (internal co-ordinates),[7] cartesian co-ordinates (external co-ordinates)[8] and internuclear distances (distance geometry)[9] have been developed. In these cases the variables involved are changed in an arbitrary fashion. In contrast, molecular dynamics simulations have also been used to carry out conformational searches.

While this latter method will also give very useful information about how the conversion from one conformer to another occurs and associated thermodynamic properties, it is slow relative to the other methods and on the evidence of Saunders, *et. al.*[10] is less effective at finding conformers.

Varying internal co-ordinates - the method used in this chapter - is an obvious way of varying the starting geometry, as conformational isomers differ primarily in their torsional angles. In contrast, the bond lengths and bond angles of these isomers vary relatively little.

The Monte Carlo (MC) method is a commonly used random method for conformational searching and the variations on it are classified according to the procedure used for the selection of starting structures. The various MC methods have been assessed by Chang, *et. al.*[11] The Metropolis MC method[12] is used in this chapter. This method involves choosing conformations with a probability $\exp(-E/kT)$, where E is the energy of a configuration, k the Boltzman constant and T is the temperature of the system in degrees kelvin. This is done by choosing a minimised conformer which could be described in terms of torsional angles, for example, and labelling each torsional angle X, Y, etc., and deforming this conformation (by varying a randomly selected torsional angle, for example) by a random amount:

$$X \quad \rightarrow \quad X \quad + \quad \alpha\varepsilon_1$$

where α is the maximum allowed displacement and ε_1 is a random number between -1 and 1.

Then the deformed structure is geometry optimised and if the energy of the resulting conformation is lower in energy than the starting conformer, the new structure is saved. If it is higher in energy a random number between 0 and 1, ε_2, is chosen and the particle is put in the new position if $\varepsilon_2 < \exp(-E/kT)$. Otherwise, it is returned it to its old position. This step is repeated for a specified number of steps or until the structures found begin to duplicate.

This method is based on the hypothesis that low-energy conformers have geometries that are more closely related to one another than that of higher-energy conformers.

However, the method is biased against finding conformers whose geometry is very different to the starting structure but which have similar or lower energies.

The Random Walk method is an MC method that works by simply starting with the latest geometry, providing that its energy is within a pre-defined limit (for example, 25 kcal mol^{-1}) of the lowest-in-energy conformer found so far. Another global search method is the so-called Usage-Directed method which records the frequency with which each starting structures has been used and then selects the structure which has been used the least or which has the lower energy, in that order of priority. This ensures that each conformer is used the same number of times (± 1). Chang *et. al.*,[11] report, that the Usage-Directed method was the most effective in terms of the number of unique structures found and the standard deviation in the energies of these conformers. However, it should be pointed out that the structures used to make the comparison between the different search methods - *n*-octane and cyclotetradecane - are relatively small and symmetric, which would make it relatively easy for the search methods to find duplicate structures and search as much as the conformational space as possible.

Changes in conformation of the calixarene upon complexation will be studied using NMR spectroscopy. A change in the chemical shift of the methylene bridging and the *t*-butyl protons should be seen upon complexation if the conformational change in the ligand is great enough. There should be no further change in the spectrum should stop when all the calixarenes are complexed to the cations and hence addition of more salt should have no effect on the calixarene conformation. This should allow the stoichiometry of the complexes to be determined.

3.2.   Experimental

3.2.1.   Potentiometric Measurements

The experimental work that is described in this section refers to work carried out on the calixarene phosphine oxides **C 3-1**, **C 3-2**, **C 3-5** and **C 3-6**. The potentiometric work that was carried out on the calixarene esters **C 3-3**[5] and **C 3-4**[6] has been previously described. The methods used to determine the potentiometric selectivity

of the phosphine oxides differ slightly to that used for **C 3-3** and **C 3-4**, the main difference being that non-linear analysis was used to treat the results in the case of the phosphine oxides, while a graphical method was used for the esters. The increase in sophistication is reflected in the fact that the log of potentiometric selectivity coefficients for the phosphine oxides are expressed to one more decimal place than that of esters. The effectiveness of non-linear analysis for the determination of ion-selective electrode characteristics has been demonstrated[13] and this work is reproduced in Chapter 4.

Materials

All metal chlorides used were of analytical reagent grade. High molecular weight PVC, lithium chloride, potassium chloride, tetrahydrofuran, bis(2-ethylhexyl)sebacate (DOS) and potassium tetrakis(4-chlorophenyl)borate (KTpClPB) were purchased from Fluka. Magnesium chloride, calcium chloride and barium chloride were purchased from BDH. Sodium chloride, ammonium chloride and sodium perchlorate were purchased from Riedel de Haen. Milli-Q grade distilled water from Millipore was used throughout. **C 3-1** and **C 3-2** were synthesised using the method previously described.[14]

Apparatus

Calcium-selective electrodes were prepared according to the procedure of Lu *et. al.*[15] The typical membrane composition was ionophore 0.66 % m/m, ion-exchanger, potassium tetra-*p*-chlorophenylborate (KTpClPB) 0.13 % m/m, plasticiser (DOS) 65.9 % m/m and PVC 33.3 % m/m. Membrane resistance and potential measurements were made with a Hewlett Packard 34401 A multimeter and a standard calomel electrode (SCE) as a reference, obtained from EDT Instruments, Ltd., Lorne Road, Dover, Kent, UK.

Procedure

The ISE and the SCE were placed in 25.0 cm^3 of a 0.01 mol dm^{-3} aqueous solution of an interfering chloride, for example, sodium chloride. Aliquots (2, 5, 20, 45, 70 and 100 μdm^3) of one mixture (0.01 mol dm^{-3} primary chloride, i.e., calcium chloride

91

(aq.), 0.01 mol dm⁻³ interfering chloride (aq.)) and then another mixture (5, 15, 30, 100, 400 and 1000 μdm³), (1.00 mol dm⁻³ calcium chloride (aq.), 0.01 mol dm⁻³ interfering chloride (aq.)) were added in the order given. These additions were made with micropipettes, keeping the tip of the micropipettes just above the surface of the solutions while making the addition.   The solution was stirred magnetically throughout. After each addition, the potential of the solution was recorded after 1 minute. After all additions had been made, the entire procedure was repeated twice. In this manner, the Ca^{2+} concentration was varied over a very wide range (8.0 x 10⁻⁷ to 0.06 mol dm⁻³) while the interfering ion concentration was kept constant without having to transfer the electrodes to new solutions.

This procedure was repeated for other interfering ions (Li^+, Na^+, K^+ and Mg^{2+}).

Treatment of Potentiometric Results

The potential, *E*, of a calcium-selective electrode in the presence of both Ca^{2+} and an interfering ion, B^{z+}, is given by the Nikolskii-Eisenman (N-E) equation:

$$E = E^0 + S \log \left(a_{Ca} + k_{CaB}^{Pot} \, a_B^{\,2/z} \right) \qquad\qquad (3\text{-}1)$$

where: E^0 is the Cell Constant

S is the Nernstian Slope Factor

k_{CaB}^{Pot} is the potentiometric selectivity coefficient

a is activity of the subscripted ion.

z is the ionic charge on the interfering ion.

The method of treatment of results is described in more detail in Chapter 4 but briefly, non-linear curve fitting was carried out to fit the mean experimental values (n = 3), when corrected for the effect of the liquid junction potential, using the Henderson formula[16] using single-ion activities, to the N-E model (Eqn. (3-1)). The curve fitting was carried out using the optimisation add-in, *Solver*, available in Microsoft Excel for Windows 95, version 7.0 and the method of Walsh and Diamond.[17] The mean experimental potentials when corrected and those obtained by *Solver* are plotted in Figure 3-3 a-d for **C 3-2** and the corresponding residual error plots are given in Figure 3-4 a-d. The response curves and residual error plots

obtained for **C 3-1**, **C 3-5** and **C 3-6** were of a similar form. The non-linear analyses yielded values for the potentiometric selectivity coefficients and these are given in Table 3-5 and Figure 3-5 for the phospine oxides and in Table 3-6 for the esters.

3.2.2.   *Molecular Modelling*

All molecular modelling calculations were carried out using *Spartan*[18] SGI Version 5.0.1. The simulations were run on an *Silicon Graphics O2* workstation with a MIPS R10000 Rev. 2.7, 195 MHz CPU running an IRIX operating system, Release 6.3, with 128 MB RAM.

The Monte Carlo algorithm was used in conjunction with the Merck Molecular Force Field (MMFF)[19] for the conformational searches. The conformational searches were carried out *in vacuo*. (It must be noted that structures containing ions or polar groups, such as the complexes under investigation here, are very likely to adopt conformations in *in vacuo* optimisations that maximise intramolecular attractive forces. However, it seems quite probable that in the presence of a solvent, these attractive forces would not be as great and many of them are likely to be replaced by solvent-ion or solvent-ligand forces of attraction. As a result, the modelled structures obtained when a solvent is included in the calculations may be so different from the *in vacuo* results, that entirely different conclusions may be drawn in attempting to explain the results of the selectivity studies). However, simulation of the PVC membrane matrix used in these studies is likely to be very difficult.

Molecular modelling studies were carried out on each of the compounds shown in Figure 3-2, each with Ca^{2+}, K^+, Na^+, Li^+ and Mg^{2+}.

All torsional angles in each pendant groups in the lower rim of each ligand were specified as torsional angles to be varied in the conformational searches. The following conditions were also used:

- The maximum difference in correlated distances between two
  conformations that are considered as duplicates: 0.25 Å

- Simulation Temperature: 298 K

93

- The number of conformers involved in the search: 35

- The maximum number of cycles: 100

- Number of bonds that were rotated per each Monte Carlo cycle   One

- Terminating gradient for minimisations: 1×10^{-5} kcal mol^{-1} $Å^{-1}$

The free ligand of the calixarene was conformationally searched and the global minimum resulting from this search was used as input when carrying out the conformational search of the complex. The searches were repeated with different initial positions: above the phenoxy oxygen atoms, below the phosphine oxide groups for **C 3-1** and **C 3-2** (or below the carbonyl groups for **C 3-3** and **C 3-4**) and intermediate between these two positions. These positions are illustrated in Figure 3-6.

All the starting conformations were geometrically optimised, via the *Minimise* module in *Spartan*, which minimises the structure based on the default force field, TRIPOS,[20] before being submitted for the conformational search.

3.2.3.   *^1H NMR Titrations*

^1H NMR titrations were carried out on the **C 3-2**:Ca^{2+}, **C 3-2**:Na^+, **C 3-4**:Ca^{2+} and **C 3-4**:Na^+ complexes in order to determine the stoichiometry of complexation by the calixarenes. The calixarene was dissolved in $CDCl_3$ and the cation salt was dissolved in CD_3OD.

Two salts were used for complexation - calcium chloride and sodium perchlorate.

Five 50 μdm^3 aliquots of a 0.1 mol dm^{-3} salt solution in CD_3OD were shaken with 0.5 cm^3 of a 20 mmol dm^{-3} solution of the calixarene in CD_3Cl_3 in the NMR tube, to give cation:calixarene mole ratios of 0:1, 0.25:1, 0.5:1, 1:1, 1.5:1 and 2:1. The ^1H NMR of each of these mixtures were then taken. A set of 'control' NMR titrations was also run, CD_3OD was substituted (with no salt added) in place of the salt solution in the above procedure. This allowed for the identification and compensatation for solvent dependent effects.

94

The NMR spectra were recorded on a Bruker Aspect 400 Series fourier transform spectrometer, operating at a frequency of 400 MHz.

3.3.   Results and Discussion

3.3.1.   *Potentiometric and Molecular Modelling Results*

General:- Potentiometric Measurements

Before testing newly fabricated electrodes, the membrane integrity was assessed by measuring the d.c. resistance. These were found to lie in the range 1.6 to 1.7 MΩ, which is typical for PVC-membrane ISE's.[21]

The response curves, plotted in Figure 3-3 a-d, show that the models fit the experimental very well. These plots also show good agreement between the mixed ion potentials and the calibration potentials at high Ca^{2+} activity as would be expected.

The residual error plots are given in Figure 3-4. They do show a sinusoidal trend, indicating that there may be some assignable cause affecting the error in the results. Similar plots were obtained for **C 3-1**.

General:- Molecular Modelling

It is encouraging to note that the position of the ion in the lowest-energy conformer of the complexes was not affected by the initial position in which the ion was placed. For example, for a given complex, the final position of the ion varied by less than 0.02 Å. Equally encouraging is the fact that the conformers found in the region of the global minimum, have a geometry that is virtually identical and they two successive conformers differ in energy by typically 1×10^{-5} kcal mol^{-1}. This would suggest that the conformational searches were effective in sampling the conformation space in the region of the global minimum.

While it is always possible that other conformational states exist with energies greater than the global minimum, that are significantly populated but which were not found by the simulations, it was found that significant changes to the geometry of the

95

complexes (for example, four-fold to three-fold co-ordination) occurred only when for those torsional states which were greater in energy from the global minimum energy by typically 3 kcal mol^{-1}. However, a Boltzmann population analysis (based on the assumption that the different torsional states have the same degeneracies) estimated that the population of such a state relative to that of the ground state, is 0.006.

Therefore, for all of the complexes modelled, I feel justified in discussing only the model of the conformer that is lowest in energy. This conformer will be referred to as the GMC (global minimum conformer) for the remainder of this chapter.

C 3-1

The results of the molecular modelling studies suggest that two different modes of complexation occur between the cations studied and **C 3-1**. Firstly, the model of the GMC of **C 3-1**:Li$^+$ (see Figure 3-7), shows that the cation is positioned at the bottom of the calixarene at a distance of 1.83 Å (see Table 3-1) from the three closest phosphine oxide oxygen atoms. The model of the GMC of **C 3-1**:Mg^{2+} (not shown) suggests that the cation is complexed in a similar mode to Li$^+$ by this ionophore.

The lithium - oxygen distance of 1.83 Å discussed above is less than the lithium - ether oxygen distances of 1.95 - 2.14 Å found in the X-ray structures of calixarene:lithium complexes.[22,23] (These and other X-ray structures of calixarene:cation complexes were obtained from the Cambridge Crystallographic Data Centre (CCDC) and the cation to ligand distances in such structures are given in Table 3-7 of the Supplementary Data section). However, such differences may be due to the fact that the calixarenes in these X-ray structures did not contain phosphine oxide groups. These differences may be due to the fact, on electronegativity grounds, that a phosphine oxide oxygen atom is probably a better electron donor than an ether oxygen atom, and because the cation - dipole bonds associated with phosphine oxide bonds in the models are much more directional than that associated with the carbon - ether oxygen bonds, causing the Li$^+$ ion to be drawn closer to the phosphine oxide oxygen atoms than they typically would be to an ether

96

oxygen atom. (The effect of the directional nature of cation - dipole bonds are explained on p. 23. See also Figure 1-2.)

The models indicate that neither Li^+ or Mg^{2+} are co-ordinated by all four of the phosphine oxide groups in **C 3-1**. Instead, a three-fold co-ordination was found with the pendant chain that is least involved in binding the cation being forced outward. That the interaction of **C 3-1** with Li^+ and Mg^{2+} is three-fold rather than four-fold is possibly due to the interaction between the relatively large phenyl groups on different pendant chains as the phosphine oxides try to co-ordinate to the relatively small Li^+ and Mg^{2+} cations (the ionic radii of the ions modelled are quoted in **Error! Reference source not found.**, which is part of the Supplementary Data section). It would appear that the three-fold co-ordination allows the phosphine oxide oxygen atoms to get close enough to the relatively small cations and at the same time minimises the steric crowding effect of the phenyl groups.

In contrast, the modelling indicated the other cations studied (Ca^{2+}, Na^+ and K^+) are co-ordinated by both the phenoxy and the phosphine oxide oxygen atoms, i.e., the other mode of complexation consists of an eight-fold co-ordination to the cation. These three ions are larger than the Mg^{2+} or Li^+ ions and therefore, it is not surprising that the molecular models of the **C 3-1** complexes formed with these cations indicate that the phosphine oxide oxygen atoms are, on average, approximately 0.5 Å further away from these cations than is the case with Li^+ or Mg^{2+}. The distance from the phosphine oxide oxygen atoms to the Ca^{2+} and Na^+ ions are approximately equal (2.36 and 2.38 Å, respectively), increasing slightly to 2.46 Å for K^+. The models of the complexes formed by **C 3-1** with Ca^{2+}, K^+ and Na^+ (see Figure 3-9 for the Ca^{2+} complex and Table 3-1), indicate that the mean distance from the phenoxy oxygen atoms to the cation was in the range 2.80 - 2.85 Å for all the three complexes. The similarity of both the cation-ligand distances and the co-ordination number for the complexes formed by these three cations with **C 3-1** would support the conclusion drawn from the potentiometric results, given in Table 3-5 and Figure 3-5, which show that the ligand has a relatively poor ability to discriminate between the primary ion (Ca^{2+}) and the other two interfering ions, K^+ and Na^+. The distances from the cation to the phenoxy oxygen atoms are greater than cation to ether-oxygen

97

distances, obtained from X-ray structures of calixarene:cation complexes, which indicate cation to ligand distances of 2.30 - 2.39 Å (6 structures) for sodium,[24] 2.57 - 2.87 Å (5 structures) for potassium[25] and 2.31 Å (1 structure) for calcium[26]. However, these calixarenes did not contain phosphine oxide groups and this may explain the differences.

The distances between the facing aryl rings of the models of **C 3-1** and its cation complexes, given in Table 3-1, suggest that the symmetry of the macrocyclic part of the ligand changes from C_{2V} to C_{4V} upon complexation with Ca^{2+}, K^+ or Na^+. The two distances between opposite aromatic rings of the macrocyclic ring were essentially the same (7.8 - 7.9 Å) for the models of these three cations, whereas these distances were 9.73 Å and 5.41 Å (Li^+) and 9.52 Å and 5.55 Å (Mg^{2+}). The C_{4V} symmetry for the ligands in their the complexed forms are best illustrated in Figure 3-9b (for **C 3-1**:Ca^{2+}) and in Figure 3-10b (for **C 3-1**:K^+). It seems likely that co-ordination by a cation to both the phenoxy oxygen atoms as well as the phosphine oxide oxygen atoms brings about the increase in symmetry, thus explaining why the macrocyclic part of **C 3-1** did not adopt this C_{4V} symmetry upon complexation with Li^+ and Mg^{2+}. The model of the GMC of **C 3-1** (see Figure 3-12) clearly shows the C_{2V} symmetry of the ligand in its 'free' form.

The average distance of the phenoxy oxygen atoms to the phosphine oxide oxygen atoms on the pendant group was in the range of 2.5 Å to 2.8 Å, which is an indication of the size of the cavity. This is relatively small, compared to the cavity size in **C 3-2** (see Section 0).

C 3-2

Potentiometric studies showed that **C 3-2,** in contrast to **C 3-1,** was much more selective for the calcium against the species ions investigated, with the exception of sodium. Furthermore, it is interesting to note that the potentiometric selectivity coefficients obtained for **C 3-1** for the singly-charged interfering ions, follow a different trend to that obtained for **C 3-2** and two calix[5]arenes, **C 3-5** and **C 3-6** (the logarithmic values are given in Table 3-5 and plotted in Figure 3-5). As Figure 3-5 very strikingly indicates, the trends of the potentiometric selectivity coefficients

of these calcium-selective phosphine oxides would appear to be strongly related to the number of methylene groups between the phenoxy oxygen atoms and the phosphorous atoms in each pendant group. **C 3-1** has one such methylene group, while **C 3-2**, **C 3-5** and **C 3-6**, all of which have two such groups.

Significantly, the model of the GMC of **C 3-2**:Ca^{2+} complex, given in Figure 3-14, obtained in this study has a geometry which is far more uniform than that of the other **C 3-2** complexes modelled and this is a strong indication of why **C 3-2** exhibits such a strong preference for the Ca^{2+} against the other ions. The **C 3-2**:Ca^{2+} model indicates that the phenoxy oxygen atoms are separated from the ion at similar distances to the phosphine oxide oxygen atoms (see Table 3-2), i.e., co-ordination is eight-fold. Table 3-2 also indicates that the ion in the other **C 3-2** complexes modelled is bound by almost entirely by the phosphine oxide groups and that the co-ordination is at most three-fold. Furthermore, upon inspection of Table 3-2, it is very noticeable that the standard deviations in all the critical distances for the **C 3-2**:Ca^{2+} complex are never greater than 0.01 Å, and that this is the only **C 3-2** complex modelled, for which this is true (for example, the phenoxy oxygen -phosphine oxide oxygen separation is 2.89 ± 0.01 Å, i.e., the small range over which this distance varies indicates just how well the Ca^{2+} ion fits the cavity created by the eight oxygen atoms and the four intermediate methylene groups). This is in contrast to the models obtained for the **C 3-2** complexes formed with sodium (see Figure 3-16 and Figure 3-17)[a] and potassium (see Figure 3-18), as these models indicate that these two ions are not bound by all eight oxygen atoms in **C 3-2**.

The model of the **C 3-1**:Ca^{2+} complex indicates that the co-ordination is also eight-fold. However, this is not unique among the **C 3-1** complexes - the models indicate that eight-fold co-ordination is observed upon complexation with Na^+ and K^+ this is strong evidence of why K^+ has the greatest interfering effect on the potentiometric signal of ion-selective electrodes constructed with **C 3-1** as the ionophore. K^+, though it is 0.2 Å larger than Ca^{2+},[30] appears to be relatively ineffective in binding

---

[a] The **C 3-2** - sodium complex was modelled as both a 1:1 complex and as a 2:1 complex because of the results of NMR titrations (see Section 0).

with **C 3-2**, perhaps because it is singly-charged. This view is reinforced by the fact that when a model of a **C 3-2**complex with K^+ having eight fold co-ordination was generated by a geometry optimisation (figure not shown), the energy of the complex increased by 175 %.

Thus, the modelling of the **C 3-1** and **C 3-2** complexes have produced very clear and positive evidence of why **C 3-2** discriminates between the primary ion (Ca^{2+}) and the interfering ions and does so to a far greater extent than **C 3-1**.

It should be stated that the model obtained in this study of the **C 3-2**:Ca^{2+} complex is very different to a previous model,[4b] which was generated by carrying out a geometry optimisation with the *HyperChem* software[27] on a personal computer. The optimised structure obtained with this method indicated that the ion was complexed in the region of the phosphine oxide groups and the difference in the latter result and that obtained in this new study emphasises the advantage of carrying out conformational searches, as opposed to geometry optimisations of single structures, the results of which are dependent on the starting geometry.

The models of the **C 3-2** complexes formed with Li^+ and Mg^{2+} (see Figure 3-11a for **C 3-2**:Li^+) suggest that these ions are positioned in the region of the phosphine oxide groups. The distances from these two cations to the three closest phosphine oxide oxygen atoms are approximately 1.8 Å (see Table 3-2) - virtually identical to that obtained for the GMC models of the complexes formed by of Li^+ and Mg^{2+} with **C 3-1**. In the case of the model of the lithium complex, this distance is less than the literature values of 1.95 -2.14 Å for Li^+ - O distances in the X-ray structures of calixarene:cation complexes.[23] However, as discussed previously, these ligands cited in the literature do not contain phosphine oxide groups and this may account for the difference.

The model for the **C 3-2**:Mg^{2+} complex indicates that the Mg^{2+} ion is higher up in the cavity than the Li^+ ion when it is complexed by **C 3-2**, by about 0.8 Å. This is possibly due to the +2 charge of the Mg^{2+} ion, which allows the ion to co-ordinate to the phenoxy oxygen atoms more effectively than the Li^+ ion.

Interestingly, the models of the **C 3-2** complexes, apart from **C 3-1**:Mg^{2+} and **C 3-1**:Li^+, were the only models obtained for which the macrocyclic ring did not adopt a C_{4V} symmetry upon complexation – see Table 3-2. However, the **C 3-2**:Ca^{2+} complex showed a slight increase in symmetry (see Figure 3-14), with distances of 6.31 and 8.86 Å between facing phenyl rings of the macrocyclic ring, compared to the 'free' ligand for which the distances were 6.26 and 9.14 Å respectively, shown in Figure 3-13. The models also showed that **C 3-2** had a C_{2V}-like symmetry upon complexation with Li^+, but was less symmetric than the free ligand with distances between the facing phenyl rings being 5.53 and 9.85 Å (the GMC model of the lithium complex is shown in Figure 3-11).

The extra methylene group in **C 3-2** between the phosphine oxide and phenoxy oxygen atoms increases the size of the cavity (in comparison to **C 3-1**), and this appears to adversely affect the ability of **C 3-2** to bind with cations. Ironically, this results in **C 3-2** having a greater ability than to discriminate between Ca^{2+} and other ions.

C 3-3

The GMC models of all the **C 3-3** complexes indicate that the cation is bound by the four carbonyl oxygen atoms, as well as the four phenoxy oxygen atoms. The models also indicate that the macrocyclic ring of all the **C 3-3** complexes have a C_{4V} symmetry (notice the similarity in the distances between facing aryl rings, given in Table 3-4). Furthermore, of the four ligands studied, it is the only ligand for which these two features are present in models of the complexes obtained with each of the ions. (See Figure 3-17 for the two-fold symmetry of the model of the uncomplexed form of **C 3-3**).

The most obvious explanation for this is the lack of relatively bulky substituents in the pendant groups attached to the macrocycle, i.e., the models suggest that in order to accommodate some or all of the ions studied, the other ligands studied, in their complexed form, are forced to adopt a conformation that minimised the interaction between these substituents but which was less symmetrical than the 'ideal' C_{4V}.

The similarity in the mode of complexation and in the distances from the cation to the carbonyl oxygen atom and phenoxy oxygen atoms for Li^+ and Mg^{2+} is again demonstrated in the models of the GMC's of the complexes of **C 3-3** formed with these cations (see Figure 3-18 for the Li^+ complex). These models show that the Li^+ and Mg^{2+} ions have positions in the region of the carbonyl groups. On average, they are separated by 2.10 and 1.98 Å, respectively, from the carbonyl oxygen atoms, and in the case of lithium, these values are in good agreement with the values of 1.95 - 2.14 Å for lithium - oxygen distances reported with X-ray structures of calixarene:lithium complexes, even if the ligating atoms were not carbonyl oxygen atoms. Li^+ - O distances in are in the range.[23] The Li^+ and Mg^{2+} ions are separated from the phenoxy oxygen atoms by distances of 2.82 and 3.01 Å, respectively, indicating that the phenoxy oxygen atoms have a minor effect on the position of the these two ions ion in the GMC's of the complexes they form with **C 3-3**.

Table 3-3 shows that the ratios of the mean cation - phenoxy oxygen distance to the mean cation - carbonyl oxygen distance are very close to unity in the case of the complexes formed with the Na^+ and K^+ ions only. Of these two complexes, the cation-ligand distances are smaller (by ca. 0.25 Å) in the case of the Na^+ complex, which is shown in Figure 3-19, and this would indicate that the **C 3-3** cavity is better suited to binding the Na^+ ion than any other ion. This postulate is consistent with the potentiometric results for **C 3-3**, given in Table 3-6, which shows that **C 3-3** is much more selective for sodium than for the other ions included in the modelling studies.

Interestingly, the fact that Ca^{2+} is doubly charged does not have the same effect when complexed by **C 3-3**, as seen in the models of the calcium complexes formed with **C 3-1** and **C 3-2**. This may be due to the absence of the relatively bulky phenyl rings near the carbonyl group, meaning that the pendant groups have greater conformational freedom than in the case of the **C 3-1** and **C 3-2**. The effect of the +2 charge on the Ca^{2+} ion can be seen in the distance from the carbonyl oxygen atoms – Table 3-3 shows that it is nearer the carbonyl group than either the Na^+ or K^+ ions. However, the phosphine oxide groups in **C 3-1** and **C 3-2** probably interact to a different extent with the Ca^{2+} ion than the carbonyl groups in **C 3-2** and this factor should not be overlooked.

C 3-4

As with the models of the cation complexes of **C 3-1**, **C 3-2** and **C 3-3**, the models of the complexes formed by **C 3-3** with Li^+ and Mg^{2+} (see Figure 3-21 for the Li^+ complex) indicate that the phenoxy oxygen atoms have little influence on the positions of these ions (both ions are approximately 2.00 Å away from the carbonyl oxygen atoms and are 3.5 to 4.0 Å away from the phenoxy oxygen atoms) and are either in or slightly below the mean plane of the carbonyl oxygen atoms. As previously discussed, this is quite likely due to the inability of these ions to adequately fill the cavities in ligands studied. However, an additional factor, unique among the four ligands, which very likely causes these two ions to have low-lying positions is the presence of the methoxy oxygen atoms (**C 3-1** and **C 3-2** have no ligating atoms below the phosphine oxide groups, while the carboxylate oxygen atoms in **C 3-3** do not have the correct orientation to bind with a cation). Table 3-4 shows that the Li^+ ion is separated from one of the methoxy oxygen atoms by 2.36 Å, while two such atoms are at distances of 2.23 and 2.49 Å from the Mg^{2+} ion and these distances are comparable to the cation to phenoxy oxygen distances in the models of the GMC's of **C 3-3**:Li^+ and **C 3-3**:Mg^{2+} and, in the case of lithium, X-ray structures of similar calixarene compounds.

The influence of the methoxy oxygen atoms is also seen upon examination of the position of the Ca^{2+} ion in the model of the GMC of the **C 3-4**:Ca^{2+} complex, (see Figure 3-22). As with the Mg^{2+} complex, at least two of the methoxy oxygen atoms (at distances of 2.68 and 2.73 Å from the ion - see Table 3-4) appear to bind with the ion to a significant extent. The lack of influence of the phenoxy oxygen atoms on the position of the Ca^{2+} ion (Table 3-4 shows that these atoms are separated from the Ca^{2+} ion by 4.05 Å) is probably the reason for the relatively small change in the symmetry of the macrocyclic ring of **C 3-4** upon complexation with calcium, since as discussed above, for the **C 3-3**:Na^+ model, for example, that binding of the ion by the phenoxy oxygen atoms causes the macrocyclic ring to take on a much more symmetrical arrangement. Table 3-4 shows that the distances between facing phenyl rings in the model of the GMC of the 'free' form of **C 3-4** (the model of which is shown in Figure 3-20) are separated by distances of 9.29 and 6.38 Å and upon complexation with Ca^{2+} (see Figure 3-22), the models predict that these distances

103

change to 8.06 and 7.83 Å, indicating that of all the **C 3-4** complexes modelled, the macrocyclic ring in **C 3-4**:Ca^{2+} was the least symmetrical.

Potentiometric selectivity coefficients for **C 3-4** are given in Table 3-6 and graphically in Figure 3-5. The models indicate that the mode of complexation for **C 3-4** with Na^+ and K^+ is similar to that for these ions with **C 3-3**, i.e., eight-fold complexation by the carbonyl and phenoxy oxygen atoms. The cation to ligand distances obtained for the model of **C 3-4**:K^+ complex are in excellent agreement with that obtained from the X-ray structure of a calixarene also co-ordinated by phenoxy and carbonyl oxygen atoms. In spite of the fact that this X-ray structure appears to be only X-ray structure of a calixarene:cation complex in the Cambridge Crystallographic Data Centre (CCDC) database that contains carbonyl oxygen atoms,[25a] this agreement is very reassuring. The model of the **C 3-4**:Na^+ complex, (see Figure 3-23 and Table 3-3), show that the Na^+ - O distances are similar for both types of oxygen and while this is also true of the model of **C 3-4**:K^+ complex, the distances in the latter case are greater by 0.25 - 0.30 Å. Moreover, of **C 3-4** complexes modelled, the symmetry of the macrocyclic ring in the sodium complex is greater than that of the other **C 3-4** complexes, with, as Table 3-4 shows, facing identical aryl rings at virtually equal separation. These facts, especially in view of the fact that such eight-fold complexation is not observed in the models of the **C 3-4** complexes fomed with the Li^+, Mg^{2+} and Ca^{2+} ions, are strong evidence of why **C 3-4** is potentiometrically selective for sodium and that potassium is the greatest potentiometric interferent of the ions modelled.

It should be pointed out that the **C 3-4**:Na^+ complex has been modelled with the *HyperChem* software[27] on a personal computer, using the same method as that described above for the **C 3-2**:Ca^{2+} complex. Both methods produced modelled structures of the **C 3-4**:Na^+ complex that are similar (four-fold symmetry of the macrocyclic ring, eight-fold co-ordination of the Na^+ ion by the carbonyl and the phenoxy oxygen atoms). However, in the case of method employed with *HyperChem*, the macrocyclic ring in the initial structure had a four-fold symmetry, since starting structures with a two-fold symmetry resulted in optimised structures, also with a twofold symmetry, but with a higher energy than that of the optimised

structure with four-fold symmetry. In contrast, when using the conformational search method reported in this chapter, it was unnecessary to adjust the starting geometry so radically. This difference in results obtained with the two methods confirms the power and sophistication of the workstation / *Spartan* conformational search option compared to that of the PC / *HyperChem* geometry optimisation approach.

3.3.2. *¹H NMR Titrations*

¹H NMR titrations were carried out for complexes of **C 3-4** and **C 3-2** with Ca^{2+} and Na^+. To detemine the stoichometry of these complexes, the change in chemical shift of the *t*-Butyl protons was plotted versus the cation:calixarene mole ratio (see Figure 3-30). These peaks were chosen because of their high intensity, making them easy to identify and because the changes in their chemical shift though small (the changes were ca. 0.03 - 0.03 ppm), were still large enough to be observed. The addition of the deuterated methanol solvent affects the position of the peaks, shifting them upfield by about 0.03 ppm and this affect has been corrected for.

C 3-2

The main features of interest in the ¹H NMR spectrum of **C 3-2** (shown in Figure 3-24a) are the chemical shifts at 3.0 and 4.5 ppm, which are assigned to the methylene bridging protons and at 1.05 ppm assigned to the *t*-butyl group protons at 1.05 ppm. The doublet of doublets due to the methylene bridging protons is conclusive evidence that the calixarene is in the 'cone' conformation.[1a] These doublets are observed in the NMR spectra (not shown) recorded for mixtures of **C 3-2** with sodium and ten with calcium, confirming that the conformation of **C 3-2** did not change from 'cone' upon complexation.

The NMR spectra of **C 3-2** and its sodium and calcium complexes (shown in Figure 3-25 and Figure 3-26, respectively) undergo little or no simplification as the cations are added, indicating that there is little or no change in the symmetry of the ligand upon complexation. The molecular modelling studies support these observations because they indicate, as has been discussed above, that the geometry of **C 3-2** retains its two-fold symmetry upon complexation with either sodium or calcium.

105

The 'free' form of **C 3-2** and its calcium complex are given in Figure 3-13 and Figure 3-12, respectively. The **C 3-2** - sodium complex was modelled as both 1:1 and 2:1 complexes and these models are given in Figure 3-14 and Figure 3-15 respectively.

The plot in Figure 3-30 clearly shows that the stoichiometry of the **C 3-2**:Ca^{2+} complex is 1:1. Virtually no further shift in the *t*-butyl protons is observed when enough Ca^{2+} had been added after the 1:1 equivalence point (this also so apparent upon examination of Figure 3-27b) and this is where the gradient of the plot changed the most.

However, Figure 3-27a and Figure 3-30 suggest that a 2:1 stoichiometry for the **C 3-2**:Na^+ complex is the most likely. The continual shift in the *t*-butyl peak can be attributed to a complexation-decomplexation equilibrium effect of the Na^+ ion with the calixarene due to weak complexation. The models of the **C 3-2**:Na^+ complex (see Figure 3-15 and Figure 3-16) indicate that the Na^+ ion is complexed in the lower region of the pendant groups, by the phosphine oxide oxygen atoms, and this would make migration of the ion away from the calixarene feasible. Attempts were made to carry out a conformational search on a (**C 3-2**)$_2$:Na^+ complex but this resulted in errors. However, a simple optimisation of this complex was carried out using the *Minimise* module after the Na^+ ion was placed in various positions. The optimised position of the ion was found to be dependent on its initial position. However, of the various conformers obtained, the Na^+ ion in the lowest-in-energy conformer, shown in Figure 3-15, was sandwiched in between two ligands and was separated from two of the phosphine oxide oxygen atoms in one ligand by 2.29 and 2.30 Å and from three of these atoms in the other ligand by distances of 2.32, 2.28 and 3.51 Å. These distances compare favourably to the distances obtained in the conformational searches on the 1:1 complexes. This is strong evidence that a 2:1 stoichiometry is feasible for the **C 3-2**-sodium complex.

C 3-4

As with **C 3-2**, the ^{1}H NMR spectra of **C 3-4** (see Figure 3-26a and Figure 3-28a) and its calcium and sodium complexes, (see Figure 3-26 b-d and Figure 3-28 b-d,

106

respectively), suggest that the ligand is in the 'cone' conformation in its 'free' and complexed forms. As was also observed in the case of the **C 3-2**, NMR spectra changed little after the addition of calcium and the molecular models of the free ligand (see Figure 3-20) and its calcium complex (see Figure 3-22) suggest that the ligand retains its symmetry upon complexation.

However, ^{1}H NMR spectra of the **C 3-4**:Na$^+$ complex (shown in Figure 3-28 b-d) do become simpler upon addition of sodium. In particular, Figure 3-28d shows the coalescence of the two *t*-butyl peaks into one peak at 1.05 ppm with 1 mole equivalent of Na$^+$, and this is a very strong indication that the symmetry of macrocyclic ring upon complexation of Na$^+$. The distances between facing aryl rings, shown in Table 3-4, indicates that the macrocyclic ring in the model of the **C 3-4**:Na$^+$ complex (shown in Figure 3-23) has a four-fold symmetry. These values and the model support the notion that the *t*-butyl protons are conformationally equivalent on the NMR timescale. In contrast, the model of the free ligand has a two-fold symmetry (see Figure 3-20) and this is backed up by the relatively complex spectrum, shown in Figure 3-28a, for the free ligand. Thus, the modelling and the NMR spectra provide very strong evidence that the symmetry of **C 3-4** increases upon complexation with Na$^+$.

No such change is seen in the NMR spectrum of **C 3-4** upon complexation with Ca^{2+} (see Figure 3-25 a-d for the full spectra, while the region of the spectrum containing peaks due to resonance of the *t*-butyl protons is shown in Figure 3-27). The modelling does predict that complexation with Ca^{2+} should bring about a slight increase in symmetry (see Table 3-4), but the model indicates that the symmetry of the macrocyclic ring remains two-fold. Therefore, it may well be that the changes in conformation of the ligand are not great enough to be observed in the NMR spectrum. The potentiometric selectivity of **C 3-4** for calcium (see Table 3-6) is so poor that it could not be measured precisely and this would imply that the stability constant for the **C 3-4**:Ca^{2+} complex is too low for any conformatational changes brought about by complexation to be detected in the NMR spectrum.

A low stability constant for this complex would also explain why the gradient of the plot in Figure 3-30 for the **C 3-4** - calcium mixture the does not change as

definitively as that for the other three complexes whose stoichiometry was also investigated by NMR spectroscopy. This is confirmed upon comparison of the overlaid plots of Figure 3-29b (for **C 3-4**:Ca^{2+}), with that of Figure 3-27a (for **C 3-2**:Na^+) Figure 3-27b (for **C 3-2**:Ca^{2+}) and Figure 3-29a (for **C 3-4**:Na^+), as the latter three overly plots show a very clear patterns of changes of the chemical shift of the *t*-butyl protons upon addition of the cation).

3.4.   Conclusion

This paper demonstrates that using the Monte Carlo conformational search algorithm in conjunction with the MMFF force field, it is possible to clearly explain the selectivity of several calixarenes for the primary ion in terms of how well the ion fits into the polar cavities of the ligands - the models indicate that the cavities are too large to effectively complex small ions such as Li^+ and Mg^{2+}, while cation to ligand distances were very useful in explaining selectivity where the co-ordination number was the same. Attempts to explain the order of selectivity were less successful.

The results of the conformational searching highlight very clearly that the effect of the increase in cavity size (as one goes from **C 3-1** to **C 3-2**) is to make the latter ligand bind less effectively with Group 1 and Group 2 cations in general but still leaving it with the capability of encapsulating the Ca^{2+} ion within its cavity, thus making it very effective at discriminating between calcium and other interferents, as measured in terms of potentiometric selectivity. The modelling results (for the **C 3-4** complexes with lithium, magnesium and calcium) suggest strongly that ligating atoms outside the calixarene cavity can cause the position of the cation to change condsiderably, from, for example, that found for the complexes of **C 3-3** with these ions.

^{1}H NMR spectra of some of the complexes modelled indicated that they were in the 'cone' conformation and this justified our decision to model these complexes as 'cone' conformers. The spectra were also consistent with the conclusion drawn from the modelling about the increases in symmetry of the ligand geometry upon complexation.

^{1}H NMR titrations provided strong evidence of the stoichiometry of the complexes under study. In the one case where such evidence was inconclusive (the **C 3-4** - calcium titration), this can be seen as support for models which depict the ion as being bound at the edge or outside the calixarene cavity

3.5. Acknowledgements

3.6. Tables

Table 3-1. *Critical distances of the models of the global minimum conformers of C 3-1 and its cationic complexes. [a]*

	C 3-1	C 3-1:Li$^+$	C 3-1:Na$^+$	C 3-1:K$^+$	C 3-1:Mg^{2+}	C 3-1:Ca^{2+}
M - Phenoxy O [b]	N/A [d]	2.33, 3.53, 3.87, 5.70	2.85 ± 0.00 (4)	2.84± 0.00 (4)	2.25, 2.96, 3.78, 5.70	2.81 ± 0.00 (4)
M - Phosphine Oxide O	N/A	1.83 ± 0.00 (3), 5.78	2.38 ± 0.00 (4)	2.46± 0.00 (4)	1.82 ± 0.00 (3), 8.27	2.35 ± 0.00 (4)
Phosphine Oxide O - Phenoxy O	2.96, 3.03, 3.69, 3.71	2.75 ± 0.12 (4)	2.69 ± 0.00 (4)	2.71± 0.00 (4)	2.44, 2.62, 2.78, 3.67	2.56 ± 0.00 (4)
Ar (I) - Ar (III) [c]	9.99	9.73	7.91	7.87	9.52	7.86
Ar (II) - Ar (IV) [c]	5.44	5.41	7.91	7.87	5.55	7.86

[a] *All distances are quoted in Angstroms. Where a distance and an error is quoted, the distance is the mean of several relatively close values, while the error is half the range of the values. The value in parentheses is the number of values used to calculate the mean and range.*

[b] *M - cation.*

[c] *These are the distances between the aryl carbon atoms in facing aryl rings that are bonded to the tertiary carbon atoms in the t-butyl groups. These distances are illustrated graphically in Figure 3-32.*

[d] N/A - Not Applicable

110

Table 3-2. Critical distances of the models of the global minimum conformers of **C 3-2** and its cationic complexes. [a]

	C 3-2	C 3-2:Li$^+$	C 3-2:Na$^+$	C 3-2:K$^+$	C 3-2:Mg^{2+}	C 3-2:Ca^{2+}
M - Phenoxy O	N/A	4.26 ± 0.01 (3), 5.87	4.64, 5.06, 5.25, 9.21	5.40, 5.51, 6.42, 6.94	2.31, 2.39, 2.90, 5.06	2.88 ± 0.00 (2), 3.09 ± 0.00 (2)
M - Phosphine Oxide O	N/A	1.82 ± 0.05 (3), 7.53	2.20 ± 0.04 (3), 5.38	2.49, 2.60, 2.98, 6.76	1.88 ± 0.02 (3), 7.90	2.48 ± 0.00 (2), 2.55 ± 0.00 (2)
Phosphine Oxide O - Phenoxy O	4.31 ± 0.0 (4)	3.21, 4.26 ± 0.01 (3)	3.17, 4.23, 4.28, 4.83	3.21, 4.36, 4.82, 4.85	2.68, 2.81, 2.93, 3.26	2.89 ± 0.01 (4)
Ar (I) - Ar (III)	9.14	9.85	9.78	9.67	9.34	8.86
Ar (II) - Ar (IV)	6.52	5.53	5.55	5.57	5.46	6.31

[a] *Footnotes a-d of Table 3-1 also apply to this table.*

Table 3-4. *Critical distances of the models of the global minimum conformers of C 3-1 and its cationic complexes. [a]*

	C 3-1	C 3-1:Li⁺	C 3-1:Na⁺	C 3-1:K⁺	C 3-1:Mg²⁺	C 3-1:Ca²⁺
M - Phenoxy O	N/A	2.82 ± 0.00 (4)	2.55 ± 0.00 (4)	2.75 ± 0.00 (4)	3.01 ± 0.00 (4)	2.68 ± 0.00 (4)
M - Phosphine Oxide O	N/A	2.10 ± 0.00 (4)	2.46 ± 0.00 (4)	2.69 ± 0.00 (4)	1.98 ± 0.00 (4)	2.37 ± 0.00 (4)
Phosphine Oxide O - Phenoxy O	2.78 ± 0.00 (2), 2.91 ± 0.00 (2)	2.66 ± 0.00 (4)	2.67 ± 0.00 (4)	2.71 ± 0.00 (4)	2.70 ± 0.05 (4)	2.71 ± 0.05 (4)
Ar (I) - Ar (III)	9.33	7.95	7.93	7.86	7.86	7.84
Ar (II) - Ar (IV)	6.30	7.95	7.93	7.86	7.87	7.84

[a] *Footnotes a-d of Table 3-1 also apply to this table.*

Table 3-6. *Critical distances of the models of the global minimum conformers of C 3-4 and its cationic complexes. [a]*

	C 3-4	C 3-4:Li$^+$	C 3-4:Na$^+$	C 3-4:K$^+$	C 3-4:Mg^{2+}	C 3-4:Ca^{2+}
M - Phenoxy O	N/A	3.51 ± 0.20 (4)	2.57 ± 0.01 (4)	2.82 ± 0.03 (4)	3.87 ± 0.12 (4)	4.05 ± 0.03 (4)
M - Carbonyl O	N/A	2.00 ± 0.05 (4)	2.41 ± 0.06 (4)	2.68 ± 0.05 (4)	1.97 ± 0.03 (4)	2.28 ± 0.05 (4)
M - Methoxy O	N/A	2.36, 4.63, 4.68, 5.12	5.14, 5.23, 5.26, 5.92	3.25, 5.47, 5.47, 5.50,	2.23, 2.49, 3.86, 5.16	2.68, 2.73, 3.85, 4.52
Carbonyl O - Phenoxy O	2.85 ± 0.02 (4)	2.73 ± 0.05 (4)	2.66 ± 0.01 (4)	2.66 ± 0.01 (4)	2.70 ± 0.05 (4)	2.71 ± 0.06 (4)
Carbonyl O - Methoxy O	4.35 ± 0.40 (4)	2.71, 3.12, 3.17, 4.32	2.98, 3.08, 3.09, 4.22	2.55, 2.83, 2.89, 4.52	3.25, 5.48 ± 0.02 (4)	2.90 ± 0.11 (4)
Ar (I) - Ar (III)	9.27	8.06	7.97	8.07	7.96	8.06
Ar (II) - Ar (IV)	6.41	7.83	7.96	7.68	7.85	7.65

[a] *Footnotes a-d of Table 3-1 also apply to this table.*

Table 3-5. *Log of Potentiometric Selectivity Coefficients, c, for the calcium-selective calixarene phosphine oxides, **C 3-1** and **C 3-2**. [a]*

	Interfering Ion			
	Li^+	Na^+	K^+	Mg^{2+}
C 3-1	-0.40	-1.04	-0.59	-1.73
C 3-2	0.11	-1.23	0.60	-1.05
C 3-5	-0.52	-1.02	-0.95	-2.40
C 3-6	-0.39	-0.98	-0.52	-1.92

[a] *The method of measurement was a modification Fixed Interference Method (FIM)[28] and is described in more detail in both Chapter 4 and Reference 13 of this chapter.*

Table 3-6. *Log of Potentiometric Selectivity Coefficients, $\log k_{NaB}^{Pot}$, for the sodium-selective calixarene esters, **C 3-3** and **C 3-3**. [a]*

	Interfering Ion			
	Li^+	Na^+	K^+	Mg^{2+}
C 3-3	-2.5 [c]	-2.2 [c]	> -6	-5.7
C 3-4	-2.7	-2.4	-3.5	-3.5

[a] *The interfering ion concentrations were 0.1 mol dm^{-3}. The results for **C 3-3** are taken from Reference 5b, while the results for **C 3-4** are taken from Reference 6.*

[b] *The method of measurement was the Fixed Interference Method (FIM),[28] except in the cases indicated in Footnote [c].*

[c] *The method of measurement used in these cases was the Separate Solution Method.[28] While less rigorous than the FIM, it is accepted that the SSM gives reliable results where the primary and interfering ions have the same ionic charge.[29]*

3.7. Figures
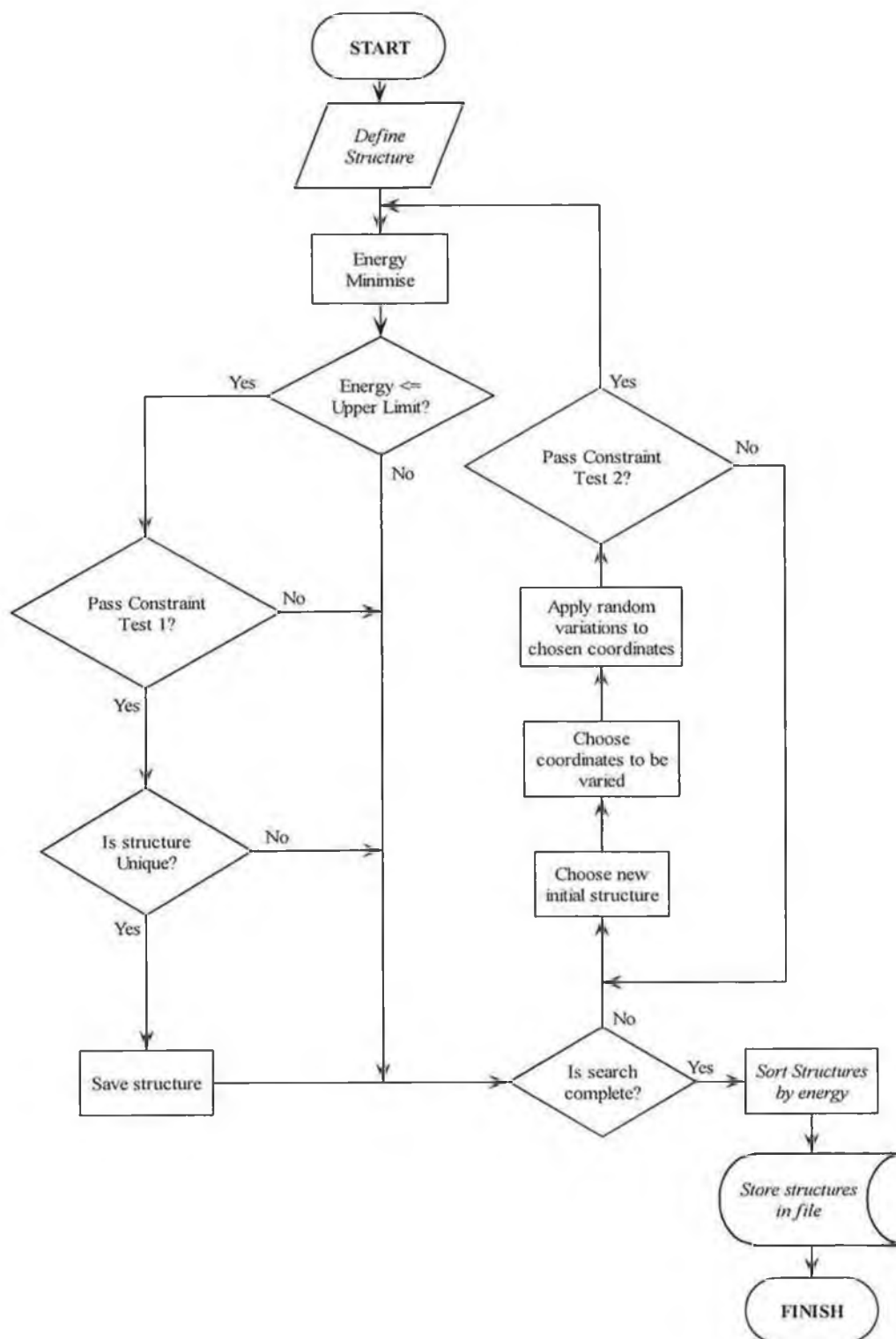
Figure 3-1. *The operation of conformational searches. Those instructions in italics are desirable but not necessarily part of a particular implementation. This structure has been reproduced with slight changes from the article by Chang, et. al.[11]*
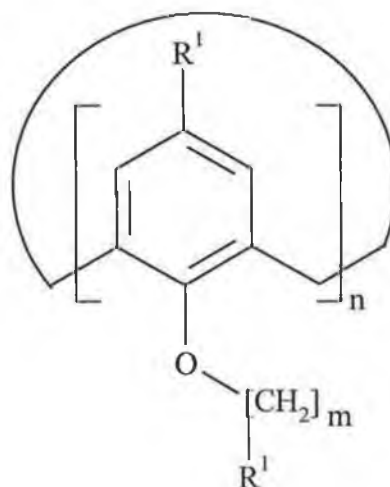
	R^1	R^2		m	n
C 3-1	*t*-Bu	Ph—**P**—Ph (O double bond)		1	4
C 3-2	*t*-Bu	Ph—**P**—Ph (O double bond)		2	4
C 3-3	*t*-Bu	O=**C**—O—CH_3		1	4
C 3-4	*t*-Bu	O=**C**—O—CH_3		1	4
C 3-5	*t*-Bu	Ph—**P**—Ph (O double bond)		2	5
C 3-6	H	Ph—**P**—Ph (O double bond)		2	5

Figure 3-2. *The compounds modelled in this study. The atom highlighted in bold in each of the R^2 susbstituents indicates the point of contact with the motif. Molecular modelling and potentiometric studies were carried out on C 3-1, C 3-2, C 3-3 and C 3-4, while potentiometric studies only were carried out on C 3-5, and C 3-6.*
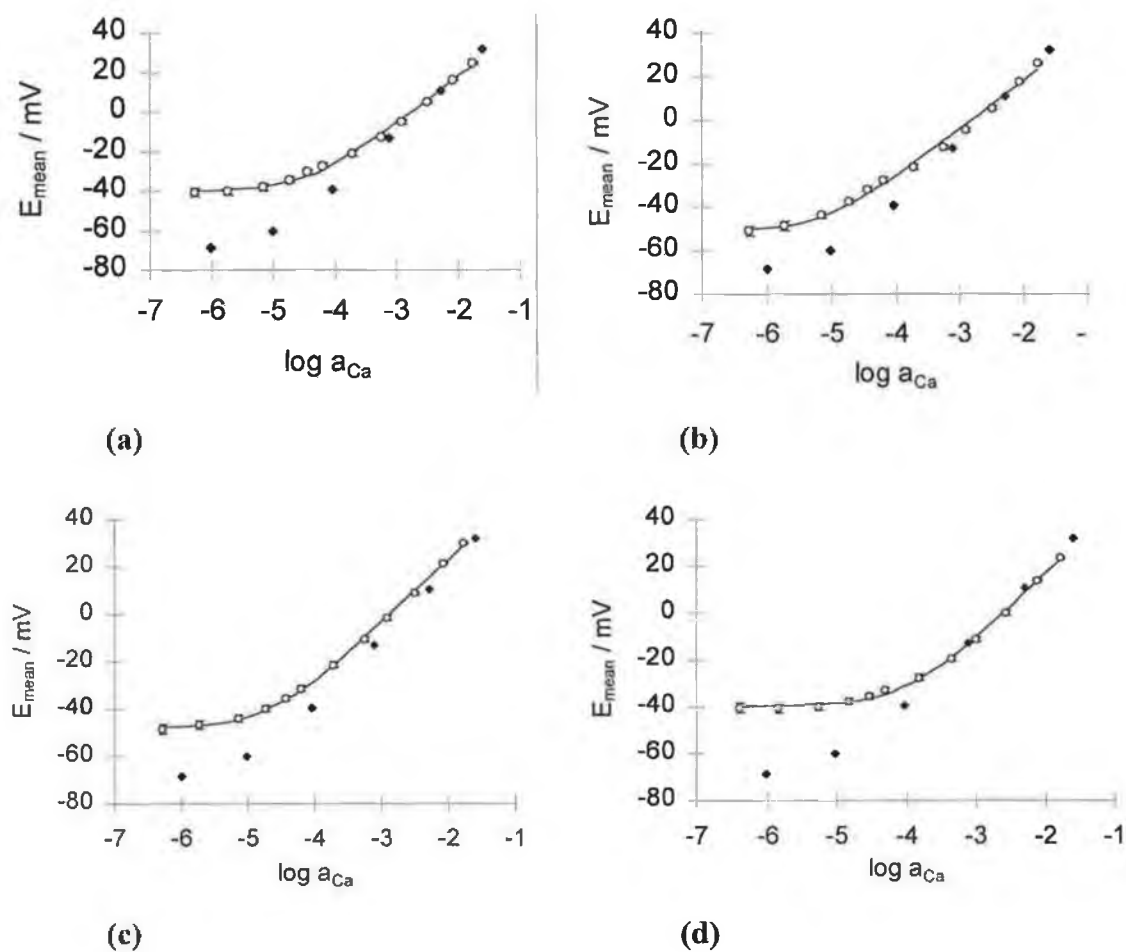
Figure 3-3. *Plot of mean experimental potentials (hollow circular points) and predicted potentials (line) versus log of the calcium ion acitivity for the ion-selective electrode based on C 3-2, according to the optimised model based on Eqn. (3-1), versus log a_{Ca} with standard deviations as error bars (n = 3). The black diamond-shaped points are the calcium chloride calibration potentials. The interfering ions are: (a) Li^+, (b) Na^+, (c) K^+ and (d) Mg^{2+}.*
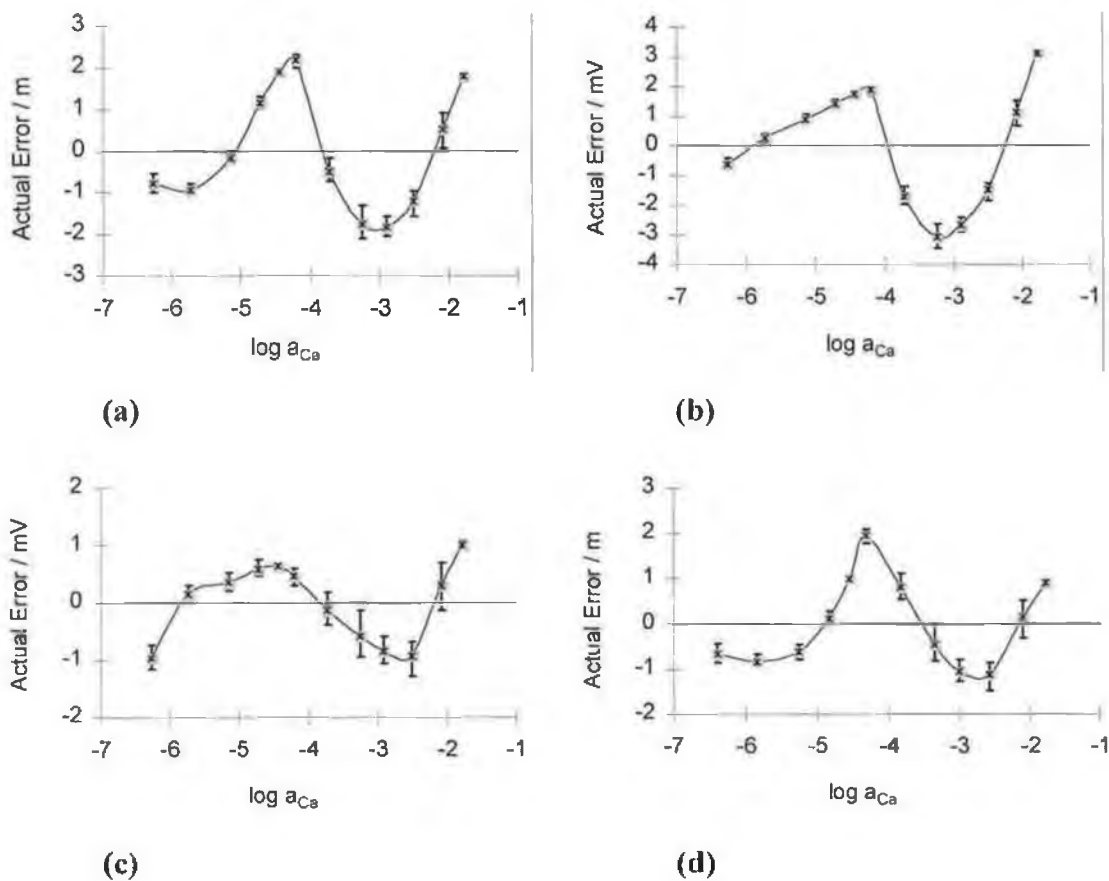
Figure 3-4. *Plot of residual error resulting from the fit of Eqn. (3-1) to the mean experimental potential versus log of the calcium ion acitivity for the ion-selective electrode based on C 3-2. The error bars show the range (n = 3) in the residual errors resulting from the fit of Eqn. (3-1) to the individual potentials. The interfering ions are: (a) Li^+, (b) Na^+, (c) K^+, (d) Mg^{2+}.*
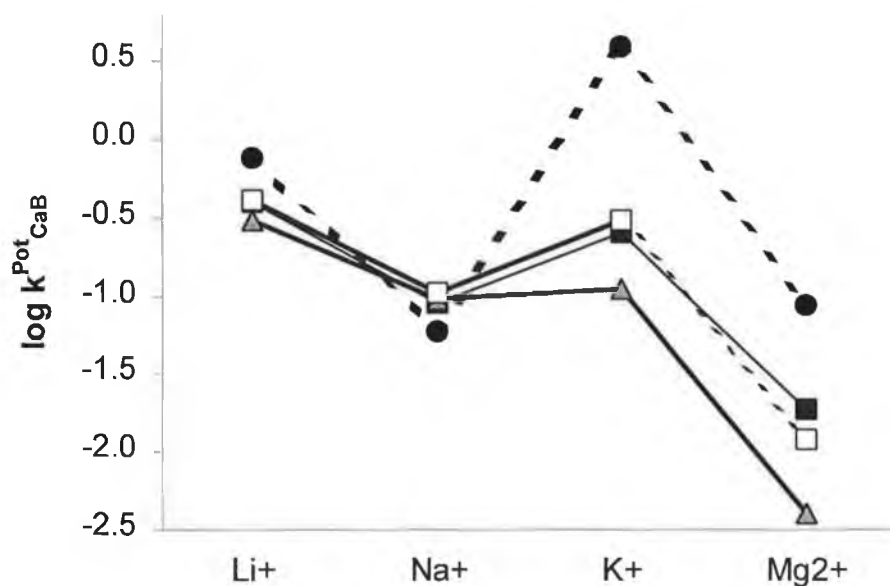
Figure 3-5. *Plot of log of potentiometric selectivity coefficients,* $\log k_{CaB}^{Pot}$, *for four interfering ions and for* ***C 3-1*** *(heavy broken line, filled circular points)* ***C 3-2*** *(unbroken line, filled square points),* ***C 3-5*** *(broken line, hollow square points) and* ***C 3-6*** *(heavy unbroken line, grey triangular points).*
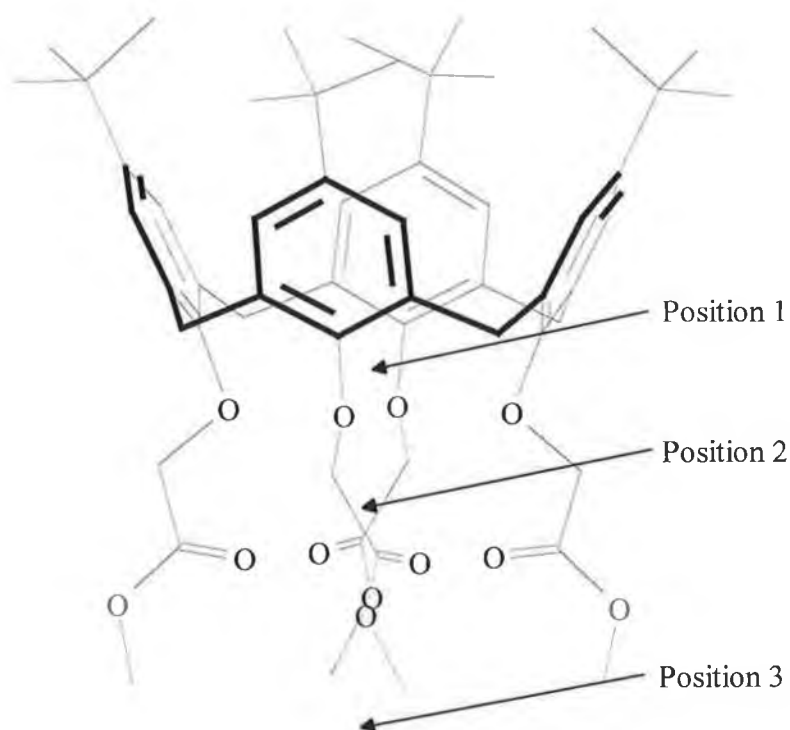
Figure 3-6. *The positions in which the cations were initially placed when carrying out conformational searches.* ***C 3-3*** *(Side-on view) is shown as an example but these positions apply to all of the complexes modelled.*
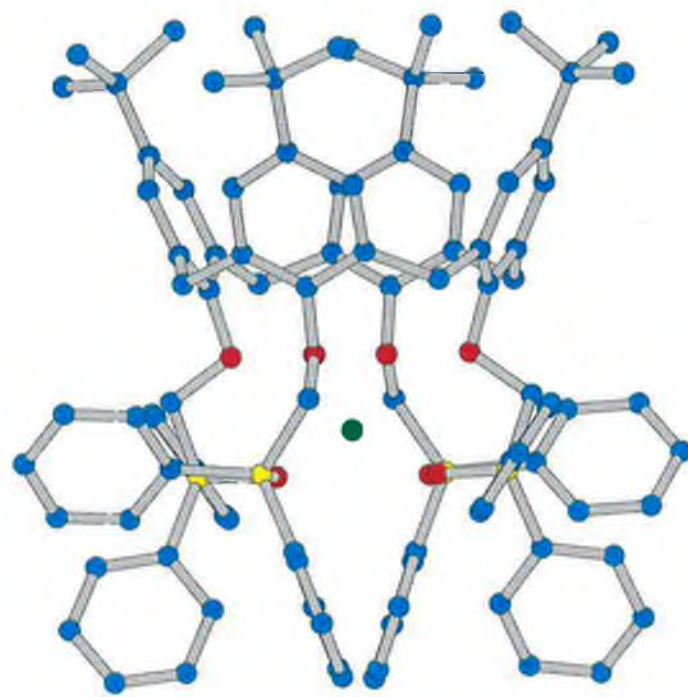
119
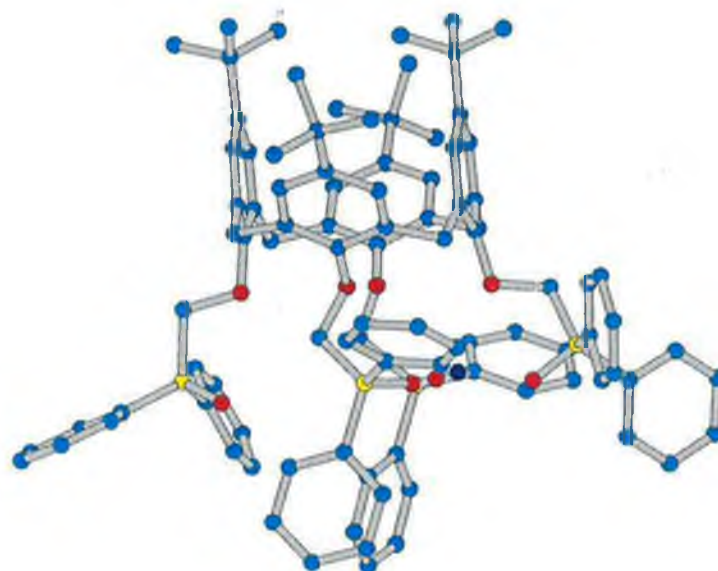
(a)
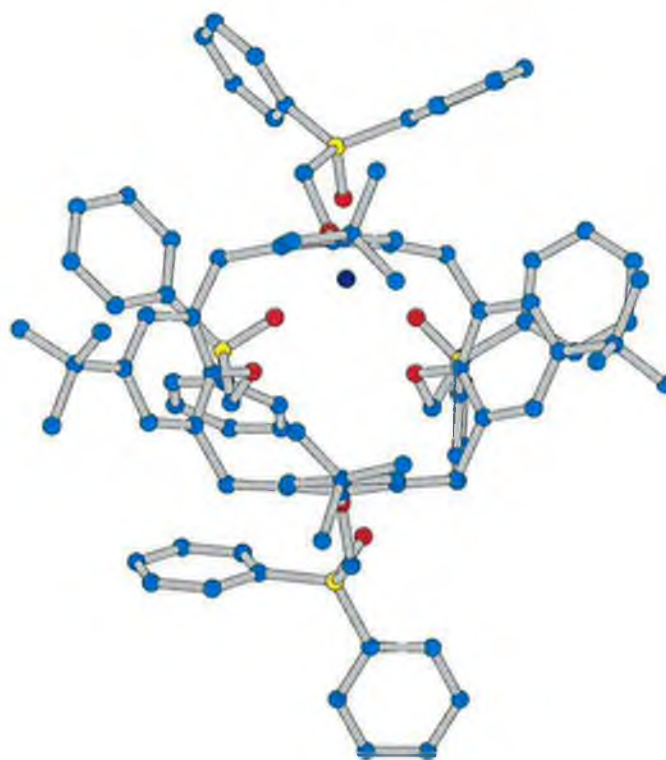
(b)
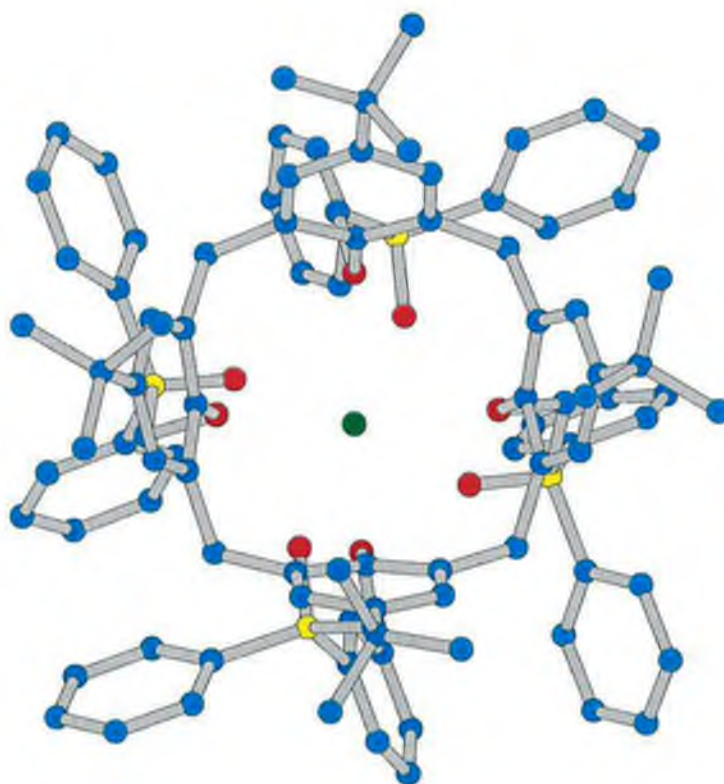
Figure 3-7. *Ball and tube rendering of the side-on view, (a) and the view through the cavity, (b) of the model of the global minimum conformer of* **C 3-1**:*Li⁺. Hydrogen atoms are not shown for the sake of clarity. Colour scheme: carbon - cyan -, oxygen - red, phosphorous - yellow, blue - lithium.*
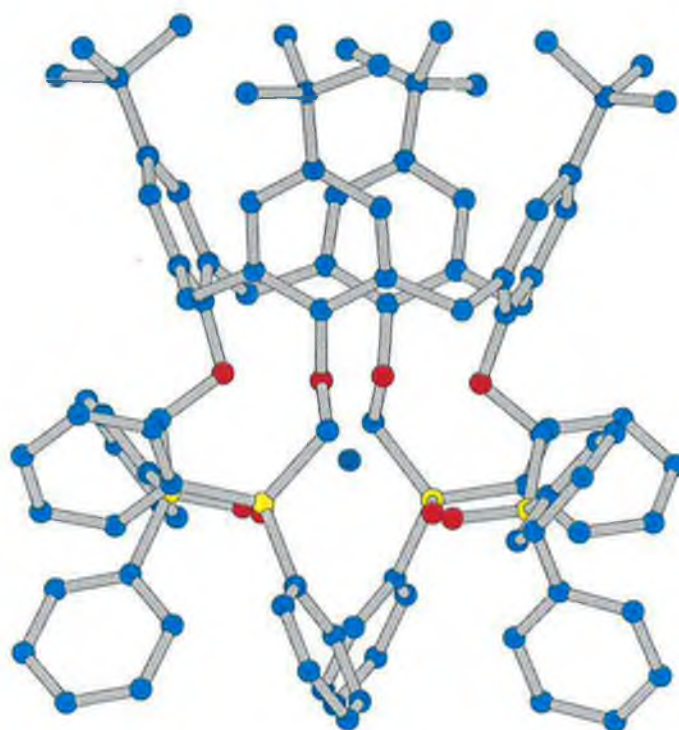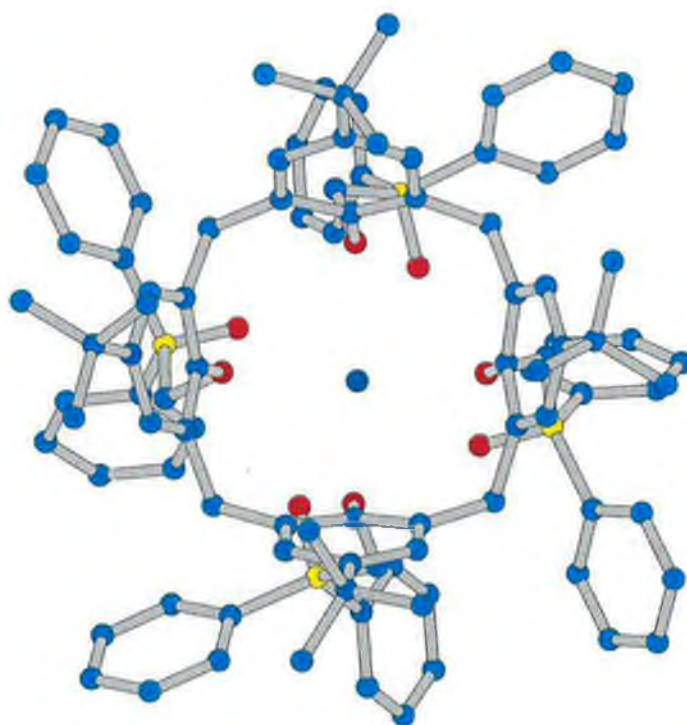
(a)

(b)

Figure 3-8. *As for Figure 3-7, except that the model of the global minimum conformer of* **C 3-1**:*Ca^{2+} is shown. Colour scheme: calcium - green.*

(a)

(b)

Figure 3-9. *As for Figure 3-7, except that the model of the global minimum conformer of* **C 3-1:**K^+ *is shown. Colour scheme: potassium - pale-grey.*

(a)

(b)

Figure 3-10. *As for Figure 3-7, except that the model of the global minimum conformer of **C 3-1** is shown.*

(a)

(b)

Figure 3-11. *As for Figure 3-7, except that the model of the global minimum conformer of C 3-2:Li⁺ is shown.*

(a)

(b)

Figure 3-12. *As for Figure 3-7, except that the model of the global minimum conformer of **C 3-2**:Ca^{2+} is shown. Colour scheme: calcium - green.*
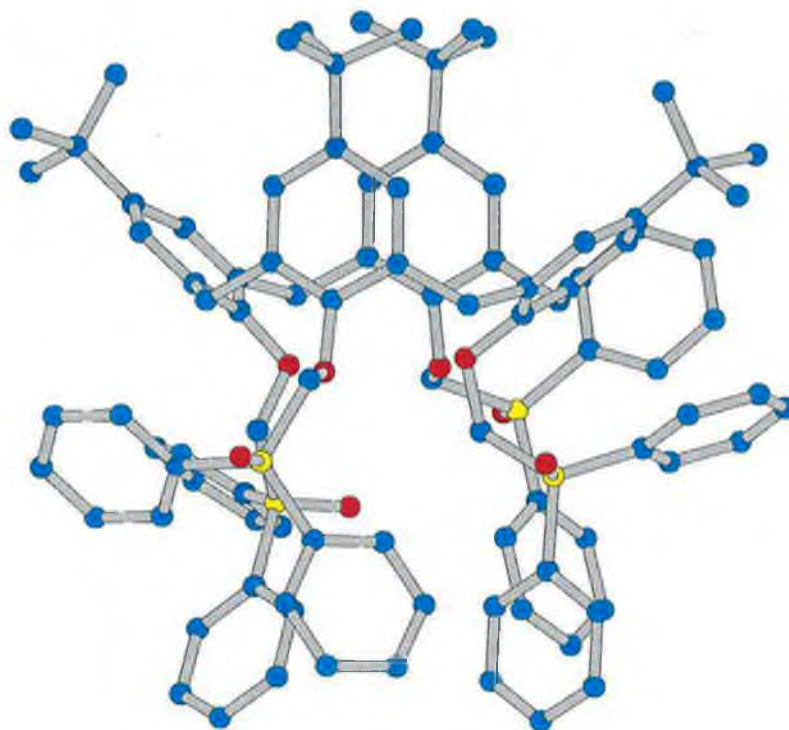
(a)

(b)

Figure 3-13. *As for Figure 3-7, except that the model of the global minimum conformer of **C 3-2** is shown.*
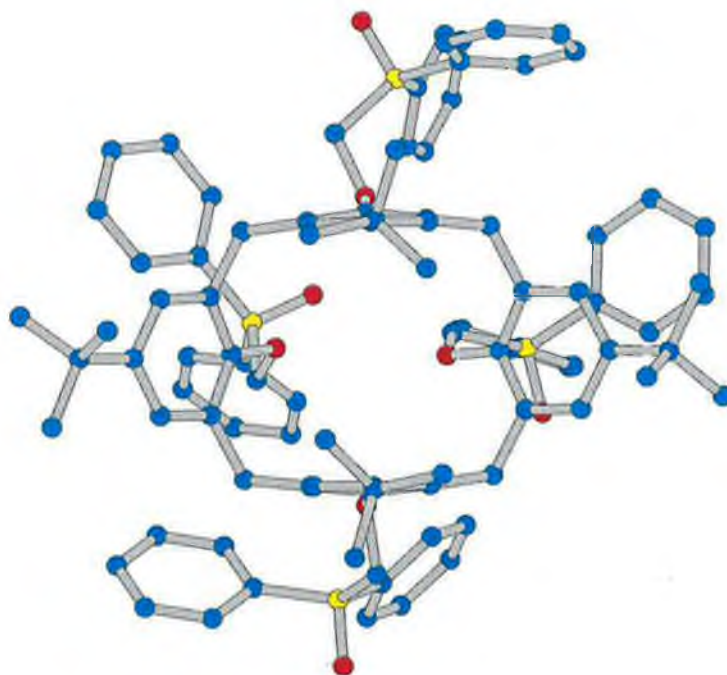
(a)

(b)
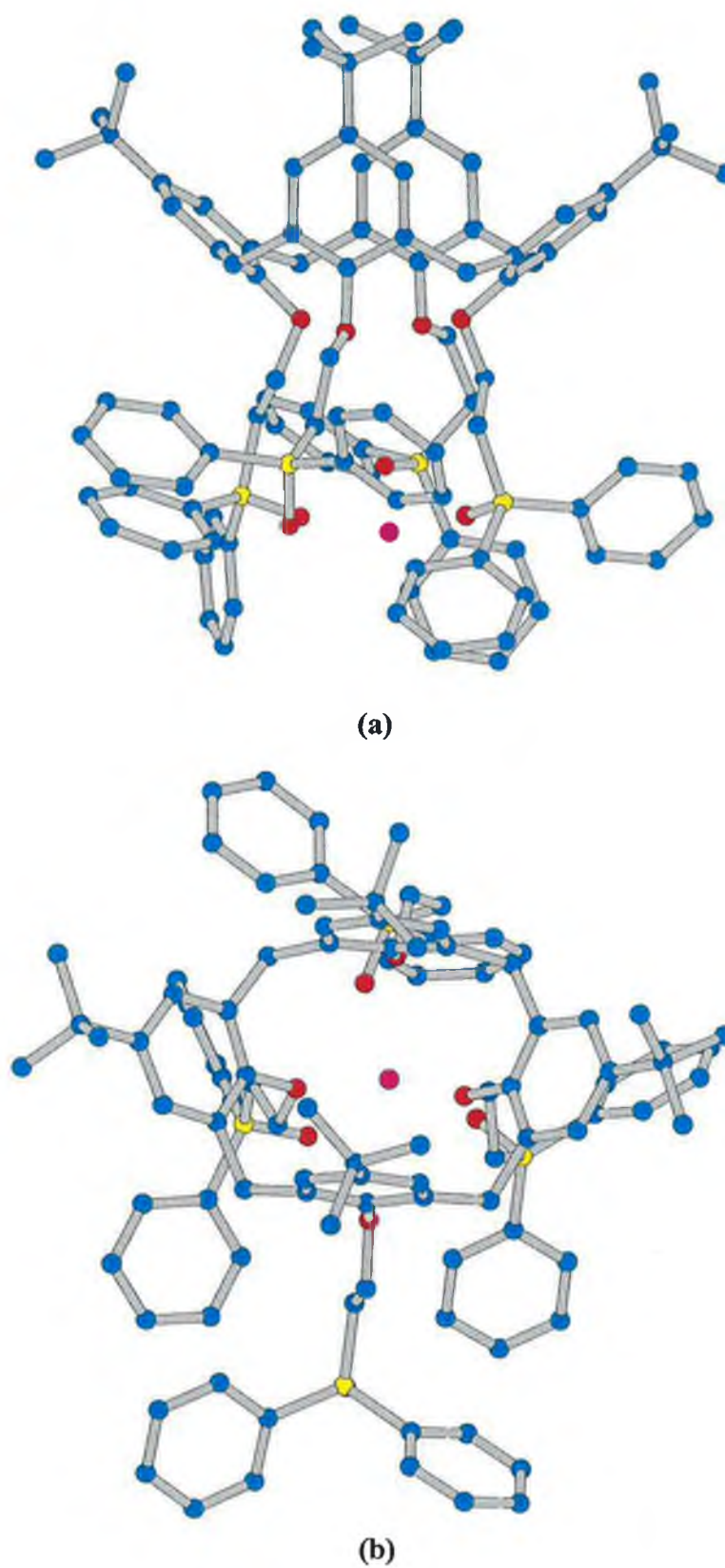
Figure 3-14. *As for Figure 3-7, except that the model of the global minimum conformer of **C 3-2**:Na⁺ is shown. Colour scheme: sodium -magenta.*

(a)

(b)
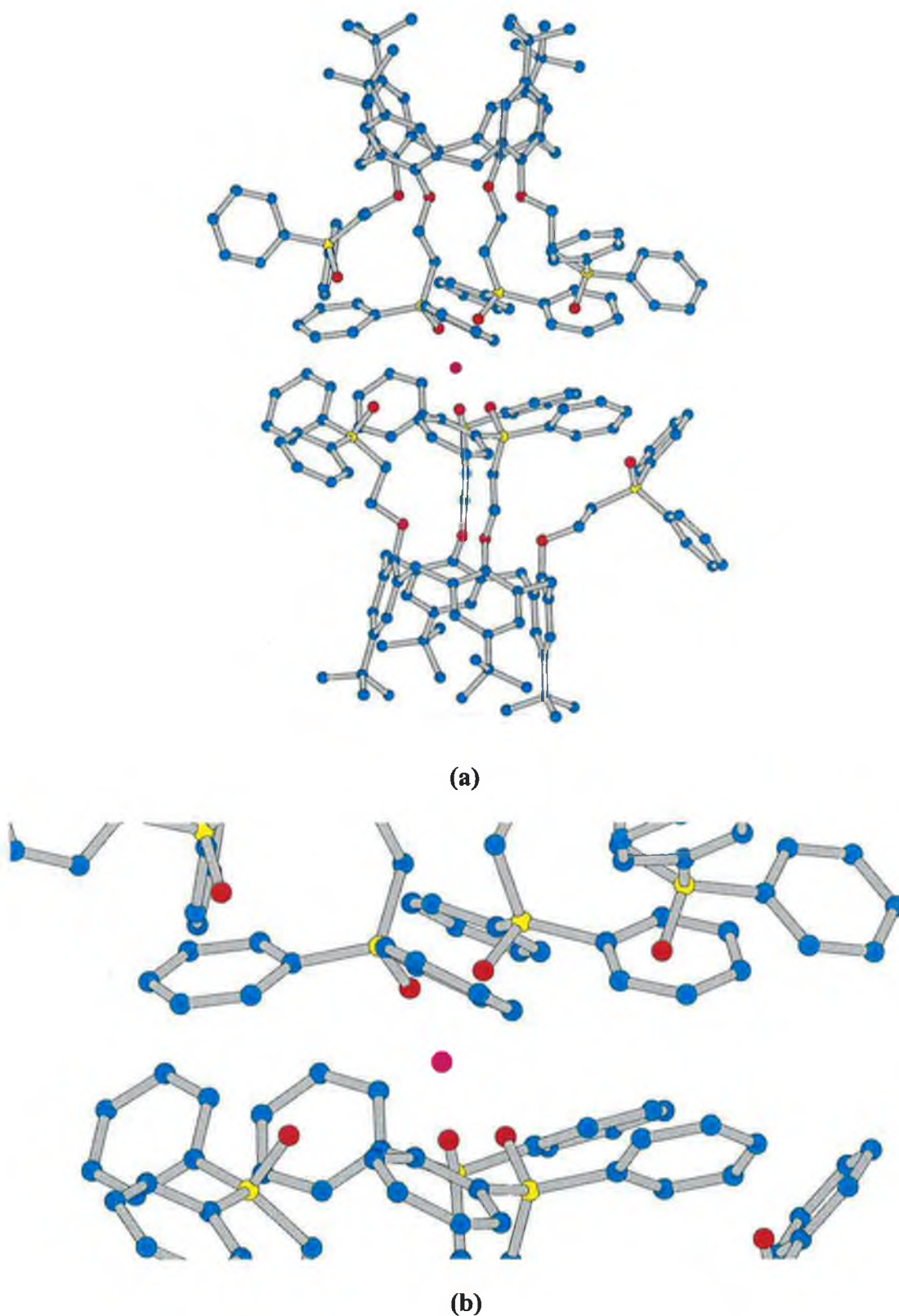
Figure 3-15. *Ball and tube rendering of the side-on view of (**C 3-2**)$_2$:Na$^+$, showing (a) the full complex and (b) the region of complexation. Colour scheme: as for Figure 3-7 and in addition, sodium -magenta.*

128
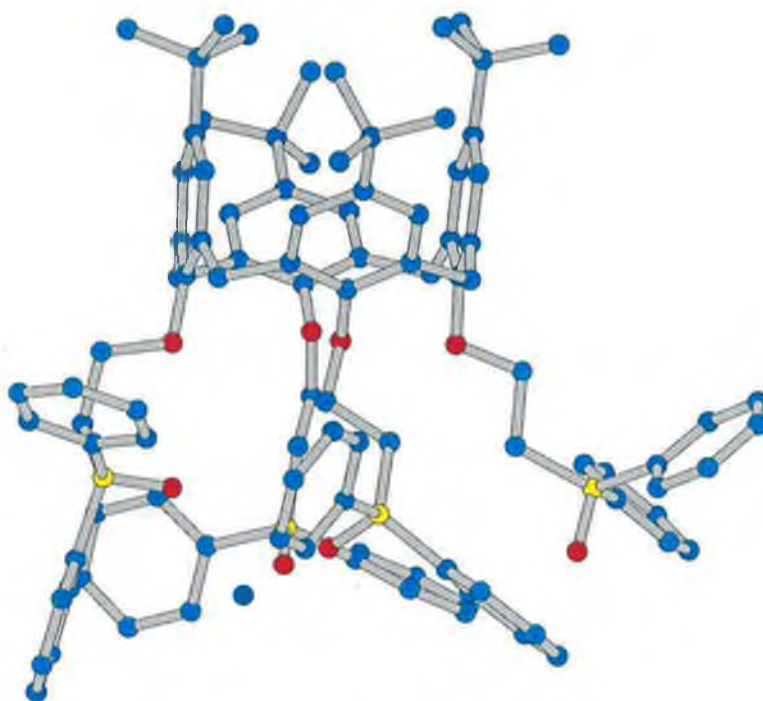
(a)
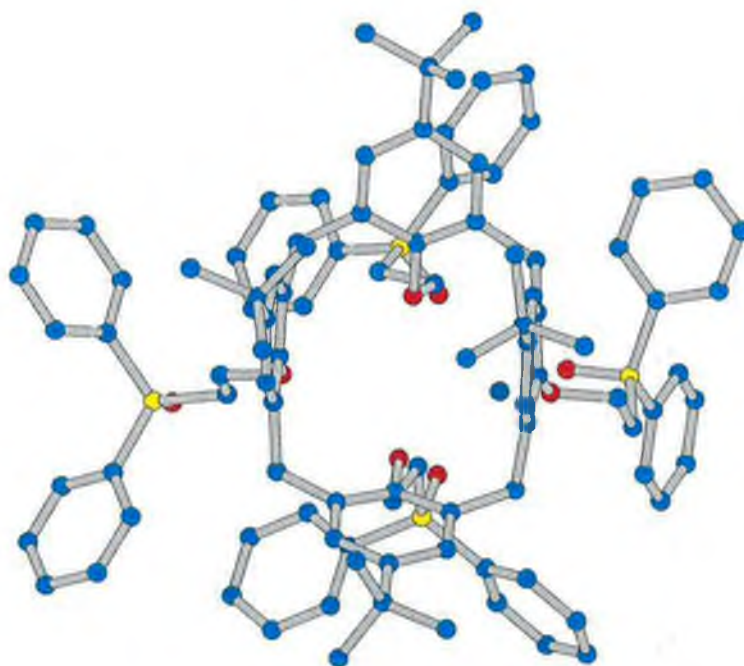
(b)

Figure 3-16. *As for Figure 3-7, except that the model of the global minimum conformer of C 3-2:K⁺ is shown. Colour scheme: potassium - blue-grey.*
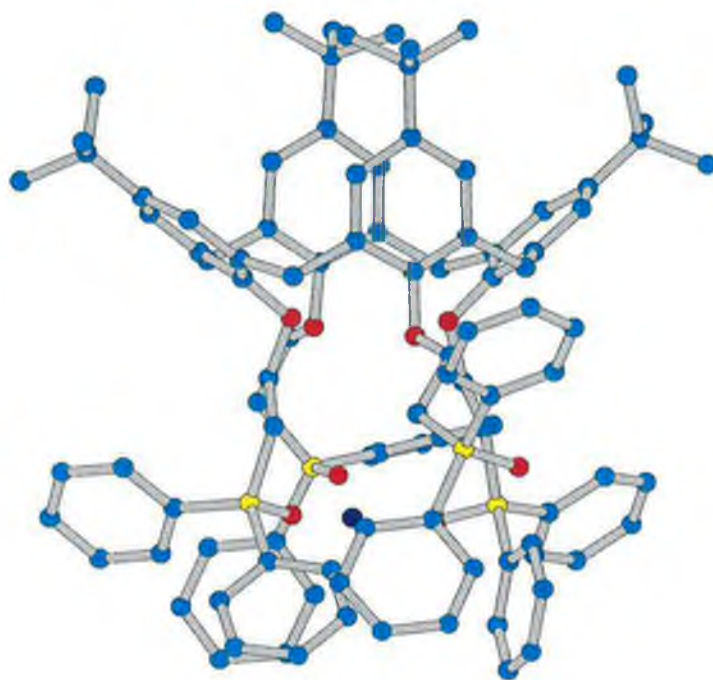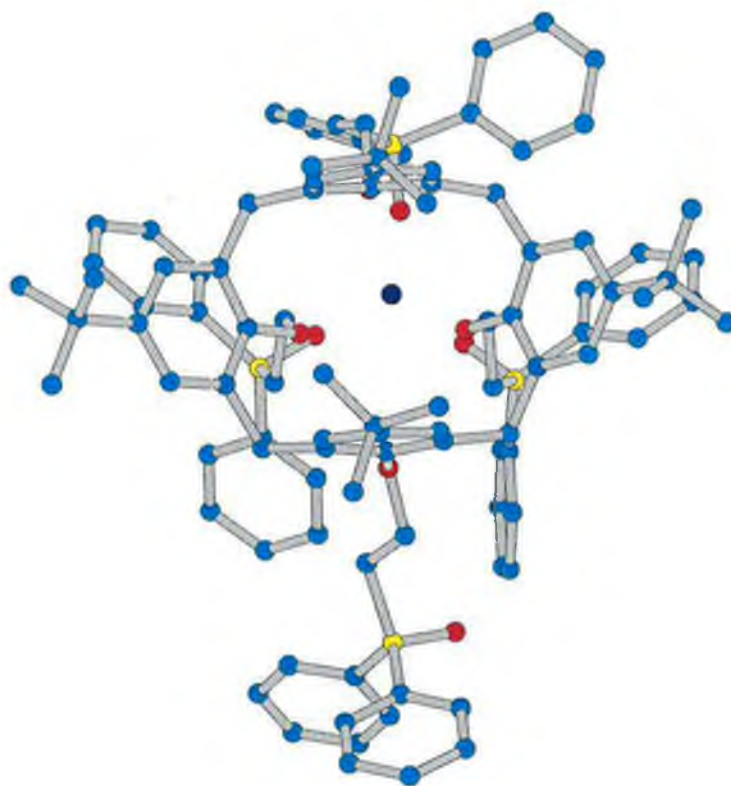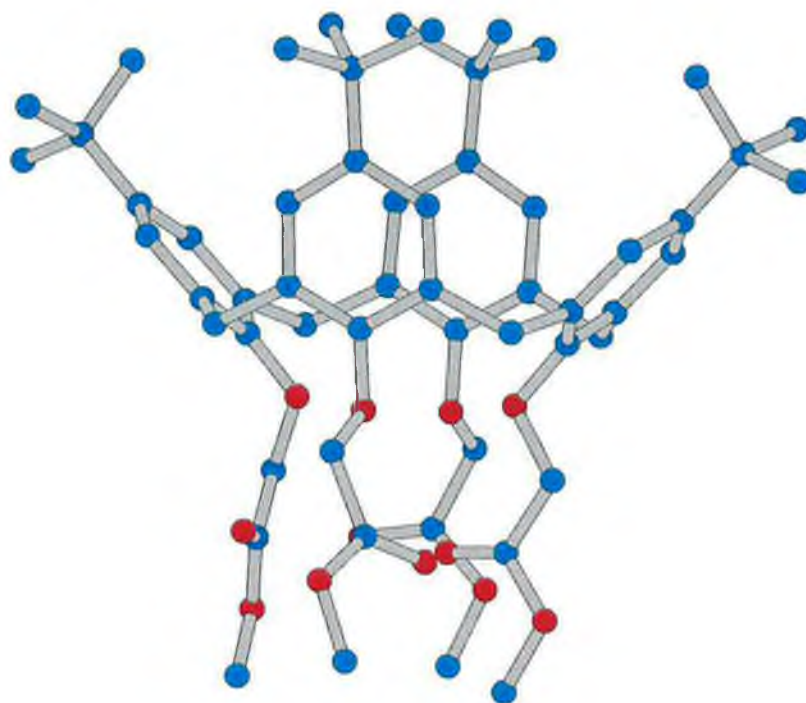
(a)
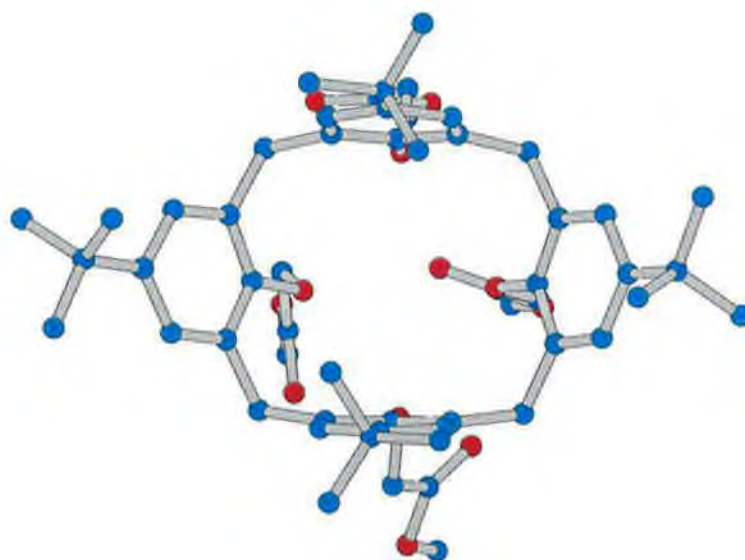
(b)

Figure 3-17. *As for Figure 3-7, except that the model of the global minimum conformer of C 3-3 is shown.*
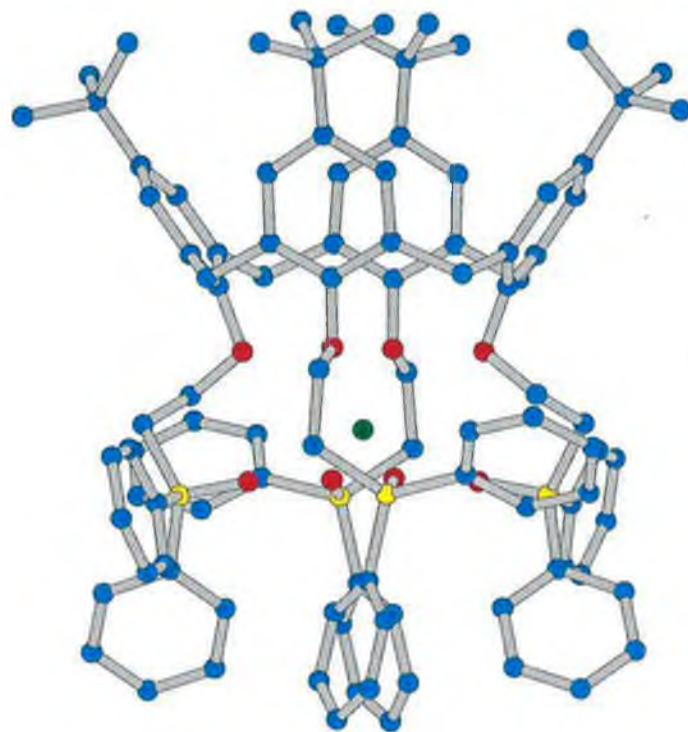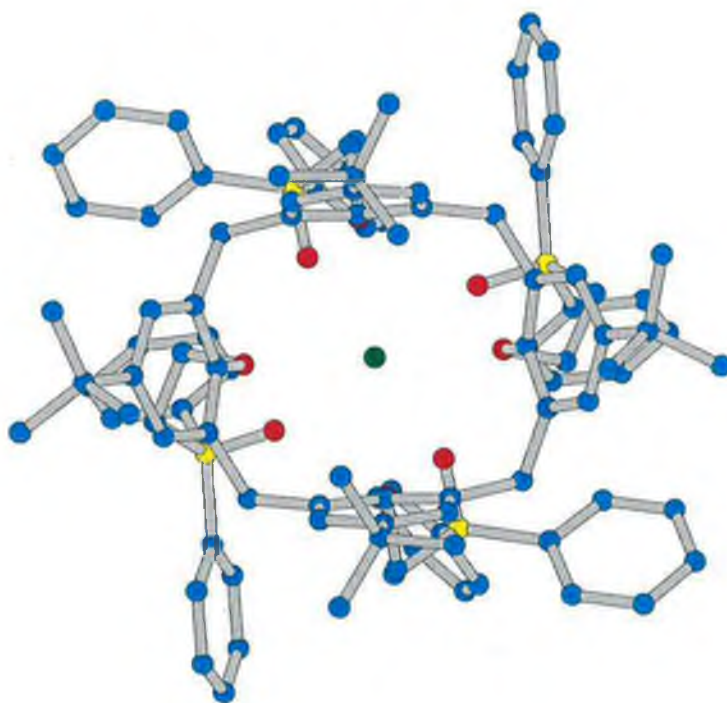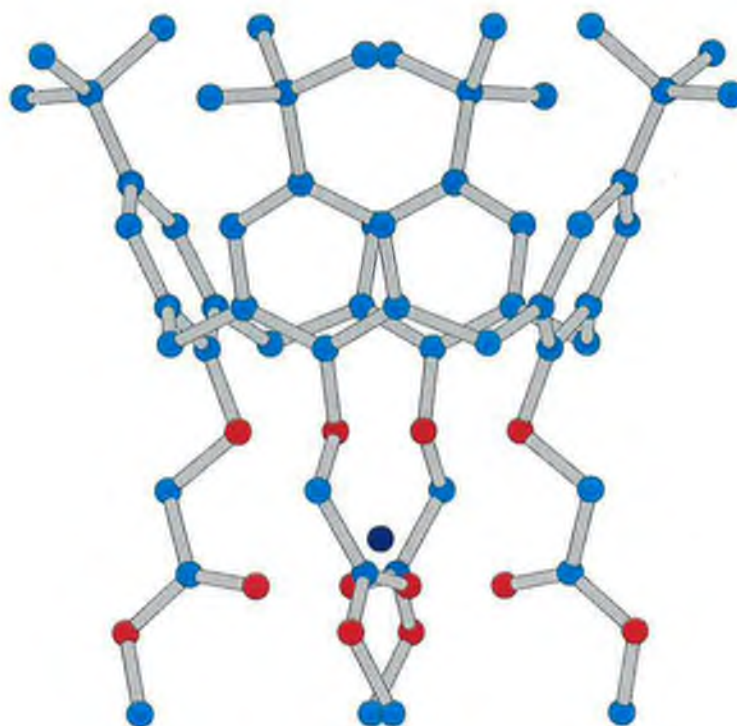
(a)
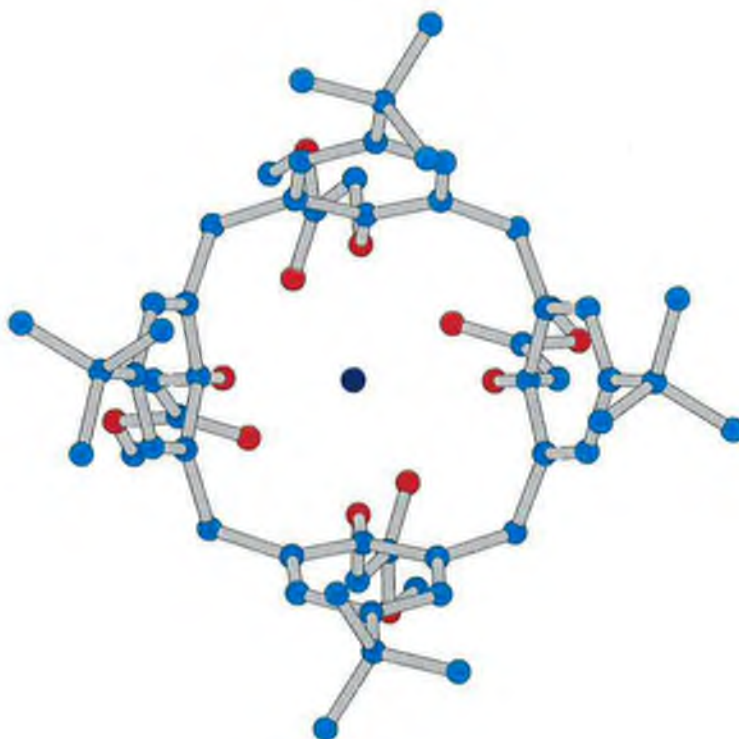
(b)

Figure 3-18. *As for Figure 3-7, except that the model of the global minimum conformer of C 3-3:Li$^+$ is shown.*
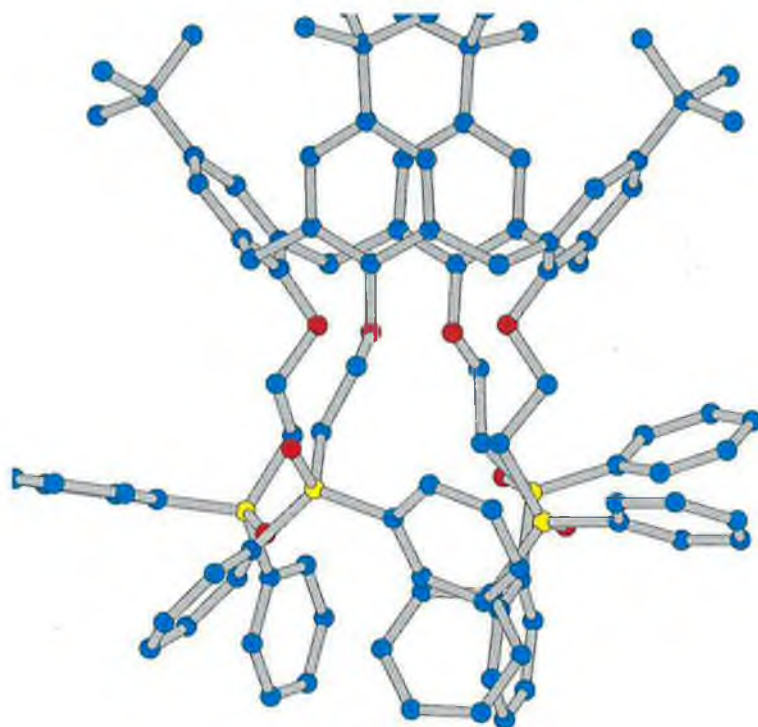
(a)

(b)
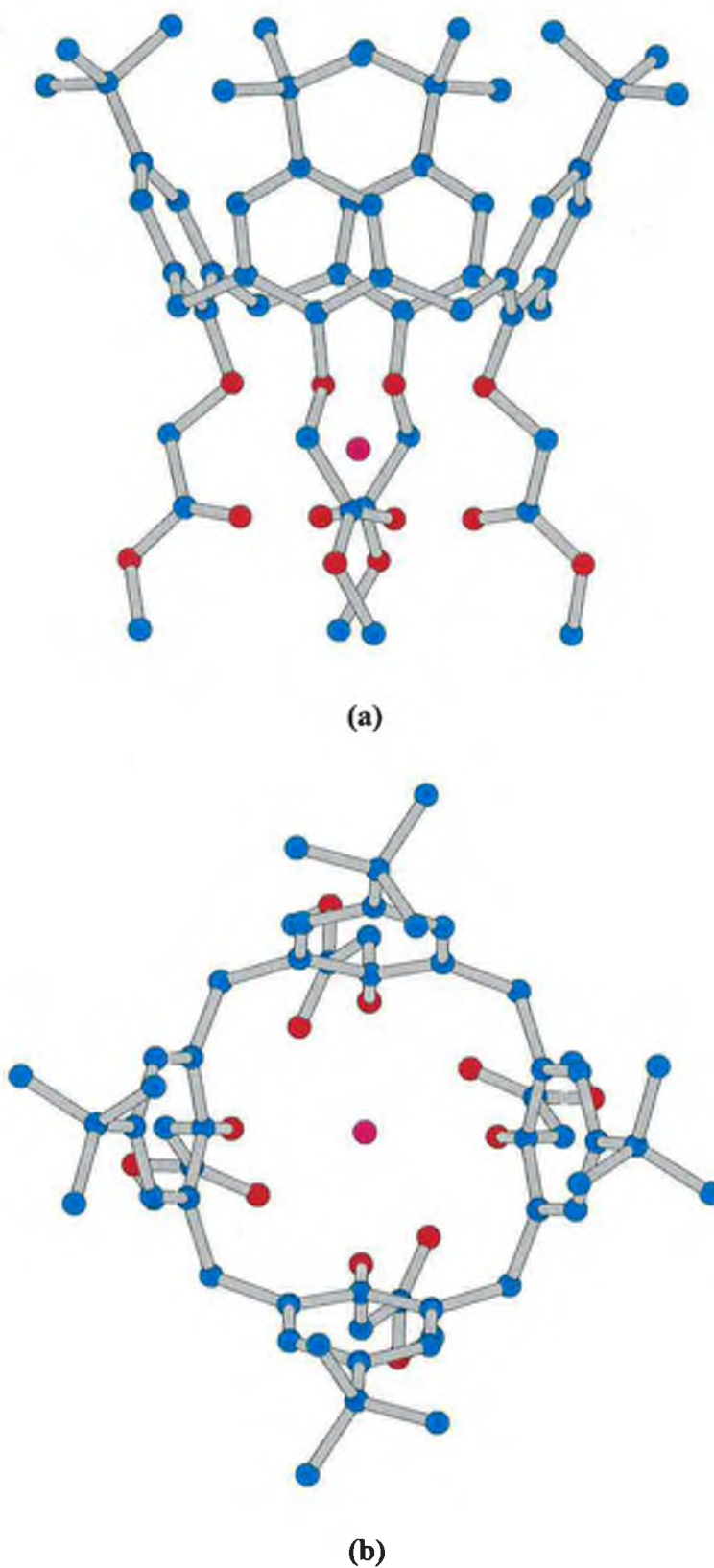
Figure 3-19. *As for Figure 3-7, except that the model of the global minimum conformer of C 3-3:Na$^+$ is shown. Colour scheme: sodium - magenta.*
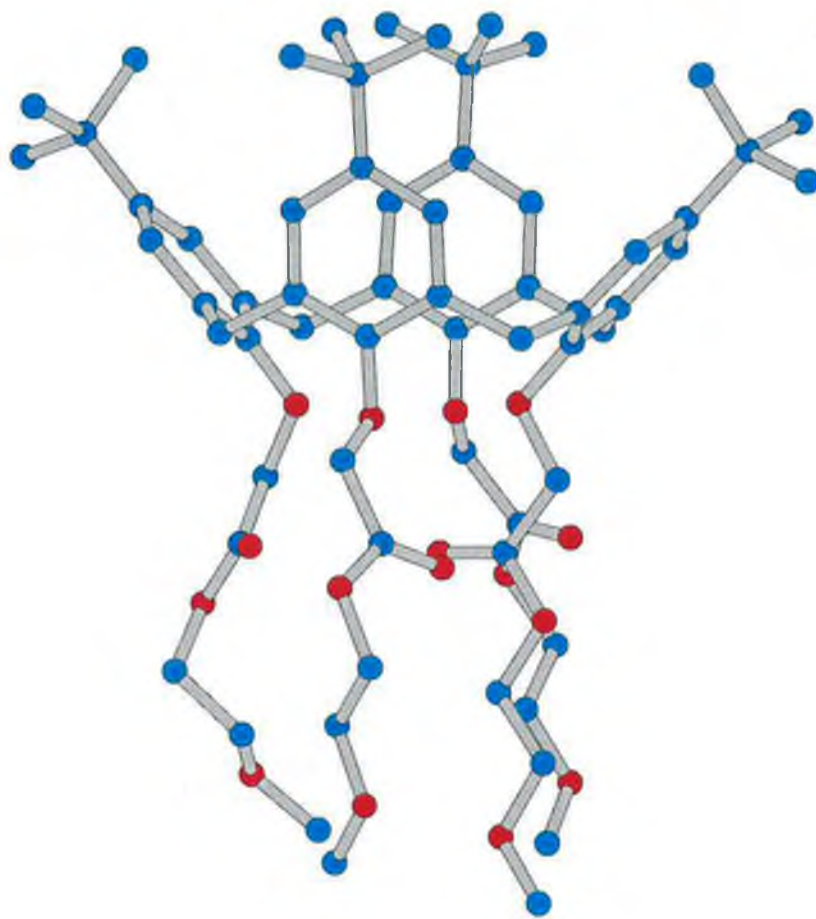
(a)
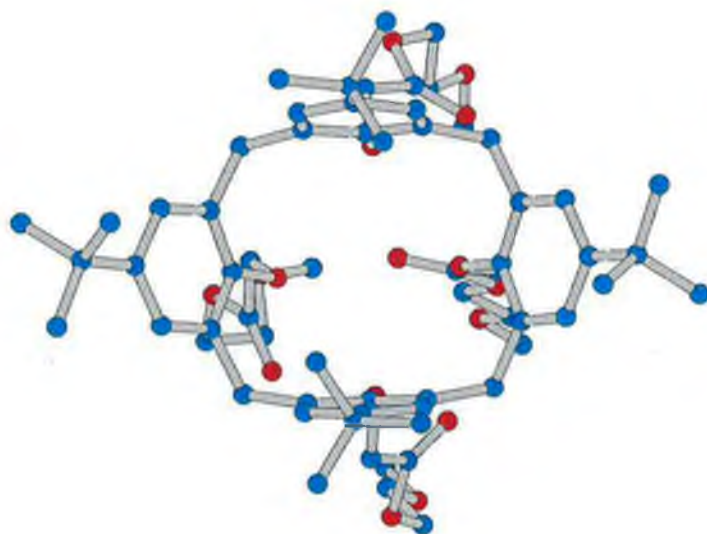
(b)

Figure 3-20. *As for Figure 3-7, except that the model of the global minimum conformer of C 3-4 is shown.*
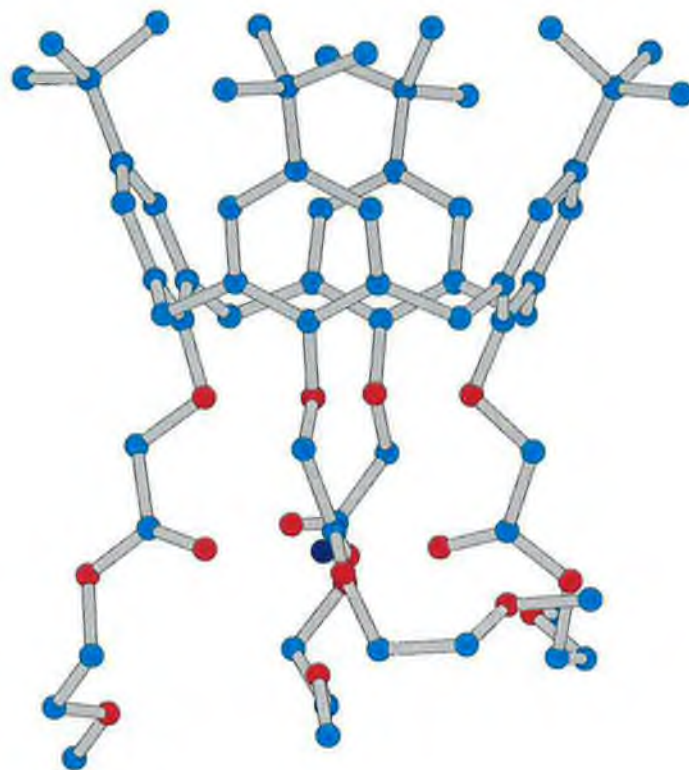
(a)
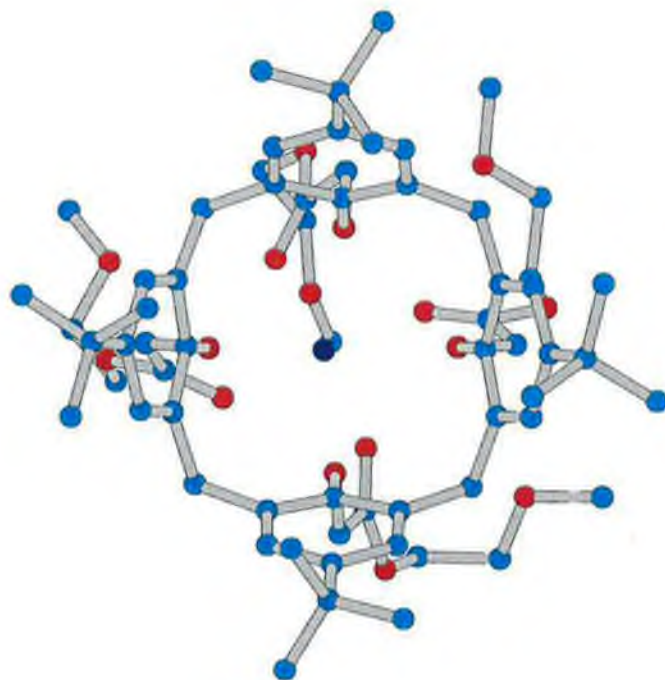
(b)

Figure 3-21. *As for Figure 3-7, except that the model of the global minimum conformer of **C 3-4**:Li⁺ is shown.*
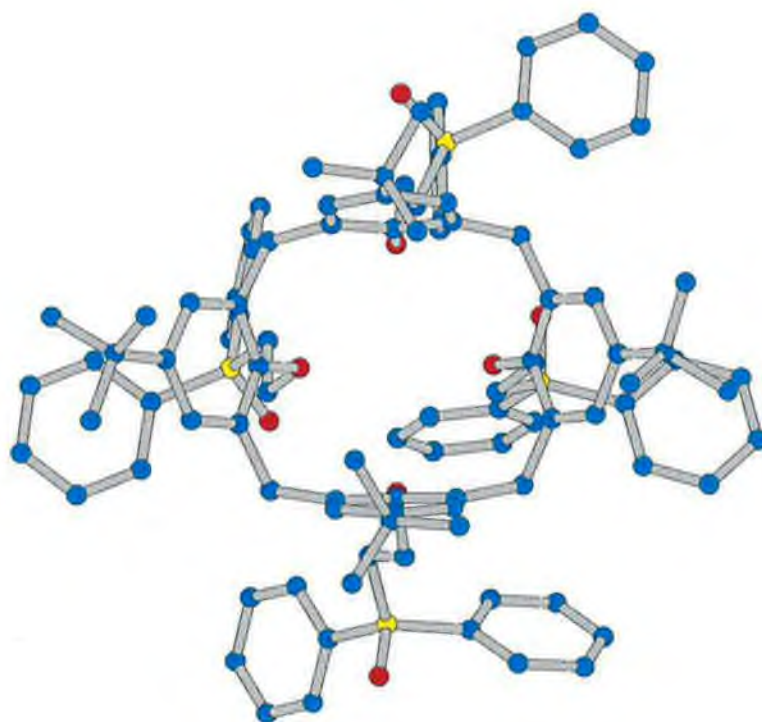
134
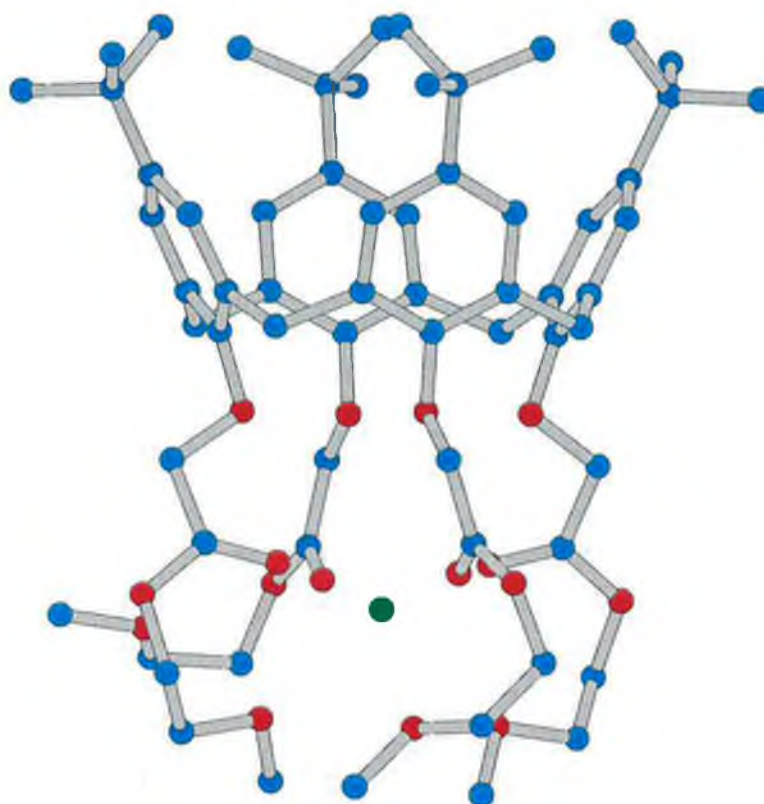
(a)
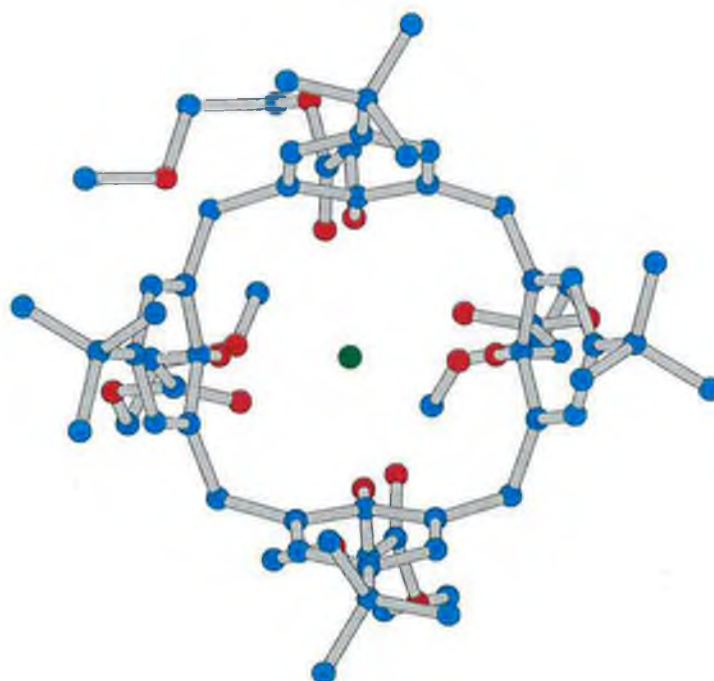
(b)

Figure 3-22. *As for Figure 3-7, except that the model of the global minimum conformer of C 3-4:Ca^{2+} is shown. Colour scheme calcium - green.*
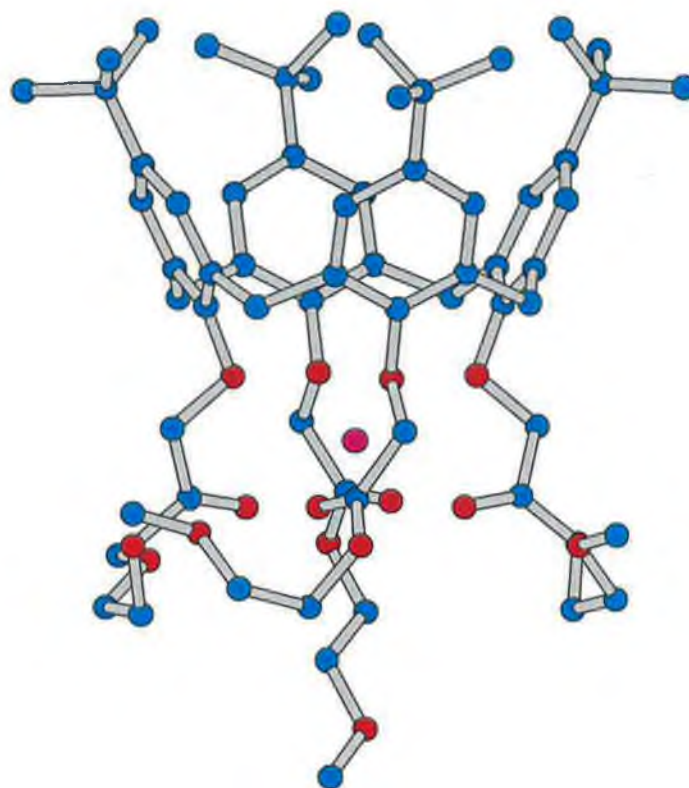
(a)
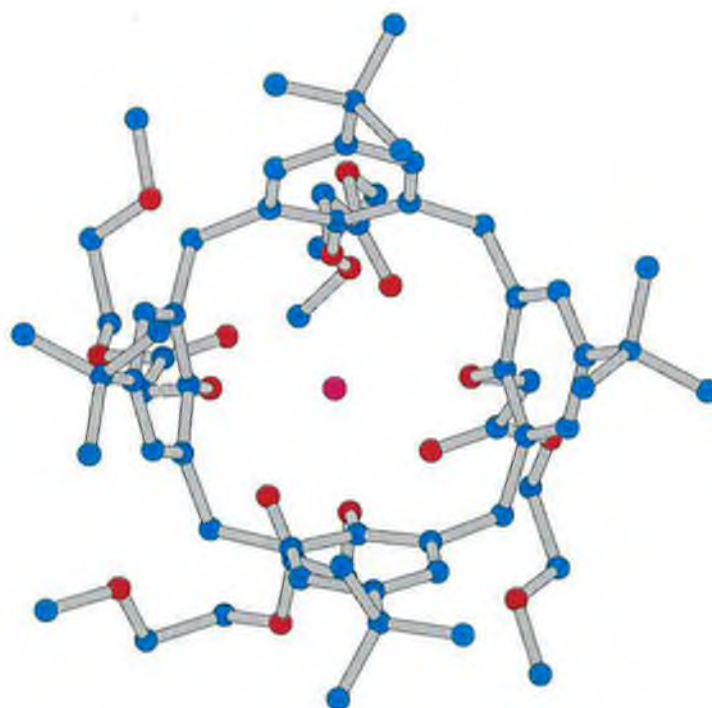
(b)

Figure 3-23. *As for Figure 3-7, except that the model of the global minimum conformer of C 3-4:Na⁺ is shown. Colour scheme: sodium -magenta.*
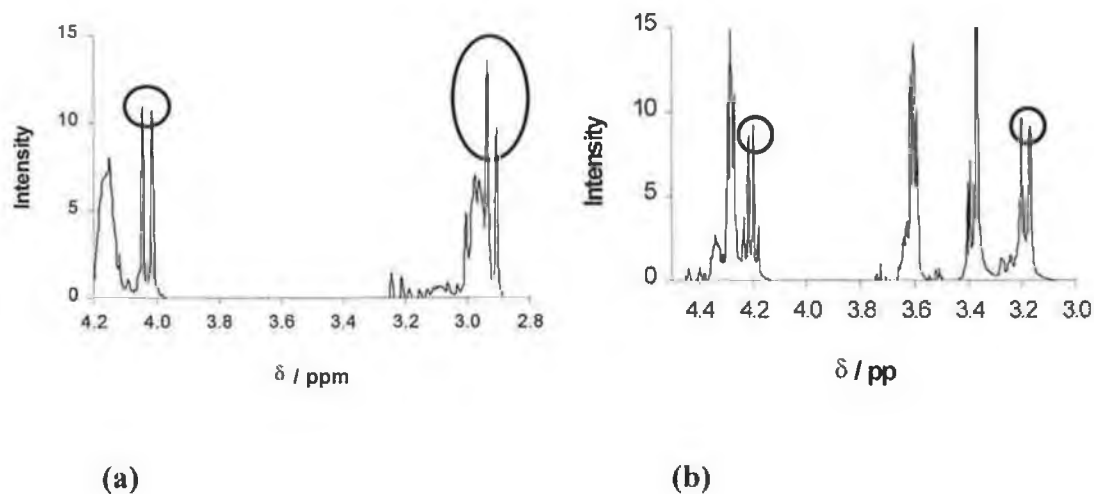
**Figure 3-24.** Partial ^1H *NMR spectrum of mixtures of* **C 3-2** *with (a) sodium and (b) calcium. The rings highlight the doublets assigned to the resonances of the methylene bridging protons.*
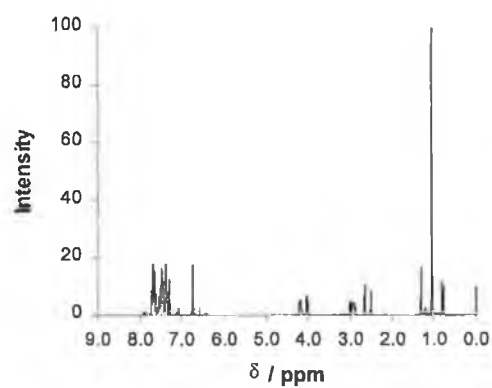
(a)
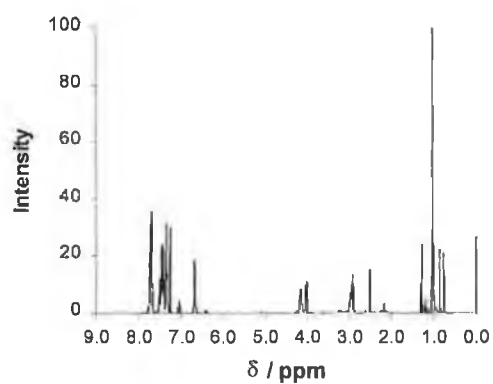
(b)
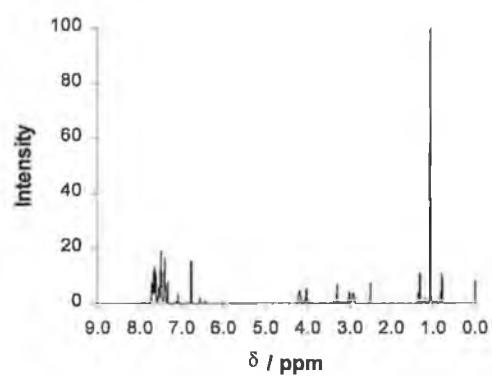
(c)

Figure 3-25. *^{1}H NMR spectra of C 3-2 - sodium mixtures for sodium:ligand ratios of: (a) 0, (b) 0.25, (c) 1.0.*

138

(a)

(b)

(c)
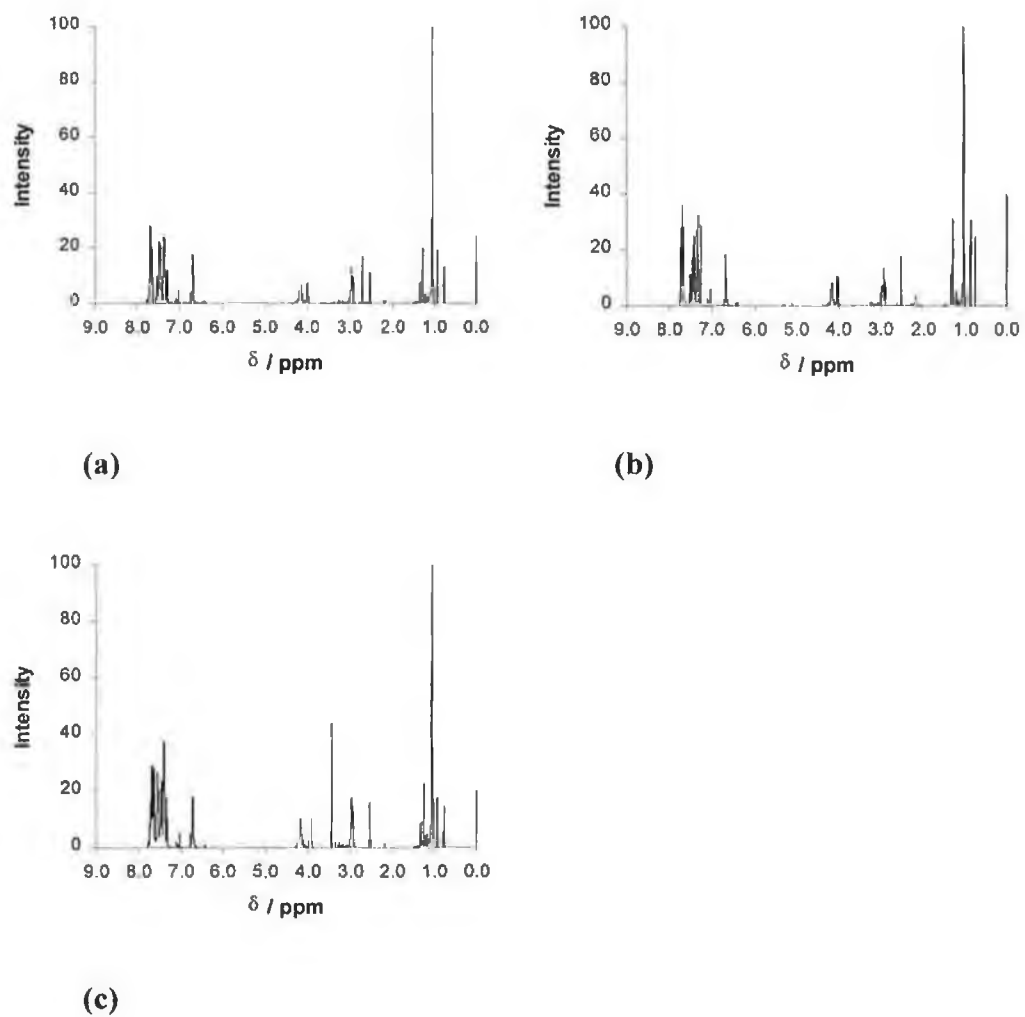
Figure 3-26. *^{1}H NMR spectra of C 3-2 - calcium mixtures for calcium:ligand ratios of: (a) 0, (b) 0.25, (c) 1.0.*

(a)   (b)
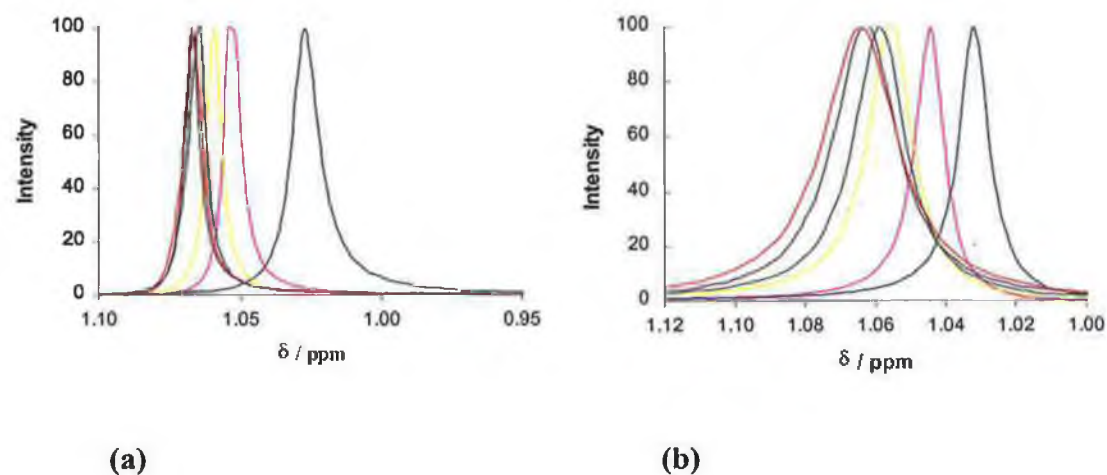
Figure 3-27. *Overlaid* partial *¹H NMR spectra of cation - **C 3-2** mixtures in the region assigned to the t-butyl protons for: (a) Na⁺ and (b) Ca²⁺ and for the cation:ligand ratios of: 0 (blue), 0.5 (pink), 1.0 (yellow), 1.5 (green), 2 (violet) and 2.5 (red).*

(a)

(b)

(c)

(d)
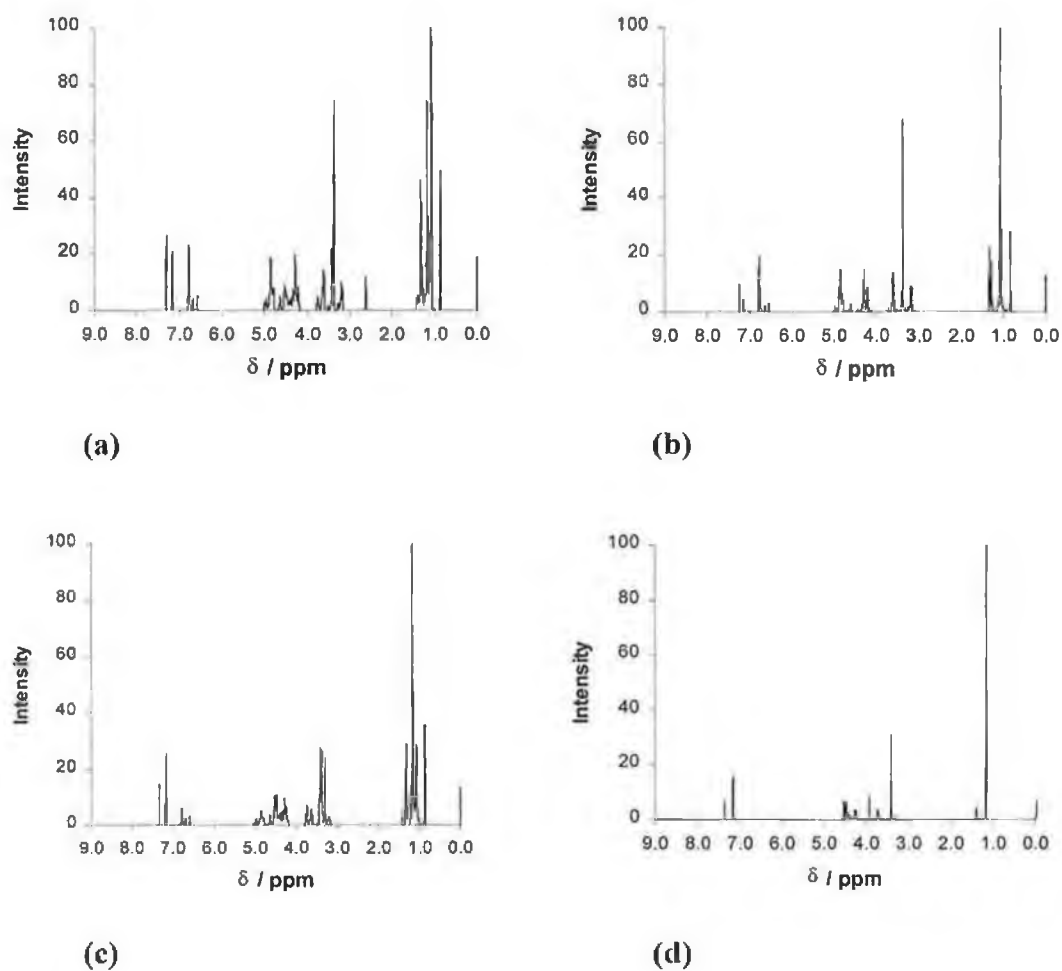
Figure 3-28. *^1H NMR spectra of **C 3-4** sodium mixtures for sodium:**C 3-4** ratios of: (a) 0, (b) 0.25, (c) 0.5, (d) 1.*

(a)   (b)
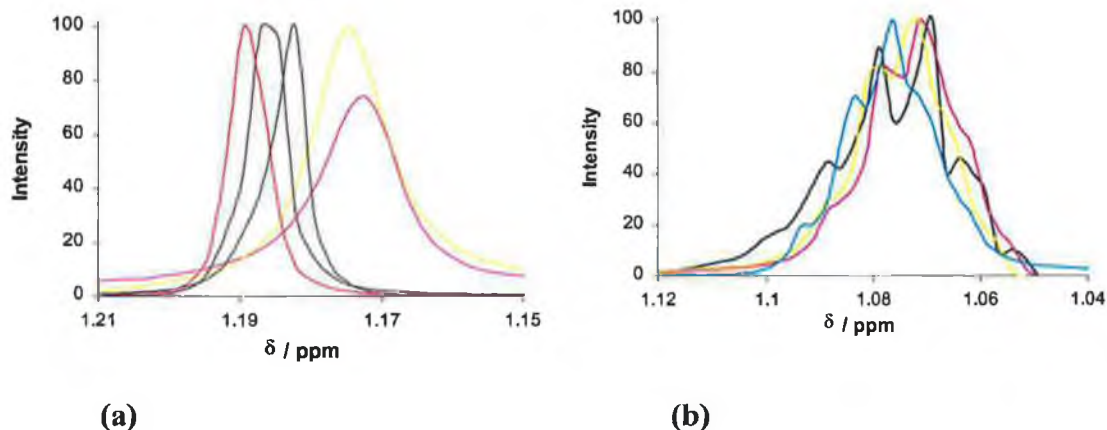
Figure 3-29. *Overlaid partial ^1H NMR spectra of cation:C 3-4 mixtures over the region assigned to the t-butyl protons for: (a) Na^+ and (b) Ca^{2+} and for the cation:ligand ratios of: 0 (blue), 0.5 (pink), 1.0 (yellow), 1.5 (green), 2 (violet) and 2.5 (red).*

Cation:Calixarene Mole Ratio
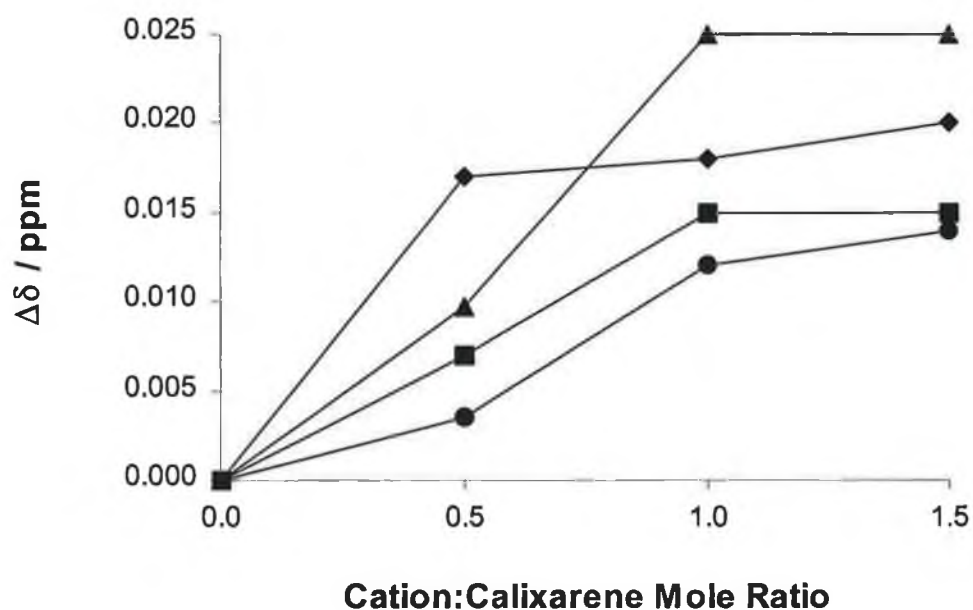
Figure 3-30. *Plot of the change in chemical shift of the most intense peak in the region assigned to the t-butyl protons of the ^1H NMR spectra of C 3-2:Na^+ (triangular points), C 3-2:Ca^{2+} (square points), C 3-4:Na^+ (diamond-shaped points) and C 3-4:Ca^{2+} (circular points).*
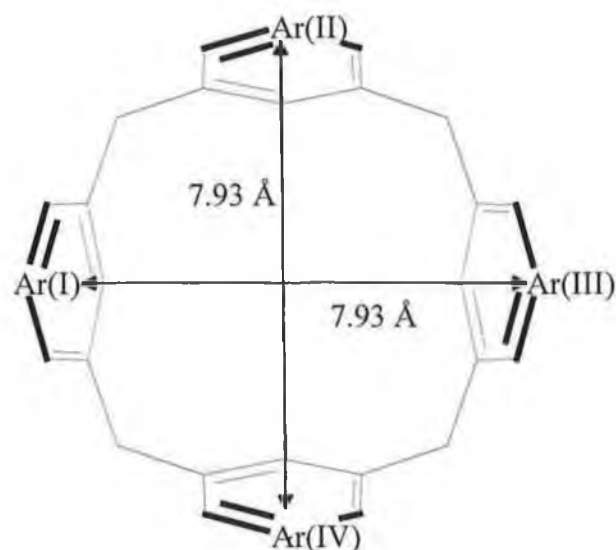
Figure 3-31. *Explanation of the distance between facing aryl rings that is used as a measure of symmetry of macrocyclic ring and which is quoted in Table 3-1 to Table 3-4, inclusive. The example used in this case is **C** 3-3:Na$^+$. Hydrogen atoms, substituents on the upper and lower rims and the Na$^+$ ion have been omitted for the sake of clarity.*

3.8.   Supplementary Data

Table 3-7.   *Cation to Ligand Distances in X-ray crystal structures* of *calixarene:cation complexes that are available from the Cambridge Crystallographic Data Centre (CCDC) and which are used in this chapter. [a]*

Cation	Cation to Ligand Distance / Å [b]	CCDC Ref.	Ref. in this chapter
Li$^+$	1.95 ± 0.07 (3)	ZESGIN	23a
Li$^+$	2.07 ± 0.11 (5)	KIPZUE	23b
Li$^+$ [c]	2.02 ± 0.00 (2)	ZALCOE	23c
Li$^+$	2.14 ± 0.00 (6)	CAXWUT	23d
Na$^+$	2.37 ± 0.04 (4)	VOYYEN	24a
Na$^+$	2.34 ± 0.01 (2)	VOYYAJ	24a
Na$^+$	2.37 (1)	VOYYIR	24a
Na$^+$	2.38 (1)	VUNHAN	24a
Na$^+$	2.30 ± 0.03 (4)	DONSAA	24b
Na$^+$	2.39 ± 0.06 (2)	YERFIK	24c
Na$^+$ [d]	2.33 ± 0.06 (2)	YERFIK	24c
Na$^+$	2.46 (1)	PEMLEE	24d
K$^+$	2.70 ± 0.01 (2)	YEYSEA	25a
K$^+$ [d]	2.66 ± 0.02 (2)	YEYSEA	25a
K$^+$	2.76 ± 0.08 (7)	SIGCUG	25b
K$^+$	2.87 ± 0.07 (9)	ZEWHUE	25c
K$^+$	2.57 ± 0.07 (6)	PIHXUZ	25d
Ca^{2+}	2.31 ± 0.03 (6)	SOGDUN	26

[a] *The ligating atoms are ether oxygen atoms except where stated.*

[b] *The distances and errors quoted are the mean and standard deviation values, respectively. The numbers in parentheses refer to how many values were used to calculate the mean and standard deviation values.*

[c] *The ligating atoms are nitrogen atoms.*

[d] *The ligating atoms are carbonyl oxygen atoms.*

Table 3-8. *The ionic radii of the cations used in the molecular modeling studies [a, b].*

Cation	Co-ordination Number			
	4	6	8	12
Ca^{2+}		1.00	1.12	1.35
Li^{+}	0.59	0.76		
Mg^{2+}	0.57	0.72	0.89	
K^{+}	1.37	1.38	1.51	1.64
Na^{+}	0.99	1.02	1.18	1.39

[a] *Data taken from Reference 30.*

[b] *All the values quoted are in Angstroms.*

3.9. Location Of Files

Description	Computer	Dir.			Comment(s)
Spartan files	Silicon Graphics workstation	usr\ people\ kevin\ storage	**Sub-dir.**		Can be opened in HyperChem if converted to PDB format
			C 3-1	tpo1	
	Serial Number: 0800 6972 B7CB		C 3-2	tpo2	
			C 3-3	tme	
	IP Address: 136.206.86.45		C 3-4	tmxyee	
Paper which focuses on the work done on **C 3-1** and **C 3-2,** as described in this chapter (in HTML format): *"Conformational Analysis ...Cations"*	Dell Pentium Pro 180 PC	C:\ _Paddy\ Talks\ ECCC5	**Filename**: Calix Conf Analy.doc		

146

3.10. References

1.   a) C. D. Gutsche, *Macrocyclic Chem*, **1987**, 3, 93; b) J. Vicens, V. Bohmer, "Calixarenes – a Versatile Class of Macrocylic Compounds"; Kluwer, Boston, MA, 1991.

2.   a) Z. Brzozka, B. Lammerink, D. N. Reinhoudt, E. Ghindini and R. Ungaro, *J. Chem. Soc., Perkin Trans. 2*, **1993**, 65, 3156; b) E. Ghindini, F. Ugozzoli, R. Ungaro, S. Harkema, A. El-Fadl and D. N. Reinhoudt, *J. Am. Chem. Soc.*, **1990**, 112, 1037; c) D. N. Reinhoudt and E. J. R. Sudholter, *Adv. Mat.*, **1990**, 2. d) US IBM Patent Database. Inventors : S. J. Harris, D. Diamond and M. A. McKervey, Patent number 5599913; e) P. L. H. M. Cobben, R. J. M. Egerbink, J. G. Bomer, P. Bergveld, W. Verboom and D. N. Reinhoudt, *J. Am. Chem. Soc.*, **1992**, 114, 10573. e) J. L. Atwood, G. A. Koutsantonis and C. L. Rason, *Nature*, **1994**, 368, 229.

3.   a) J. Stary, *Talanta*, **1966**, 13, 421; b) T. H. Sidall III, *J. Inorg. Nucl. Chem.*, **1964**, 1991; c) M. K. Chmutova, N. E. Kochetova, O. E. Koiro, B. F. Myasoedov, T. Y A. Medved, N. P. Nesterova and M. I. Kabachnik, *J. Radioanal. Chem.*, **1983**, 80, 63; d) K. Farah, S. Elbayoumy and A. T. Kandil, *J. Radioanal. and Nuc. Chem.* **1992**, 157 (1), 87; e) K. Chaneching, M. Lequan, R. M. Lequan, C. Runser, M. Barsoukas and A. Fort, *J. Mat. Chem.*, **1995**, 5, (4), 649.

4.   a) T. McKittrick and D. Diamond, *Talanta*, **1996**, 43, 1145; b) S. O'Neill, P. Kane, M. A. McKervey and D. Diamond., *Anal. Comm.*, **1998**, 35, 127.

5.   a) D. Diamond, G. Svehla, E. M. Seward and M. A. McKervey, *Anal. Chim. Acta*, **1988**, 204, 223; b) A. M. Cadogan, D. Diamond, M. R. Smyth, M. Deasy, M. A. McKervey, S. J. Harris, *Analyst*, **1989**, 114, 1551.

6.   K. Cunningham, G. Svehla, S. J. Harris and M. A. McKervey, *Analyst*, **1993**, 118, 341.

7.　　a) M. Lipton and W. C. Still, *J. Comp. Chem.*, **1988**, 9, 1669; b) M. Dyert, N. Go and H. A. Scheraga, *Macromolecules*, **1975**, 8, 750; c) W. C. Still and I. Galynker, *Tetrahedron*, **1981**, 37, 3981.

8.　　a) M. Saunders, *J. Am. Chem. Soc.*, **1987**, 109, 3150; b) D. M. Ferguson and D. J. Raber, *J. Am. Chem. Soc.*, **1989**, 111, 4371.

9.　　P. K. Weiner, S. Profeta, G. Wipff, T. Havel., I. D. Kuntz, R. Langridge and P. A. Kollman, *Tetrahedron*, **1983**, 39, 1113.

10.　　M. Saunders, K. N. Houk, Y.-D. Wu, W. C. Still, M. Lipton, G. Chang, W. C. Guida, *J. Am. Chem. Soc.*, **1990**, 112, 1419.

11.　　G. Chang, W. C. Guida and W. C. Still, *J. Am. Chem. Soc.*, **1989**, 111, 4379.

12.　　a) N. Metropolis, A. W. Rosenbluth, M. N. Rosenbluth, A. H. Teller and E. Teller, *J. Chem. Phys.*, **1953**, 21, 1087; b) Z. Li and H. A. Scheraga, *Proc. Nat. Acad. Sci.,* **1987**, 84, 6611; c) A. R. Leach in "Computational Chemistry" Vol. 2, 1, K. B Lipkowitz. & D. B. Boyd, Eds., VCH Publishers, New York, 1994.

13.　　P. Kane and D. Diamond, *Talanta*, **1997**, 44, 1847.

14.　　J. F. Malone, D. J. Marrs,. M. A. McKervey, P. O' Hagan, N. Thompson, A. Walker, F. Arnaud-Neu, O. Mauprivez, M.-J. Schwing-Weill, J. F. Dozol, H. Rouquette and N. Simon., *J. Chem. Soc., Chem. Commun.*, **1995**, 2151.

15.　　J. Lu, Q. Chen, D. Diamond and J. Wang, *Analyst*, **1993**, 118, 1131.

16.　　P. C. Meier, D. Ammann, W. E. Morf and W. Simon, in J. Koryta, Editor, "Medical and Biological Applications of Electrochemical Devices", John Wiley, Chichester, 1980, p.22.

17.　　S. Walsh and D. Diamond, *Talanta*, **1995**, 42 (4), 561.

18.　　Spartan, Wavefunction Inc., 18401 Von Karman Ave., Suite 370, Irvine, CA 92612, U.S.A. http://www.wavefun.com/.

19.　　T. Halgren, *J. Am. Chem. Soc.*, **1992**, 114, 7827.

20.   M. Clark, R. D. Cramer and N. van Opdenbosch, *J. Comput. Chem.*, **1989**, 10, 982.

21.   D. Diamond and F. Regan, *Electroanalysis* (N. -Y.), **1990**, 2 (2), 113.

22.   a) The crystal structures referred to in this chapter are available from the Cambridge Crystallographic Data Centre (CCDC), 12 Union Road, Cambridge CB2 1EW, UK, e-mail: deposit@ccdc.cam.ac.uk; (b) F. H. Allen and O. Kennard, *Chem. Des. Auto. News*, **1993**, 8, 1 & 31-37.

23.   a) H. Bock, A. John, C. Nather and Z. Havlas *J. Am. Chem. Soc.*, **1995**, 117, 9367, (CCDC Reference: ZESGIN);   b) D. V. Khasnis,   J. M. Burton, M. Lattman and H. Zhang *J. Chem. Soc., Chem. Comm.*, **1991** 562, (CCDC Reference: KIPZUE);   c) J. Jubb, P. Berno, S. Shoukang Hao and S. Gamarotta, *Inorg. Chem.*, **1995**, 34, 3563, (CCDC Reference: ZALCOE);   d) K. N. Trueblood, C. B. Knobler, E. Maverick, R. C. Helgeson, S. B. Brown and D. J. Cram, *J. Am. Chem. Soc.*, **1981**, 103, 5594, (CCDC Reference: CAXWUT).

24.   a) J. L. Atwood, G. W. Orr, N. C. Means, F. Hamada, H. Zhang, S. G. Bott and K. D. Robinson, *Inorg. Chem.*, **1992** 31, 603, (CCDC References: VOYYEN, VOYYAJ, VOYYIR, VUNHAN);   b) S. G. Bott, A. W. Coleman and J. L. Atwood *J. Am. Chem. Soc.*, **1986**, 108, 1709, (CCDC Reference: DONSAA);   c) A. Ikeda, H. Tsuzuki and S. Shinkai, *Tetrahedron Lett.*, **1994**, 35, 8417, (CCDC Reference: YERFIK);   d) J. L. Atwood, G. W. Orr, S. G. Bott and K. D. Robinson. *Angew. Chem., Int. Ed. Engl.*, **1993**, 32, 1093, (CCDC Reference: PEMLEE).

25.   a) P. D. Beer, M. G. B. Drew, P. A. Gale, P. B. Leeson, and M. I. Ogden, *J. Chem. Soc., Dalton Trans.*, **1994**, 3479, (CCDC Reference: YEYSEA); b) E. Ghidini, F. Ugozzoli, R. Ungaro, S. Harkema, A. A. El-Fadl and D. N. Reinhoudt, *J. Am. Chem. Soc.*, **1990**, 112, 6979.   (CCDC Reference: SIGCUG); c) P. D. Beer, M. G. B. Drew, R. J. Knubley and M. I. Ogden, *J. Chem. Soc., Dalton Trans.*, **1995**, 3117, (CCDC Reference: ZEWHUE);   d)

W. I. I. Bakker, M.Haas, C. Khoo-Beattie, R. Ostaszewski, S. M. Franken, and H. J. den Hertog Juni, *J. Am. Chem. Soc.*, **1994**, 116, 123, (CCDC Reference: PIHXUZ).

26.   J. M. Harrowfield, M. I. Ogden, W. R. Richmond and A. H. White, *J. Chem. Soc., Dalton Trans.*, **1991**, 2153, (CCDC Reference: SOGDUN).

27.   HyperChem is available from Hypercube, Inc., 1115 N.W. 4th Street, Gainesville, Florida, 32601 U.S.A.

28.   G. G. Guilbault, R. A. Durst, M. S. Frant, H. Freiser, E. H. Hansen, T. S. Light, E. Pungor, G. Rechnitz, N. M. Rice, T. J. Rohm, W. Simon and J. D. R. Thomas, *Pure Appl. Chem.*, **1976**, 48, 127.

29.   Y. Umezawa, K. Umezawa. and H. Sato, *Pure Appl. Chem.*, **1994**, 67, 507.

30.   J. A. Dean, "Lange's Handbook of Chemistry", 14th Ed., McGraw Hill, Inc., 1992 and references contained therein.

4. Determination of Ion-Selective Electrode Characteristics by Non-Linear Curve Fitting

4.1. Introduction

The most widely used methods for determining potentiometric selectivity coefficients of ISE's have been the separate solution (SS) method,[1] the fixed interference (FI) method[1] or what Umezawa et. al.[2] refer to as the two-solution method. The fixed primary ion (FPI) method[1] has also been used but is less popular. The matched potential (MP) method, developed by Gadzekpo and Christian,[3] has been recommended by Umezawa et. al.[29] when the ionic charges of the primary and interfering ions are unequal or when the electrode response to either ion is non-Nernstian. In a variation on the SS method, Bakker[4] has described a method where the ISE is conditioned in a solution of interfering ion.

In practical terms, all of these methods involve the transfer of electrodes to different solutions and as such, are subject to 'carryover' error. The SS method and Bakker's variation on it,[4] have the disadvantage that they are not realistic representations of the practical behaviour of the electrode since in practice, measurements are made in the presence of both primary and interfering ions, and competitive processes can have a significant effect on the electrode response. However, Bakker's approach is interesting in that the ISE, with a membrane containing the tetraphenylborate salt of

an interfering ion, is conditioned in an interfering ion solution. The difficulty that the interfering ion has in displacing the primary ion from the membrane when the ISE is conditioned in a primary ion solution and then transferred to an interfering ion solution, is thus avoided and a Nernstian response is expected from interfering ions, something which does not always occur when electrodes are conditioned in primary ion solutions. The potentiometric selectivity coefficients obtained are therefore more representative of the ion-exchange process. However, they are not representative of practical electrode behaviour, where the conditioning and calibration of the ISE in solutions of the primary ion, is standard practice.

The FI method, as traditionally used,[1] involves the preparation of a range of solutions with different primary ion activities but with a constant activity of interfering ion and, as such, the method is both tedious and open to operator error. Furthermore, analysis of the data obtained by this method usually involves manually finding the point of intersection of the extrapolated linear portions of a plot of the cell potential versus the log of the activity of the primary ion.[1] This has two disadvantages; firstly, a decision has to be made as to which portions of the response curve are linear and this makes the method subjective. Secondly, as Moody and Thomas[5] point out, the potentials in the plateau region of this plot are subject to an unacceptable degree of irreproducibility and drift. Srinivasan and Rechnitz[6] derived two equations for high and low values of potentiometric selectivity coefficients, respectively, and these allow potentiometric selectivity coefficients to be determined from data relating to a range of activities. However, their methods require some *a priori* knowledge of selectivity before choosing the activities of the primary and interfering ions and the appropriate equation. Furthermore, their methods allow no "at a glance idea" of selectivity, as provided by the traditional FI method.

In principle, the MP method requires just two experimental points to calculate the potentiometric selectivity coefficient (or the interference ratio since, as Maccà[7] points out, the quantity obtained by the MP method is by definition, different to the traditional potentiometric selectivity coefficient). In practice, however, this method requires measurements to be made in solutions of different concentrations of interfering ion and then sophisticated interpolation if it is to be accurate. As such, it

is no less tedious or time consuming than the traditional FI method. Another disadvantage of the MP method is that for electrodes which are very selective, the level of interferent required to equalise the potentials may be so high as to make the method unrealistic since, in practice, such levels of interferents are unlikely to be encountered and extrapolation to lower interfering ion activity is not generally advisable. Furthermore, Maccà[7] claims that the interference ratio is more concentration dependent than the potentiometric selectivity coefficient.

Therefore, there is a need for an approach which is practically simple to implement, and which removes the subjectivity of the conventional FI method.[1] Previously, Yuliang *et. al.*[8] used a non-linear regression approach with electrode measurements of halide ion mixtures. However, they have given no indication (either numerical or graphical) of the quality of the fit to the Nikolskii-Eisenman equation. Furthermore, they give no details of how their approach was implemented, and therefore, it is impossible to comment on the reliability of their results or how easy it is to process data with their method. In a variation on the FI method, Davey *et. al.*[9] plotted the peak heights obtained using a flow-analysis approach versus the log of the primary ion activity at constant concentration of interfering ion. They then used values in the curved region of the plot to determine potentiometric selectivity coefficients using a data linearisation technique based on the Nikolskii-Eisenman equation. Unfortunately, their method did not yield a value for the Nernstian Slope Factor. Diamond and Forster[10, 11] and Saez de Viteri and Diamond[12] have proposed very rigorous non-linear modeling approaches based on multivariate calibration and simplex optimisation which enabled potentiometric selectivity coefficients to be obtained in mixed solutions containing up to four interfering ions. However, these methods are not simple to implement, as even with partial factorial design, 32 calibration solutions are required to characterise a four-electrode array.

There has been some discussion in the literature on alternatives to the Nikolskii-Eisenman equation. Morf *et. al.*[13] proposed an equation for neutral carrier-based calcium-selective ISE's, relating to mixed-ion solutions where the interfering ion is singly charged. Meyerhoff and co-workers[14] have developed a formalism for ISE's

153

of three different carrier types, for mixed-ion solutions which is applicable to all combinations of primary and interfering ions of different charge.

In this chapter, I describe a very simple procedure for obtaining experimental data, and subsequently fitting the data to a mathematical model in order to obtain estimations of the electrode characteristics (the cell constant, the Nernstian Slope Factor and potentiometric selectivity coefficients). In the proposed method, the interfering ion concentration is kept constant and the primary ion concentration is varied by means of a series of small volume 'spikes', added to a single solution, with the electrodes continually in contact, and measuring the cell potential after each addition. Therefore, no transfer of electrodes between measurements is involved and the preparation of relatively few solutions is required. The entire response curve is then fitted to an appropriate model (for example, the Nikolskii-Eisenman equation or the Meyerhoff formalism[14]) to obtain the electrode characteristics which provide the best-fit to the experimental data through minimisation of the least-squares error. This non-linear analysis is carried out using the *Solver* optimisation add-on available in Microsoft Excel for Windows 95, version 7.0 which, with its graphical user interface, is very simple to use. As Excel is normally bundled with PCs these days, the user does not have to invest in any relatively expensive specialised mathematical or statistical packages to perform the calculations.

Despite the known limitations of the Nikolskii-Eisenman, Eqn. (4-1), (strictly speaking, the equation should be applied only when the primary and interfering ions should have Nernstian slopes and a different ionic charge[2]), it was decided to use this model because of the large database of information on this model in existence in the literature. Similarly, a valinomycin-based potassium selective electrode was chosen because of the wealth of data available for this ISE to which I could compare my results.

4.2.   Experimental

4.2.1.   *Materials*

All metal chlorides used were of analytical reagent grade. High molecular weight poly(vinyl chloride) (PVC) lithium chloride, potassium chloride, valinomycin, tetrahydrofuran, bis(2-ethylhexyl)sebacate (DOS) and potassium tetrakis(4-chlorophenyl)borate (KTpClPB) were purchased from Fluka. Magnesium chloride, calcium chloride and barium chloride were purchased from BDH. Sodium chloride and ammonium chloride were purchased from Riedel de Haen. Milli-Q grade distilled water from Millipore was used throughout.

4.2.2.   *Apparatus*

A potassium-selective electrode was prepared according to the procedure of Lu *et. al.*[15] using valinomycin as the ionophore. The components and composition of the membrane used in the ion-selective electrode (ISE) are the same as that used by Knoll *et. al.*[16] and are given in Table 4-1. Membrane resistance and potential measurements were made with a Hewlett Packard 34401 A multimeter and a standard calomel electrode (SCE) as a reference, obtained from EDT Instruments, Ltd., Lorne Road, Dover, Kent, UK.

4.2.3.   *Determination of Potentiometric Characteristics*

The ISE and the SCE were placed in 25.0 cm^3 of a 0.1 mol dm^{-3} aqueous solution of an interfering chloride, for example, sodium chloride. Aliquots (2, 5, 20, 45, 70 and 100 μdm^3) of mixture **1** (0.01 mol dm^{-3} potassium chloride (aq.), 0.1 mol dm^{-3} interfering chloride(aq.)) and then mixture **2** (5, 15, 30, 100, 400 and 1000 μdm^3), (1.00 mol dm^{-3} potassium chloride (aq.), 0.1 mol dm^{-3} interfering chloride (aq.)) were added in the order given. These additions were made with micropipettes, keeping the tip of the micropipettes just above the surface of the solutions while making the addition. The solution was stirred magnetically throughout. After each addition, the potential of the solution was recorded after 1 minute. After all additions had been made, the entire procedure was repeated twice. In this manner, the primary ion (K^+) concentration was varied over a very wide range (8.0 x 10^{-7} to 0.06 mol dm^{-3}) while

155

the interfering ion concentration was kept constant without having to transfer the electrodes to new solutions.

This procedure was repeated for other interfering ions (Li^+, NH_4^+, Ca^{2+}, Mg^{2+} and Ba^{2+}).

Potentiometric selectivity coefficients were also determined by the SS method[1] (0.1 mol dm^{-3} solutions of metal chlorides) for comparison.

4.2.4.   *Treatment of Results*

The potential, E, of a potassium-selective electrode in the presence of both K^+ and an interfering ion, B^{z+} is given by the Nikolskii-Eisenman equation:

$$E = E^0 + S \log \left(a_K + k_{KB}^{Pot} a_B^{1/z} \right)$$ (4-1)

where: E^0 is the Cell Constant

S is the Nernstian Slope Factor

k_{KB}^{Pot} is the potentiometric selectivity coefficient

a is activity of the subscripted ion.

z is the ionic charge on the interfering ion.

Single-ion activity coefficients, f, were calculated using the Davies equation:

$$\log f = -A z^2 \left(\frac{\sqrt{I}}{1+\sqrt{I}} - 0.2I \right)$$ (4-2)

where I is the ionic strength of the solution

and A is the Debye-Hückel parameter which was determined using:

$$A = 1.82481x10^6 (DT)^{-1.5} \quad mol^{1.5} \, dm^{-0.5}$$ (4-3)

where T is the absolute temperature

and D is the dielectric constant of the solvent.

156

The values used for D for the solvent water were either the known value at 20^0C[17] or calculated values based on the temperature of the experiment and empirical equations.[18] Corrections were made to experimental potentials using estimations of the liquid junction potentials, E_J, of the reference electrode, calculated according to the Henderson formula[19] using single-ion activities. A typical set of results are given in Table 4-2 for Na^+ as the interfering ion.

Non-linear curve fitting was carried out to fit the mean experimental values (n = 3) of the corrected (for the effect of the liquid junction potential) cell potentials given in Table 4-2, to the Nikolskii-Eisenman model (Eqn. (4-1)), using the optimisation add-in, *Solver,* available in Microsoft Excel for Windows 95, version 7.0 and the method of Walsh and Diamond.[20] The optimised model returned estimates for the model parameters k_{KB}^{Pot} (see in Table 4-3, Study 1), E^0 and S (both given in Table 4-4). In the case of each interfering ion, the potential of the solution containing interfering chloride only was ignored in the analysis as the drift in this reading was far greater than that for any other reading (typically after 1 minute, when the reading was taken, the drift was 0.1 mV s^{-1} for the solution containing interfering chloride only but for any other reading, it was approximately 0.2 mV min^{-1} after 1 minute). It is worth noting that for a given set of measurements, optimisations with Solver produced the same set of values for E^0, S and k_{KB}^{Pot} regardless of the initial values of these parameters. Thus I can be confident that the optimisations converged at the global minimum, and that the error space is relatively smooth. The experimental potentials and those obtained by Solver are plotted in Figure 4-1 a-f.

An alternative to Eqn. (4-1) for a mixture of a primary ion and an interfering ion with ionic charges of +1 and +2 respectively has recently been proposed by Meyerhoff and co-workers[14]:

$$E = E^0 + \frac{RT}{F}\ln\left(\frac{a_K}{2} + \frac{\sqrt{a_K^2 + 4a_B\left(k_{KB}^{Pot}\right)^2}}{2}\right) \qquad (4-4)$$

157

Replacing the RT/F term with the Nernstian Slope Factor, S, and using common logs, Eqn. (4-4) becomes:

$$E = E^0 + S\log\left(\frac{a_K}{2} + \frac{\sqrt{a_K^2 + 4a_B\left(k_{KB}^{Pot}\right)^2}}{2}\right) \qquad (4\text{-}5)$$

Using the same experimental data, Eqn. (4-5) was fitted to the mean values of the corrected cell potentials (n = 3), in the cases of the doubly charged interfering ions. See Figure 4-2 a-c for the response curves and in Table 4-3, Study 2 and in Table 4-4 for the electrode characteristics obtained using Eqn. (4-5) as the model for the response curve.

The data obtained from calibration of the ISE (i.e., where measurements are made on solutions containing the primary salt only) can also be modeled with this Solver technique, simply by assuming that the sum of the $k_{KB}^{Pot} a_B^{1/z}$ terms in the extended form of Eqn. (4-1) for several interfering ions (present because of the background electrolytes in the deionised water) is constant for each of the calibration solutions. However, Eqn. (4-5) was not used to model the calibration results as it is applicable only for a mixture of a primary ion of charge +1 and one interfering ion of charge +2.

The goodness of fit of the optimised model to the experimental data can be quantified by the standard deviation of the experimental values from best-fit curve, σ[21]:

$$\sigma = \sqrt{\frac{\Sigma(E^* - E)^2}{n - p}} \qquad (4\text{-}6)$$

where: E^* is the predicted potential

E is the measured potential

n is number of measurements (12 in this case)

p is the number of parameters to be varied to determine the curve of best fit (3 in this case).

σ, unlike the correlation coefficient which can be used in linear regression only, is approximately equal to experimental error of the dependent variable and has the same unit of measurement.

For comparison, in Table 4-3 also lists potentiometric selectivity coefficients, obtained using the SS method[1] (Study 5), and the FI method[1] (Study 3, and Study 4 in the case of the doubly charged interfering ions) using the same FI experimental data and Eqn. (4-7).[22] The limit of detection (LOD) used when applying Eqn. (4-7) is estimated by determining the K^+ activity for which the linear and rising portion of the graph deviates by $2.303\,R\,T\log 2/F$ mV from the curved part as described by the Nikolskii-Eisenman model (Study 3) or by Eqn. (4-5) (Study 4). As the interfering ion activity varies slightly (for example, see in Table 4-2), the mean value of a_B^{1/z_B} in the region of the LOD was used to calculate the potentiometric selectivity coeffcient when using Eqn. (4-7).

$$k_{KB}^{Pot} \ = \ LOD/a_B^{1/z_B} \tag{4-7}$$

The estimated limits of detection are given in Table 4-4.

4.3. Results and Discussion

Before testing newly fabricated electrodes, the membrane integrity was checked by measuring the d.c. resistance. These were found to lie in the range 1.0 to 1.1 MΩ, which is typical for PVC-membrane ISE's.[23]

Table 4-3 shows that the $\log k_{KB}^{Pot}$ values obtained using the data analysis method based on Nikolskii-Eisenman model (Study 1) are very similar to those obtained for similar membrane compositions using both the conventional FI method (Study 3) and the SS method (Study 5). Given the variety of experimental conditions, methods and conditions under which the measurements were made, the degree of agreement between the results of the various studies illustrated in Table 4-3 is very encouraging. In almost every case, the general trend is the same ($Li^+ < Na^+ < NH_4^+$ and $Mg^{2+} < Ca^{2+}$), and the values are within an order of magnitude of each other. In the case of Ca^{2+} and Ba^{2+}, good selectivity is obtained by all three methods used in this research,

159

although there are some slight differences in the values of the coefficients. However, such discrepancies are to be expected in these types of measurements, and is reflected in the variations reported by other researchers (see in Table 4-3). For example, the value for the Li^+ potentiometric selectivity coefficient reported by Moody et al (Study 15)[31] which is significantly lower than all other studies. Gadzekpo and Christian[3] obtained very different $\log k_{KB}^{Pot}$ values (by four different methods) for a valinomycin-based potassium ISE (see value for Na^+ potentiometric selectivity coefficient for example, Studies 19-22). Metzger *et. al.*[24] and Gadzekpo *et. al.*[25] have also demonstrated with a number of ionophores that different values for potentiometric selectivity coefficients are obtained depending on whether the FI method or the MP method is used. I believe that our new method is to be preferred as it involves minimising the sum of the squares of the errors over the entire data set (covering a wide range in primary ion activity) rather than using selected portions of the response curve in a very subjective way.

Of the results quoted from other researchers in Table 4-3, those from Knoll *et. al.*[16] (Study 6) are important as the membrane components and composition employed are identical to those used in this investigation, and they used the FI method[1] for determining potentiometric selectivity coefficients. Cosofret *et. al.*[26] (with Membrane L in their paper) used membranes with similar components and composition to this investigation but estimated the potentiometric selectivity coefficients by means of the SS method (Study 7). In both cases, while the values are not an exact match with our data (Study 1), the variations are reasonable given the differences in experimental methods and design.

Table 4-3 also lists the $\log k_{KB}^{Pot}$ values obtained with the formalism (Eqn. (4-5)) recently proposed by Meyerhoff and co-workers for situations where the primary ion charge is +1 and the interfering ion charge is +2 (Study 2). These values were calculated using the same experimental data used for the Nikolskii-Eisenman model (Study 1), but with the least squares error generated from Eqn. (4-5). The trends in the $\log k_{KB}^{Pot}$ values using both models are the same ($Mg^{2+} < Ca^{2+} \approx Ba^{2+}$), but Eqn. (4-5) generates slightly more negative values. With both models, the average relative standard deviation of the potentiometric selectivity coefficient for the three doubly

charged interferents is 15-16% (n=3). The trends in the $\log k_{KB}^{Pot}$ values obtained with the conventional FI method[1] (Study 4) using both the Nikolskii-Eisenman equation and Eqn. (4-5), are also the same ($Mg^{2+} \approx Ca^{2+} < Ba^{2+}$, see the Study 3 and Study 4 results).

In the light of Bakker's work on ISE's conditioned in an interfering ion solution,[4] it could be argued that the potentiometric selectivity coefficients obtained are merely an indication of the detection limit of the ISE. If our results were in fact a measure of the LOD of the electrode, then one would expect that the effect of the interfering ion would be the same in each case. However, the response curves in Figure 4-1 invalidates this latter argument as the location of the plateau region of the graph is clearly dictated by the identity of the interfering ion. Clearly therefore, the potentiometric selectivity coefficients obtained with our new method are a measure of practical selectivity.

The Nernstian Slope Factors, S, obtained using the Nikolskii-Eisenman model and Eqn. (4-5) (given in Table 4-4), are all close to the ideal Nernstian values, as would be expected for a valinomycin ISE.

The Cell Constants, E^0 obtained with the Nikolskii-Eisenman model (see Table 4-4), are similar for interfering ions of a given charge but are different for ions of different charge. One reason for this difference is that the E^0 values for the doubly charged ions decreased by approximately 2 mV on correcting the experimental potentials for variation in the liquid junction potentials but this correction brought about negligible change in the E^0 values for the singly charged ions (i.e., agreement was closer prior to correction). Similar values are obtained with Eqn. (4-5) as the model as would be expected. Nernstian Slope Factors obtained in the presence of doubly charged interfering ions are slightly (by ca. 0.6 mV) higher and the LOD's are slightly more negative using Eqn. (4-5) as the model. The differences in electrode characteristics returned by the two models are small. Given the ease with which Excel can be set up to model either equation with the same data sets, it would be useful for other groups to compare electrode characteristics obtained with both approaches. I have obtained data showing similar agreement for characteristics determined with Meyerhoff's

formalism and the Nikolskii-Eisenman equation from data obtained with a calcium selective electrode and several singly charged interferents (results not shown).

In any curve fitting exercise, it is useful to compare the quality of the fits obtained to the experimental data. One approach is to use the standard deviations of the experimental values from the best-fit curves, σ (see Eqn. (4-6)).

Table 4-5 lists the σ values obtained using Eqn. (4-1) (and Eqn. (4-5) for the doubly charged interfering ions) as the models. These values are low enough to suggest that both equations, in their optimised form, fit the experimental data very well for each interfering ion and that therefore, the values returned for the model parameters are accurate. For example, in the case of Na^+, the σ value of 0.86 mV, which is very low considering the large range in potentials covered (more than 200 mV), and the standard deviation in the experimental mean potentials which vary from 0.8 mV (at high K^+ activity) to 4.1 mV (n=3). The utility of the σ parameter is well illustrated by comparing the values for the different ions. Clearly, Ba^{2-} gives by far the worst fit for both models, and this is confirmed by visually comparing the actual curves (see Figure 4-1f in comparison to other curves in Figure 4-1 and Figure 4-2c in comparison to other curves in Figure 4-2).

The σ values obtained when using Eqn. (4-5) as the model for the doubly charged interfering ions, are greater than that obtained when using the Nikolskii-Eisenman model. This would suggest, in the case of our data, that the Nikolskii-Eisenman model (Eqn. (4-1)) gives a better fit to the experimental data than Eqn. (4-5).

The residual plots resulting from the fits obtained by the two models are illustrated in Figure 4-3 a-c. These plots confirm that the Nikolskii-Eisenman model give better fits in all three cases to those obtained with Eqn. (4-5). Our results therefore suggest that there is no major difference in the electrode characteristics obtained with either model, but that the quality of the fit is superior with the Nikolskii-Eisenman model.

162

4.4.   Conclusion

I believe that the method of determination of potentiometric selectivity coefficients described in this paper is superior to the conventional mixed solution and SS methods for the following reasons;

1. Conventional beaker-to-beaker measurements are prone to carry-over contamination between measurements; this cannot occur in the experimental procedure that I have developed as all measurements are performed in a single vessel.

2. Relatively few solutions need to be made up, and the experimental procedure is practically simple to implement. Hence it is easy to replicate data sets.

3. Transfer of electrodes between beakers results in the formation of an open cell with associated large transient shifts in cell potential, which the cell may or may not fully recover from. This does not happen in the proposed method as the electrodes are in continuous contact with the sample, and no open circuit is generated at any time during an experimental run.

4. The use of a non-linear curve fitting approach means that all the experimental data are used to estimate the electrode parameters. Unlike the conventional FI method,[1] there is no element of subjectivity, and the approach can easily cope with ions of differing charge.

5. The ease with which Excel spreadsheets can be modified allows the analyst to quickly investigate the usefulness of models other than the Nikolskii-Eisenman equation such as Eqn. (4-5). A macro can be easily written (with the Record Macro option on the Tools menu) for modifying the Worksheet relating to one interfering ion and this macro is then executed for each of the other interfering ions.

6. The quality of the electrode characteristics can be compared at a glance through the σ value in a single run. Furthermore, examination of the response curves in Figure 4-1 and Figure 4-2, or the residual error plots (see Figure 4-3 for the

163

doubly charged interfering ions) enable a very comprehensive picture of the data quality to be obtained.

7. Finally, *Solver* can change up to 200 parameters simultaneously and so, in principle, potentiometric selectivity coefficient measurements can be made for a primary ion in the presence of many interfering ions, should this be required.

In conclusion, I feel that this approach, if adopted by other investigators, would enable electrode characteristics to more rigorously measured, and would lead to much greater confidence in the applicability of these data.

4.5. Tables

Table 4-1. *Membrane Composition (m/m %) for Valinomycin ISE's.*

	valinomycin	Other Components [a]		
This Report	2.0	KTpClPB, 0.5	DOS, 64.7	PVC, 32.8
Knoll et. al.[16]	2.0	KTpClPB, 0.5	DOS, 64.7	PVC, 32.8
Cosofret et. al.[26] (Membrane L)	1.0	KTpClPB, 0.5	DOS, 49.5	PVC [b], 49.0
Ammann et. al.[27] (Membrane 23)	5.0	KTpClPB, 2.0	DBS, 68.0	2,3 DMNB, 25.0
Ammann et. al.[27] (Membrane 8)	1.0	_	DOS, 66.0	PVC, 33.0
Anker et. al.[28] (PVC / DOS)	1.0	_	DOS, 66.0	PVC, 33.0
Jenny et. al.[29] (PVC / DOS)	1.0	_	DOS, 66.0	PVC, 33.0
Miyahara and Simon[30] (PVC / DOS)	1.0	_	DOS, 66.0	PVC, 33.0
Miyahara and Simon[30] (PVC / TOTM)	1.0	_	TOTM, 66.0	PVC, 33.0
Miyahara and Simon[30] (OH-PVC / DOS)	1.0	_	DOS 66.0	OH-PVC, 33.0
Moody et. al.[31]	0.9	_	NPOE, 67.3	PVC, 31.8
Anker et. al.[28] (PVC / BBA)	1.3	_	BBA, 68.3	PVC, 30.4

165

	valinomycin	Other Components [a]	
Anker et. al.[28] (Silopren K 1000)	2.5	_	Silopren K 1000, 83.0	Cross-linking agent K11, 14.5
Jenny et. al.[29] (Silopren K 1000)	2.5	_	Silopren K 1000, 83.0	Cross-linking agent K11, 14.5
Gadzekpo and Christian[3] [c]	_			

[a] *Abbreviations (those not listed in this footnote are given in the experimental section)*:

    DBS - dibutylsebacate

    2,3 DMNB - 2,3-dimethyl-nitrobenzene

    TOTM - tri-(2-ethylhexyl)trimellitate

    NPOE - ortho-nitrophenyloctylether

    BBA - bis(1-butylpentyl)adipate

[b] *Carboxylated.*

[c] *This valinomycin ISE used was obtained from Beckmann Instruments.*

Table 4-2. *Potentials With Na$^+$ As The Interfering Ion.*

a_K	a_{Na} [a]	E_{mean} / mV	SD [b] / mV	E_J / mV
0	0.07726	-176.0 [c]	3.8	0.052
6.18E-07	0.07726	-172.9	4.1	0.052
2.16E-06	0.07726	-168.8	3.8	0.052
8.34E-06	0.07726	-160.0	3.5	0.052
2.22E-05	0.07726	-149.2	3.2	0.052
4.37E-05	0.07726	-138.6	2.7	0.052
7.41E-05	0.07725 [d]	-128.8	2.5	0.052
2.27E-04	0.07724 [d]	-104.4	1.4	0.052
6.86E-04	0.07720	-77.6	1.3	0.052
0.001599	0.07713	-57.1	1.1	0.051
0.004618	0.07689	-31.4	0.5	0.050
0.016499	0.07600	0.5	1.5	0.045
0.043794	0.07433	25.3	0.8	0.037

[a] *The Na$^+$ activity is effectively constant except for the most concentrated solution.*

[b] *S.D.; standard deviation.*

[c] *This value was not used in the non-linear analysis as the drift in the reading was too great, as is explained in Section 4.2.4.*

[d] *the mean of these a_{Na} values were used to calculate the LOD (see Eqn. (4-7)).*

Table 4-3: *Log of Potentiometric Selectivity Coefficients,* $\log k_{KB}^{Pot}$, *for Valinomycin ISE's*

Study		Method	Li⁺	Na⁺	NH₄⁺	Mg²⁺	Ca²⁺	Ba²⁺
						Interfering Ion		
1	This Report	[a, b]	-4.16	-3.71	-1.94	-4.30	-4.08	-4.03
2	This Report	[b]				-4.35	-4.13	-4.09
3	This Report	[b]	-4.11	-3.60	-2.22	-4.17	-4.10	-3.87
4	This Report	[b]				-4.04	-3.98	-3.73
5	This Report	SS [b]	-4.39	-3.98	-1.85	-4.70	-4.01	-4.44
6	Knoll *et. al.*[16]	MS [b]	-4.3	-4.2	–	–	–	–
7	Cosofret *et. al.*[26] (Membrane L)	SS [b]	-3.98	-3.56	-1.81	–	-4.30	–
8	Ammann *et. al.*[27] (Membrane 23)	SS [b]	-4.0	-3.5	–	-5.1	-4.4	-5.0
9	Ammann *et. al.*[27] (Membrane 8)	SS [b]	-4.3	-4.1	-2.0	-4.9	-4.7	-4.6
10	Anker *et. al.*[28] (PVC/DOS)	SS [b]	-4.3	-4.0	-2.0	-4.8	-4.6	-4.5
11	Jenny *et. al.*[29] (PVC/DOS)	SS [b]	-4.28	-4.04	-2.01	-4.82	-4.59	-4.51
12	Miyahara and Simon[30] (PVC/DOS)	SS [b]	-4.47	-3.92	-1.87	-4.97	-4.50	–
13	Miyahara and Simon[30] (PVC/TOTM)	SS [b]	-4.80	-4.09	-2.04	-4.92	-4.82	–
14	Miyahara and Simon[30] (OH-PVC/DOS)	SS [b]	-3.53	-2.40	-1.82	-3.44	-3.98	–
15	Moody *et. al.*[31]	SS [f]	-2.88	-3.02	–	-3.96	-3.80	–
16	Anker *et. al.*[28] (PVC/BBA)	SS [b]	-4.7	-3.7	-1.9	-4.6	-4.8	-5.4

Study		Interfering Ion						
		Method	Li^+	Na^+	NH_4^+	Mg^{2+}	Ca^{2+}	Ba^{2+}
18	Jenny *et. al.*[29] (Silopren K 1000)	SS [b]	-4.33	-4.00	-1.81	-4.31	-4.16	-3.77
19	Gadzekpo and Christian[3]	MS [g]	_	-3.54	_	_	_	_
20	Gadzekpo and Christian[3]	SS [h]	_	-2.15	_	-3.92	-3.74	_
21	Gadzekpo and Christian[3]	SS [i]	_	-3.17	_	-3.70	-3.68	_
22	Gadzekpo and Christian[3]	MP	_	-4.08	_	-3.68	-3.43	_

[a] *Modified FI method combined with non-linear analysis based on Eqn. (4-1).*

[b] *0.1 mol dm^{-3} solutions of metal chloride.*

[c] *Modified FI method combined with non-linear analysis based on Eqn. (4-5).*

[d] *Eqn. (4-7) was used with an LOD value found using Eqn. (4-1) as the model.*

[e] *Eqn. (4-7) was used with an LOD value found using Eqn. (4-5) as the model.*

[f] *0.01 mol dm^{-3} solutions of metal chloride.*

[g] *0.140 mol dm^{-3} solution of sodium chloride.*

[h] *equal concentrations of primary and interfering ions.*

[i] *unequal concentrations of primary and interfering ions.*

Table 4-4: *Other ISE Characteristics.*

Interfering ion	S / mV decade^{-1} [a, b]	E^0 / mV [a, b]	LOD (log a$_K$)	Model Equation
--	57.84 ± 0.24	100.65 ± 0.65	-5.70	(4-1)
Li$^+$	58.23 ± 0.06	101.28 ± 0.33	-5.22	(4-1)
Na$^+$	56.87 ± 0.49	101.83 ± 0.30	-4.72	(4-1)
NH$_4^+$	56.67 ± 0.50	99.44 ± 0.83	-3.17	(4-1)
Mg^{2+}	57.00 ± 0.13	96.27 ± 0.27	-4.97	(4-1)
Ca^{2+}	56.88 ± 0.04	96.98 ± 0.33	-4.90	(4-1)
Ba^{2+}	55.94 ± 0.68	96.09 ± 1.56	-4.67	(4-1)
Mg^{2+}	55.43 ± 0.20	92.82 ± 0.12	-4.84	(4-5)
Ca^{2+}	55.05 ± 0.11	93.14 ± 0.14	-4.78	(4-5)
Ba^{2+}	53.98 ± 0.81	91.95 ± 1.80	-4.53	(4-5)

[a] *The S and E^0 values quoted were obtained by non-linear analysis on the mean of the corrected potentials.*

[b] *The errors quoted are the standard deviation of the values obtained from non-linear analysis of three replicate data sets for the interfering ion studies. In the case of pure K+ solutions (first row), the error is the standard error of the slope of the regression line calculated over the concentration range 10^{-4} to 0.1 mol dm^{-3}.*

Table 4-5. *Standard Deviation of the experimental values from the curve of best fit, σ. [a, b]*

Interfering Ion	Model: Eqn.: (4-1)	Model: Eqn.: (4-5)
Li^+	0.68 ± 0.02	
Na^+	0.86 ± 0.22	
NH_4^+	0.51 ± 0.04	
Mg^{2+}	0.96 ± 0.12	2.28 ± 0.18
Ca^{2+}	0.71 ± 0.02	2.03 ± 0.04
Ba^{2+}	2.07 ± 0.58	3.50 ± 0.35

[a] *obtained by non-linear analysis of the mean corrected potentials.*

[b] *The errors quoted are standard deviation of the values obtained from non-linear analysis on the individual potentials.*

4.6. Figures
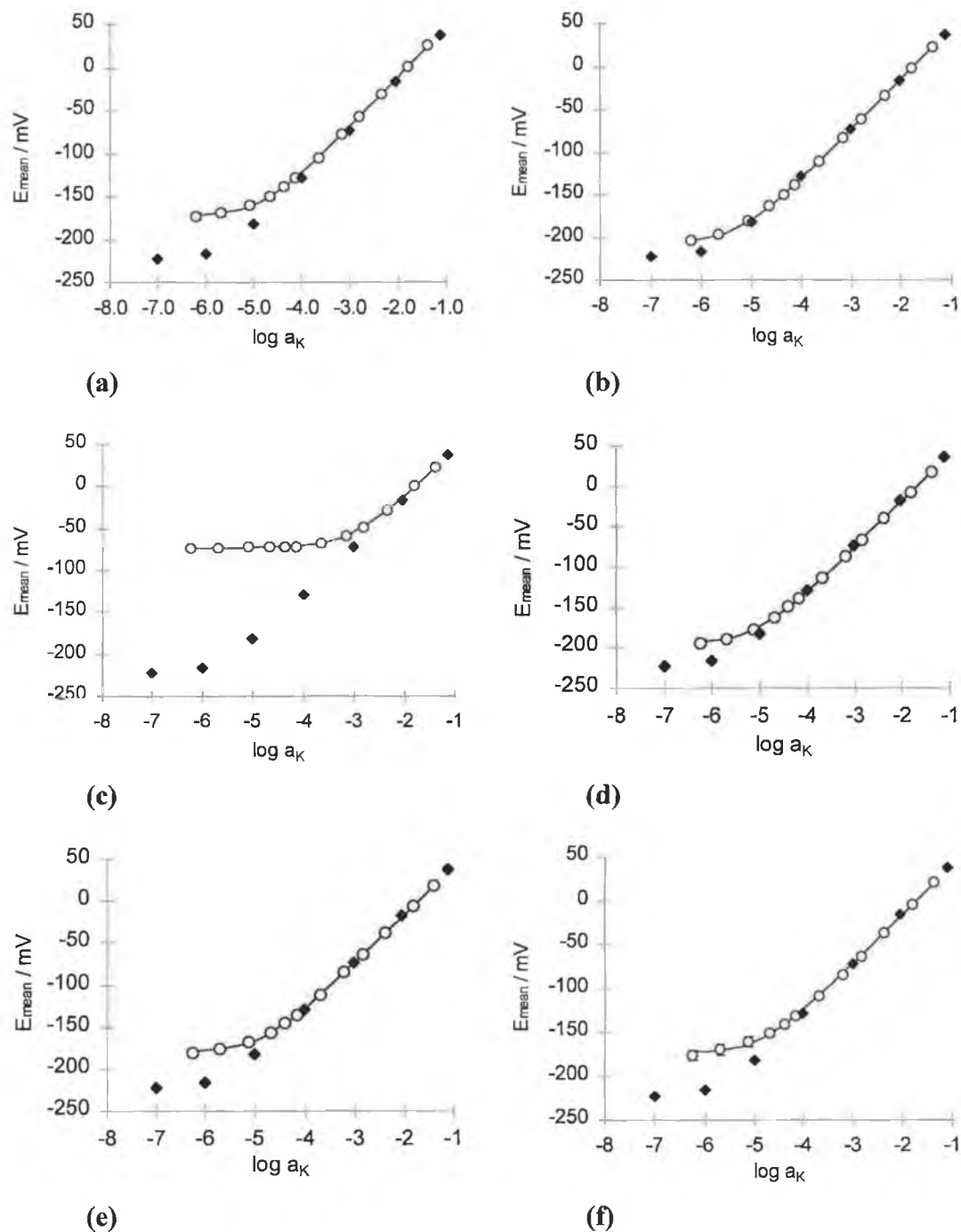
Figure 4-1. *Plot of mean experimental potentials (hollow circular points) and predicted potentials (line) according to the optimised model based on Eqn. (4-1), versus log of potassium ion activity with standard deviations as error bars (n = 3). The interfering ions are: (a) Li^+, (b) Na^+, (c) NH_4^+, (d) Mg^{2+}, (e) Ca^{2+} and (f) Ba^{2+}. The black diamond-shaped points are the potassium chloride calibration potentials.*

172

(a)

(b)

(c)
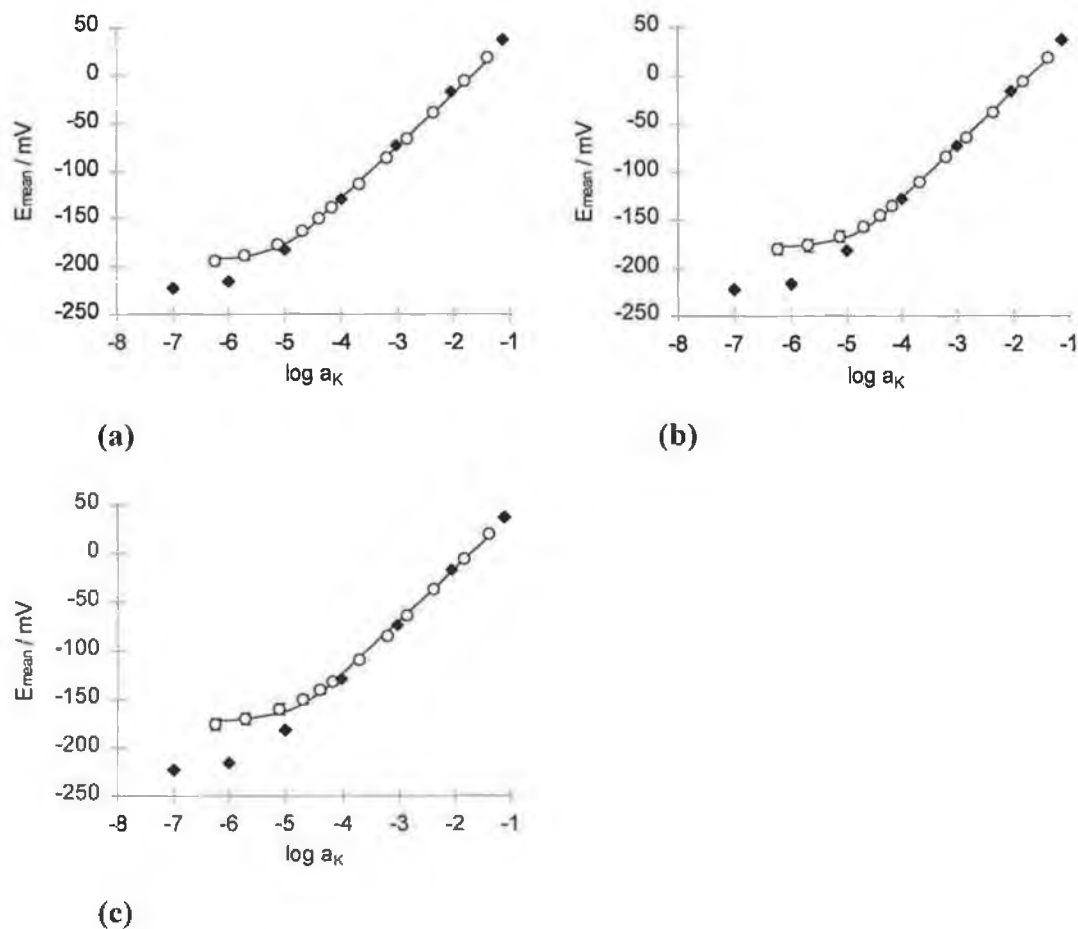
Figure 4-2. *Plot of mean experimental potentials (hollow circular points) and predicted potentials (line) according to the optimised model based on Eqn. (4-5), versus log of potassium ion activity with standard deviations as error bars (n = 3). The interfering ions are: (a) Mg^{2+}, (b) Ca^{2+} and (c) Ba^{2+}. The filled diamond-shaped points are the potassium chloride calibration potentials.*

(a)

(b)

(c)
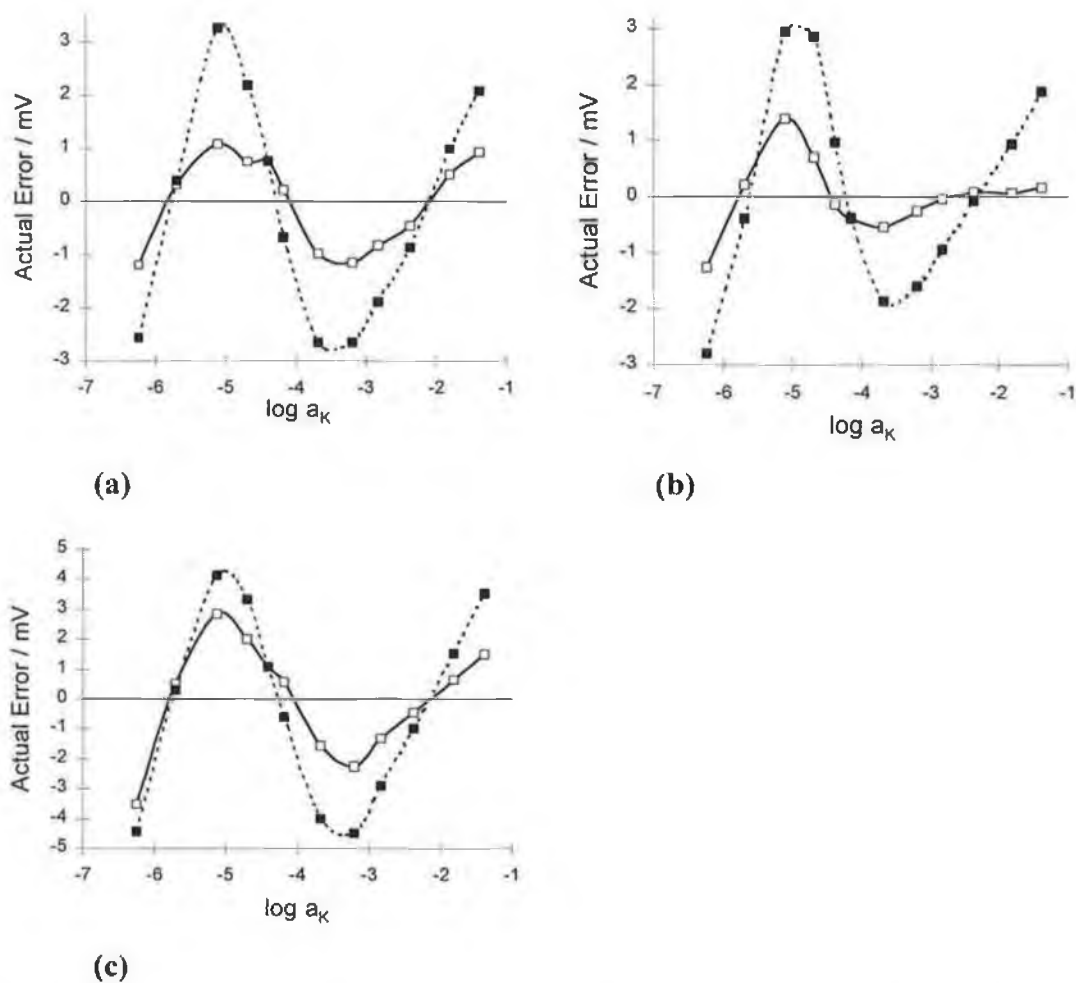
Figure 4-3. *Plot of residual error resulting from the fit of the Eqn. (4-1) (solid line, hollow points) and Eqn. (4-5) (broken line, filled points) to the mean experimental potential versus log of the potassium ion activity. The interfering ions are: (a) Mg^{2+}, (b) Ca^{2+} and (c) Ba^{2+}.*

174

4.7.   Location Of Files

Reprints of the paper which forms the basis of this chapter (P. Kane and D. Diamond, "*Determination of Ion-Selective Electrode Characteristics by Curve Fitting*", Talanta, **1997**, 44, 1847-1858.) are available from myself or Dr. Dermot Diamond.

Description	Computer	Directory	File Name	Comment(s)
Excel files containing the electrode characteristics	Gateway P5-100	C:\ __Paddy\ Potentio\ Val ISE Modelling	Val_Sel_7a.xls (Eqn (4-1) is used as the model) Val_Sel_8_Bakker.xls (Eqn (4-5) is used as the model)	

4.8.   References

1.   G. G. Guilbault, R. A. Durst, M. S. Frant, H. Freiser, E. H. Hansen, T. S. Light, E. Pungor, G. Rechnitz, N. M. Rice, T. J. Rohm, W. Simon and J. D. R. Thomas, *Pure Appl. Chem.*, **1976**, 48, 127.

2.   Y. Umezawa, K. Umezawa. and H. Sato, *Pure Appl. Chem.*, **1994**, 67, 507.

3.   V. P. Y. Gadzekpo, and G. D. Christian, *Anal. Chim. Acta,* **1984**, 164, 279.

4.   E. Bakker, *J. Electrochem. Soc.*, **1996**, 143, L83.

5.   G. J. Moody, and J. D. R. Thomas, "Selective Ion Sensitive Electrodes", Marrow, Watford, 1971.

6.   K. Srinivasan, and G. A. Rechnitz, *Anal. Chem.*, **1969**, 41, 1203.

7.   C. Maccà, *Anal. Chim. Acta,* **1996**, 321, 1.

8.   W. Yuliang, Z. Zhiang, and Z. Zhiyi, *Fenxi Shiyanshi*, **1994**, 13 (4) 56.

9.   D. E. Davey, D. E. Mulcahy and G. R. O'Connell, *Electroanalysis* (N. -Y.), **1996**, 8 (3), 274.

10.   R. Forster, and D Diamond, *Anal. Chem.*, **1992**, 64, 1721.

11.   D. Diamond, and R. J. Forster, *Anal. Chim. Acta*, **1993**, 276, 75.

12.   F. J. Saez de Viteri and D. Diamond, *Analyst*, **1994**, 119, 749.

13.   W. E. Morf., D. Ammann, E. Pretsch and W. Simon *Pure Appl. Chem.*, **1973**, 36, 421.

14.   E. Bakker, R. K. Mervura, E. Pretsch, and M. E. Meyerhoff, *Anal. Chem.*, **1994**, 66, 3021.

15.   J. Lu, Q. Chen, D. Diamond, and J. Wang, *Analyst*, **1993**, 118, 1131.

16.   M. Knoll, K. Cammann, C. Dumschat, M. Borchardt, and G. Högg, *Sens. Actuators B,* **1994**, B20, 1.

17.   D. Lide., Editor-in-Chief, "CRC Handbook of Chemistry and Physics", 76 th ed., CRC Press Inc., 1995, p. 6-160.

176

18. *Ibid*, p. 6-193.

19. P. C. Meier, D. Ammann, W. E. Morf and W. Simon, in J. Koryta, Editor, "Medical and Biological Applications of Electrochemical Devices", John Wiley, Chichester, 1980, p.22.

20. S. Walsh, and D. Diamond, *Talanta*, **1995**, 42 (4), 561.

21. J. H. Noggle, "Practical Curve Fitting and Data Analysis", Ellis Horwood, 1993.

22. A. K. Covington, Editor, "Ion Selective Electrode Methodology", Vol. 1, CRC Press, Boca Raton, Florida, 1979.

23. D. Diamond and F. Regan, *Electroanalysis* (N. -Y.), **1990** 2 (2), 113.

24. E. Metzger, D. Ammann, R. Asper, and W. Simon, *Anal. Chem.,* 1986, **58**, 132.

25. V. P. Y. Gadzekpo, J. M. Hungerford, A. M. Kadry, Y. A. Ibrahim, R. Y. Xie, and G. D. Christian, *Anal. Chem.,* **1986**, 58, 1948.

26. V. V. Cosofret, E. Erdösy, R. P. Buck, W. J. Kao J. M. Anderson, E. Lindner, and M. R. Neuman, *Analyst*, **1994**, 119, 2283.

27. D. Ammann, W. E. Morf, P. Anker, P. C. Meier, E. Pretsch, and W. Simon, *Ion-selective Revs.,* **1983**, 5, 3, 38.

28. P. Anker, H.-B. Jenny, U. Wuthier, R. Asper, D. Ammann, and W. Simon, Clin., Chem., **1983**, 29, 1447.

29. H.-B. Jenny, C Riess, D. Ammann, B. Magyar, R. Asper, and W. Simon, Mikrochim Acta, **1980**-II, 309.

30. Y. Miyahara, and W. Simon, *Electroanalysis* (N. -Y.), **1991** 3, 287.

31. G. J. Moody, B. Saad Bahruddin, and J. D. R. Thomas, *Analyst*, **1989**, 114, 15.